Investigating the effects of cooperative vehicles on highway traffic flow homogenization: analytical and simulation studies

Julien Monteil



Investigating the effects of cooperative vehicles on highway traffic flow homogenization: analytical and simulation studies

by

Julien Georges Monteil

A dissertation submitted for the degree of Doctor of Philosophy

at the

Mécanique - Energétique - Génie civil - Acoustique (MEGA) Doctoral School

in the

Traffic Engineering Laboratory (LICIT)

Joint Research Unit of IFSTTAR, ENTPE

Examining committee:

Hesham RAKHA	Professor, Virginia Tech
Masao KUWAHARA	Professor, Tohoku University
Philippe GOUGEON	R&D Director, Valeo
Salima HASSAS	Professor, Université de Lyon
Jacques SAU	Professor, Université de Lyon
Nour-Eddin EL FAOUZI	Research Director, IFSTTAR

Manuscript submitted on December 3, 2013

Investigating the effects of cooperative vehicles on highway traffic flow homogenization: analytical and simulation studies

by
Julien Georges Monteil

A Georges Emile Monteil
Officier de la Légion d'honneur
Mon grand-père

Abstract

The traffic engineering community currently faces the advent of a new generation of Intelligent Transportation Systems (ITS), known as cooperative systems. More specifically, the recent developments of connected and autonomous vehicles, *i.e.* cooperative vehicles, are expected to cause a societal shift, changing the way people commute on a daily basis and relate to transport in general.

The research presented in this dissertation is motivated by the need for proper understanding of the possible inputs of cooperative vehicles in a traffic stream. Beyond legal aspects regarding the introduction of such vehicles and considerations on standardization and harmonization of the communication norms, the research focuses on the use of communication for highway traffic flow homogenization. In particular, the selected approach for the introduction of cooperation inherits from the theory of traffic flow and the recent developments of microscopic traffic models.

Cooperation can first be introduced as a form of multi-anticipation, which can either come from drivers' behaviors or from communication. A mathematical framework for investigating the impact of perturbations into a steady-state traffic is proposed for the class of time continuous car-following models. Linear stability analyses are refined for forward and backward multi-anticipation, exploring the underlying importance of considering upstream information. The linear stability analyses for all wavelengths can be deepened by the mean of the graphical root locus analysis, which enables comparisons and design of strategies of cooperation. The positive influence of bilateral cooperation and of added linear control terms are highlighted. Weakly non-linear analyses are also performed, and the equations of solitary waves appearing at the frontier of the instability domain are obtained. A simple condition over the partial derivatives of the dynamical system is found to determine the acceleration regime of the leading edge of the travelling wave.

Following these analytical results, one aim is to simulate a realistic traffic thereby reproducing the driving behavior variability. A Next Generation Simulation trajectory dataset is used to calibrate three continuous car-following models. A methodology involving data filtering, robust calibration, parameters estimation and sampling of realistic parameters is detailed, and allows realistic traffic with stop-and-go waves appearances to be replicated. Based on these simulated trajectories, previous analytical results are confirmed, and the growing perturbations are removed for various coverage

rates of cooperative vehicles and adequately tuned cooperative strategies.

Finally the issue of information reliability is assessed for a mixed fleet of cooperative and non-cooperative vehicles. The modelling choice consists in building a three layers multi-agent framework that enables the following properties to be defined: the physical behavior of vehicles, the communication possibilities, and the trust each vehicle -or agent- has in another vehicle information or in itself. The investigation of trust and communication rules allow the model to deal with high rates of disturbed cooperative vehicles sensors and to learn in real time the quality of the sent and received information. It is demonstrated that appropriate communication and trust rules sensibly increase the robustness of the network to perturbations coming from exchanges of unreliable information.

Acknowledgments

My first, sincere and deep affectionate thoughts are for my beloved family, my parents Bruno and Eveline, my sisters Marie and Clémence and my brother Jean-Baptiste. They have guided me through adversity, and they have all my admiration and love.

I would like to start by expressing my gratitude to the members of my PhD committee, Professors Hesham Rakha, Masao Kuwahara, Salima Hassas, Jacques Sau, Philippe Gougeon and Nour-Eddin El Faouzi, for all their comments and reviews. I felt honored to have my work examined by them and I would like to thank them again for the day of my PhD defense, which I will remember.

I am extremely indebted and thankful to my supervisor Professor Nour-Eddin El Faouzi, who gave me the opportunity to enter into the research field as a young civil servant graduated engineer. He oriented my research work, sent me to research labs and conferences worldwide, and above all never stopped supporting me.

My first research experience is the reason of where I am today. I had the deep honor to join the laboratory of Professor Kuwahara at the University of Tokyo, on March 2009, for a six months internship. Since this wonderful research experience, I have always felt like any good thing happening in my young academic career would be related to sensei and his team, and to Japan.

I had the chance to join the CCIT team at UC Berkeley in March 2010 for my master thesis. During this five months training, Professor Alexandre Bayen and Joe Butler were role models for me and never gave up on advising me and spending their time with the young student I was. I could not have dreamt of a better learning experience at that time.

I would like to express my extreme gratitude to Professor Jacques Sau, who guided me all along my PhD work. He kept reminding me how entertaining developing mathematical expressions and how rigorous writing

scientific papers should be. He accompanied my journey into the fascinating wild world of dynamical systems.

Professor Edward Chung gave me the opportunity to join his team at QUT for a three months stay at the beginning of my second year. I am very grateful to him and to Dr Mark Miska for all the insights they gave me from a traffic engineering perspective. I have always respected Professor Christine Buisson a lot, for the passion she communicates and the availability she demonstrates. Her guidance for car-following parameter identification was precious. The exchanges I had with Dr Jean-Luc Ygnace were a unique experience. He made the world look small and his constant sharing of his revolutionary ideas on congestion pricing was a day to day sunbath. The elegance and simplicity of Wei-Bin Zhang have always impressed me, and I must say he is probably the one along with my supervisor who steered me in the right direction after the first few months of my PhD. I am very thankful to Fabrice Reclus for his regular inputs on ITS technologies, and the numerous discussions we had always provided me with knowledge. I am very grateful to Professeur Salima Hassas and Dr Frederic Armetta, whom I went to see at the beginning of my second year with a few questions on multi-agent systems, and who since then never stopped encouraging me and sharing with me their vast expertise in the multi-agent field. I would also like to thank Professor Ludovic Leclerq, who was always available and insightful, and Professor Robert Bertini, who allowed me to benefit from his incredible knowledge and experience. To go back in college years, and my year at Lycée Saint-Louis in particular, I must acknowledge the great influence that Professeur Eric Leborgne had on my education.

I would like to particularly thank two colleagues and friends of mine, Dr Romain Billot and Dr David Rey. Romain hosted me at QUT while he was in the middle of a postdoc, and this was the start of a good collaboration. I shared the office with David on the first two years of my PhD, and also tons of good moments. Their friendly and scientific insights have always been sharp and accurate. I also have to thank Fouad, who has been a wonderful colleague and friend and has become like a brother to me, Matthieu, who was always ready to share his excellent mood and knowledge in statistics, Maxime, who kindly helped me in the last rush of the PhD, Sonia, who patiently guided me through administrative tasks, and Anne-Christine, who has always helped me a lot.

Along my work and academic visits, I have met colleagues who became friends and all inspired me through their spirit and belief. I learnt a lot from all of them. I would like to particularly thank Michael, Babak, Samitha, Alfredo, Shiomi and Filmon. My close family as well as my old and not

so old friends have also made it possible, and I am very grateful to all of them for their permanent support. My aunt Françoise, my cousin Julien, Mehdi, Julien, Tim, Vanessa, Matthis, Nicolas, Salwa, Alex, Cyril, Thibaud, Moussa, Adrien, Romain, Yannis, Sylvain, Julio, Francisco, Michelle, Ono. I feel extremely happy to have Kristen in my life, and her energy has made the supposedly difficult last months of PhD look easy.

Contents

List of Figures

List of Tables

Chapter 1

Introduction

The advent of new technologies in transportation, known as Intelligent Transportation Systems (ITS), and their introduction into daily city and intercity traffic has become a major preoccupation for car manufacturers, road authorities, traffic operators, and researchers. High technology is sought-after in the current climate agitated by growing challenges related to emerging technologies. The exponential growth rate of smartphone use, the rising challenges of cloud computing and big data call for new solutions and at the same time bring new means to move towards those new solutions [1]. This technological context paves the way for the concept of connected roads, enabling infrastructure and vehicles to cooperate and exchange their data *via* various communication means thereby facilitating traffic monitoring in order to increase safety and efficiency, and decrease environmental impact. The diversity of data sources, including fixed cameras, infrared beacons, loop detectors, bluetooth detectors, GPS devices, drivers' smartphones, vehicle radars and on board devices, provides many data sets and enables the establishment of sensor networks with unprecedented scalable monitoring capabilities.

The microscopic scale has always been an important area of interest and research as it directly affects the way people drive. Stakeholders and researchers have been insistently working for a future in which the human driving task would be considerably reduced or even removed, in order to minimize human errors. When Ralph Teetor thought of the first cruise control system which was later launched on a few 1958 Chrysler models, while traffic theory was still in its very early stages, the first step towards automated (driverless) and autonomous (driver present) vehicles was made. Autonoumous vehicles refer to the vehicles in which the driver is partially

or fully assisted in his driving task by an electronic system, without any communication with other vehicles or infrastructure. At the same time, in-vehicle sensors, communication devices, and infrastructure units enable the frequent exchanges of information between vehicles and infrastructure and contribute to develop the connected vehicles, which designate vehicles with endowed communication capabilities. Cooperative vehicles are connected vehicles that share some of the functionalities of autonomous vehicles [2].

The constant progress in the implementation of Advanced Driver Assistance Systems (ADAS) has well expressed this paradigm shift towards mobility and safety. Now a multitude of ADAS systems [3] include infotainment, adaptive cruise control, lane changing assistant, night vision, automatic parking, among others, that aim at providing safer and more efficient traffic by supporting the driving task. A complete shift towards fully assisted vehicles was introduced in the last two decades, with the California Partners for Advanded Transportation TecHnology (PATH) pioneer work on platoons of automated vehicles, and very recently the autonomous Google driverless car. The industry's move towards automation is mainly motivated by the perspective of a safer traffic where automated electronic systems prevent human mistakes and inefficiencies, as well as by the potential to reduce environmental impact. Prospective standardization efforts on ITS technologies has been made at an international level resulting in numerous funded Research and Development (R&D) projects, which give particular attention to the potential of ITS in decreasing hazardous situations and reducing greenhouse gas emissions. These emerging technologies also stimulate investment because they have the potential to make vehicles more marketable: where the technology is seen as fashionable it may attract customers and boost a company's image.

In this context, a driver would legitimately claim to benefit from these cutting edge technologies. While the liability question in the case of collisions related to systems failures gives way to legal issues, especially in the case of fully automated vehicles, the safe behavior of ADAS and any integrated automated system must be a guarantee. Some open debates may then be raised with a system that potentially informs the driver, warns the driver or even takes over the driving task during identified critical situations:

- Does a partial support system offered to the driver lead to a less careful and less reactive driver?
- What is an appropriate design for the in-vehicle Human Machine Interface (HMI), as too much information may cause a lack of attention

to the driving task?

- Are drivers ready to let an automated system drive for them, especially in critical situations?
- What happens in the case of a crash involving a normal vehicle and a cooperative vehicle?
- Is it possible to mix an equipped fleet of cooperative vehicles with normal vehicles without deteriorating the traffic flow characteristics?

Facing these concerns relating to the reality of a mixed traffic made of normal and cooperative vehicles, prospective simulation studies are much needed to counterbalance the lack of cooperative vehicles data and to figure out to which extent cooperative vehicles can help reduce traffic flow heterogeneities and collision-prone situations.

It is known that congestion wastes a massive amount of time, fuel and money. However congestion does not systematically come from a capacity default as about half of it is due to non-recurrent events [4], which are typically due to crashes, disabled vehicles, convoys of trucks or adverse weather conditions. Non-recurrent events follow irregular patterns in time, and their consequences on traffic flow efficiency and safety could therefore be dramatic [5]. A legitimate idea would consist in using the potentialities of cooperative vehicles to reduce the occurences of such non-recurrent events. The presented research takes on the problem of a mixed traffic on highways, in which cooperative vehicles have to interact with normal drivers, with an emphasis on the question of congestion appearance and spontaneous traffic jams, when shock waves appear "out of nowhere". More specific challenges may then emerge regarding the use of cooperative vehicles for traffic flow management:

- What physics can explain the formation of non-recurrent traffic jams?
- What type of information, and how much information, can be utilized to control the dynamics of cooperative vehicles, and to reduce undesirable traffic situations?
- What control algorithms to integrate such data exchanges, and to prevent cooperative vehicles from adopting abnormal driving behavior?
- What traffic safety and efficiency indicators can well reflect traffic conditions?

- What is the proportion of cooperative vehicles needed to get positive effects?
- Can negative effects result from vehicle cooperation?
- How can the different sources of noise (drivers behavior, communication latency time, sensors faults) be integrated?

This dissertation aims at considering and addressing these questions, while the main intention is to operate cooperative vehicles to homogenize highway traffic flow thereby reducing the formation of spontaneous shock waves. First, an analytical framework was needed to understand the physics of traffic and the potential of cooperation, therefore, stability analyses of defined cooperative car-following models were conducted. Real data based calibration of car-following models was performed using a robust methodology in order to reproduce drivers behavior variability in simulation. Finally, a multi-agent modelling framework was introduced to consider all sources of perturbations, with the perspective of achieving self-organization in highway traffic.

The organization of the dissertation is as follows. Chapter 2 relates to ITS technologies with an emphasis on cooperative vehicles. It reflects what might be expected in terms of technology development, presenting the main European and international research on ITS technologies. Chapter 3 presents the state of the art in traffic modelling as well as its utility for ITS applications. Chapter 4 addresses the problem of congestion appearance in a longitudinal traffic stream via a mathematical formulation. For a microscopic steady-state traffic, stability analyses allow conditions to be derived for the stability of the dynamical system, defined in the case of cooperative and non-cooperative traffic. Linear stability analyses, weakly linear stability analyses and root locus analyses of cooperative and non-cooperative car following models are conducted. A discussion about the type of cooperation needed for the stabilization of the dynamical system concludes the chapter. Chapter 5 discusses the reproduction of realistic traffic conditions from trajectory data. A robust methodology for parameter identification of car-following models is much needed to capture the variability of drivers' behaviors. Realistic estimated parameters enable the assessment of the potential of cooperative vehicles. Data filtering, estimation and sampling techniques are explained in detail. Chapter 6 documents the research conducted using simulation studies. Results from chapter 5 are verified and are used to evaluate the effect of cooperation and distributed control strategies over the

shock waves appearances and various traffic efficiency and safety indicators. Chapter 7 introduces perturbations from communication, as in-vehicles sensors are considered potentially sources of error. A multi-agent framework with a physical layer defining behavioral traffic laws, a communication layer enabling information exchanges, and a learning layer for sensors unreliability diagnosis is built-in to adapt control strategies while using the available information in the network. Chapter 8 reflects on the contributions of the dissertation and the research perspectives that are of future interest.

Along with this work, the following research has been published in peer-reviewed journals and conference papers and presented at conferences and international projects, all listed below.

Peer-reviewed journal publications

- Monteil, J., Billot, R., Sau, J., Buisson, C., El Faouzi, N.-E., Calibration, estimation and sampling issues of car-following parameters. *Transportation Research Records, journal of the Transportation Research Board, 2014.* Submitted.
- Sau, J., Monteil, J., Billot, R., El Faouzi, N.-E., The root locus method: application to linear stability analysis and design of cooperative car-following models. *Tranportmetrica B: Tranport Dynamics, 2014.*
- Monteil, J., Billot, R., Sau, J., El Faouzi, N.-E., Linear and weakly non-linear stability analyses of cooperative car-following models. *IEEE Transactions on Intelligent Transportation Systems, 2013.*
- Monteil, J., Nantes, A., Billot, R., El Faouzi, N.-E., Microscopic cooperative traffic flow: calibration and simulation based on a NGSIM dataset. *IET Intelligent Transport Systems, 2013.*
- Monteil, J., Billot, R., Sau, J., Armetta, F., Hassas, S., El Faouzi, N.-E., Cooperative highway traffic: multi-agent modelling and robustness assessment to local perturbations. *Transportation Research Records, journal of the Transportation Research Board, 2013.*
- Monteil, J., Billot, R., El Faouzi, N.-E., Des véhicules coopératifs pour une gestion dynamique du trafic : approche théorique et simulation. *Recherche Sécurité Transports, 2012.*

Peer-reviewed conference publications

- Monteil, J., Billot, R., Guériau, M., Armetta, F., Hassas, S., El Faouzi, N.-E., A three-layer multi-agent framework for sensor reliability issues: application to cooperative highway traffic. *Association for the Advancement of Artificial Intelligence, AAAI 2014*. Submitted.

- Monteil, J., Billot, R., Sau, J., Buisson, C., El Faouzi, N.-E., Calibration, estimation and sampling issues of car-following parameters. *93rd Annual Meeting of Transportation Research Board (TRB) 2014*, Washington D.C., USA.
- Monteil, J., Billot, R., Sau, J., Armetta, F., Hassas, S., El Faouzi, N.-E., Cooperative highway traffic: multi-agent modelling and robustness assessment to local perturbations. *92nd Annual Meeting of Transportation Research Board (TRB) 2013*, Washington D.C., USA.
- Monteil, J., Nantes, A., Billot, R., El Faouzi, N.-E., Microscopic cooperative traffic based on NGSIM data. *Proceedings of the 19th ITS World Congress 2012*, Vienna, Austria.
- Monteil, J., Billot, R., Rey, D., El Faouzi, N.-E., Distributed and centralized approaches for cooperative road traffic dynamics. *Procedia of Social and Behavioral Sciences, Volume 48, pp. 3198 - 3208*, *4th Transportation Research Arena, TRA 2012*, Athens, Greece.
- Monteil, J., Billot, R., El Faouzi, N.-E., Towards cooperative traffic management: methodological issues and perspectives. *Australasian Transport Research Forum 2011 Proceedings*, Adelaide, Australia.

Presentations in conferences/ international projects

- Monteil, J., Modélisation multi-agents pour la régulation dynamique des flux microscopiques de trafic de véhicules. *Plateforme francophone de l'intelligence artificielle (PFIA)*, Lille, France, July 2013.
- Monteil, J., Analytical studies and real data based simulation for assessing the potential of cooperative systems. *Final NEARCTIS workshop*, Trinity College Dublin, Ireland, June 2013.
- Monteil, J., Stability techniques for assessing cooperation in highway traffic. *OPTIMUM workshop*, EPFL Lausanne, Switzerland, March 2013.
- Monteil., J., Cooperative highway traffic: multi-agent modelling and robustness assessment to local perturbations. *92th Annual Meeting of Transportation Research Board (TRB)*, Washington D.C., USA, January 2013.

- Monteil, J., Microscopic Cooperative Vehicular Traffic Flow Modelling: Analytical considerations and calibration issues based on NGSIM data. *19th ITS World Congress 2012*, Vienna, Austria, October 2012.
- Monteil, J., Distributed and Centralized Approaches for Cooperative Road Traffic Dynamics. *4th Transportation Research Arena, TRA*, Athens, Greece, May 2012.
- Monteil, J., Towards cooperative traffic management: methodological issues and perspectives. *Australasian Transport Research Forum*, Adelaide, Australia, September 2011.
- Monteil, J., Samoili, S., Weather sensitive calibration of microscopic models. *COST TU0702 Action*, Brno, Czech Republic, May 2011.

Chapter 2

Cooperative systems for connected mobility: origins and ongoing projects

The objective of this chapter is to place the dissertation in historical context. The technical needs to operate future connected and autonomous vehicles constitute a scientific challenge which solution may be inspired from human behavior. A quote from Paul Ricoeur explores this concept, before a brief history of autonomous and connected vehicles is presented, followed by a description of ongoing projects in the field. The multiple projects and developing test sites contribute to making cooperative systems an imminent reality.

2.1 Ricoeur and the organization

"Life does not belong wholly to the necessary, to the absolute necessary, it also belongs to the relative involuntary, docile to willing. In other words, the paradox is not only one of the will and life in general, but also is already present at the core of my experience of life. My life is ambiguous: it is at the same time a resolved problem insofar as it is structure -and a problem to be solved, insofar as it is spontaneity of need, of habit, and emotion. It is the marvel of structure and a pressing appeal to the sovereignty of decision. I have nothing to do with the beating of my heart, and everything to do with nourishing, caring for, and guiding my body. Thus I constantly experience within myself the mixture of two involuntaries: the absolute involuntary of a life that allows my existence as a consciousness -and in this way premises

my humanity, and the relative involuntary of a life that appeals for my decision and my effort -and in this way expects my humanity". (Freedom and nature: the voluntary and the involuntary, p. 419-420, [6]). Ricoeur entitled the third chapter of his book "The life: the organization". The semi-collon, in the tradition of the phenomenological method, heralds a confrontation between the life and the organization. It is nothing certain that a synthesis is possible between the two terms. The life may limit the organization, the organization may exclude the life, or maybe their ambiguous relation makes it impossible to specify for the human consciousness. Ricoeur's effort consists in supporting the confrontation of these two concepts to an extent where this confrontation is the reflection of the fundamental contradiction between life and consciousness. Starting from the organization is an epistemologic question. The organization can simultaneously be two things: the production of an order applying appropriate techniques, and the natural construction of a living structure. Thus, a scientific organization is a will that aims at creating an order -organization- able to subdue other wills, and this order can follow two opposed directions. First, it is question of conditioning wills that could perturb the desired order by playing on involuntary mechanisms that act upon potentially rebellious wills from the inside. One may risk a parallel with traffic, where the operating mechanims could be the contamination of cooperation, *via* the influence that cooperative vehicles with desired behaviors can have on non-cooperative vehicles. Secondly, it is question of integrating the particular wills to create, as in the living, a spontaneous organization. The absolute and relative involuntary can be used in traffic to control and condition the drivers' behaviors. Drivers should not be surprised in their habits, but they can be conditioned in their needs, habits, and emotions. Following this idea, a mixed traffic made of cooperative and non-cooperative drivers should be as close as possible to a real traffic, with the idea to smoothly constrain and modify unwanted driving behaviors.

2.2 Towards cooperative vehicles

2.2.1 A brief history of autonomous vehicles

The concept of autonomous vehicles dates from the second half of the twentieth century. In 1960, the New York Times [7] published that electronic roads made of guided cars were feasible. A long experiment conducted by General Motors and the Radio Corporation of American (RCA) Laboratories at Princeton lead to demonstrations of infrastructure built-in detector

circuits that were able to conduct any metallic vehicle driving on the road surface. Radio receivers enable the acceleration or deceleration of such cars. Earlier, in 1948, Ralph Teetor invented the first cruise control system, which automatically controlled the speed of the vehicle using a solenoid to modify speeds when necessary. The way his lawyer used to drive irritated Teetor and motivated him to work on the conception of this automated system. In the 60s the United Kingdom's Transport and Road Research laboratory (TRRL which later became TRL Limited) conducted experiments on magnetic cable embedded roads. They demonstrated that an automated vehicle was more responsive than an actual driver in terms of speed and direction deviation under adverse weather conditions. However, the funding for this research was withdrawn in the early 70s. The Programme for a European Traffic of Highest Efficiency and Unprecedented Safety (PROMETHEUS) project was launched in 1987 following the effort of the team of Ernst Dickmanns at the Bundeswehr University of Munich, which consisted of building vision-guided Mercedes cars that can circulate on streets without traffic. The intergovernemental organization Eureka funded the ambitious 749 M€project for a duration of 8 years, involving 11 European countries [8]. A few experiments were planned, and the arguably very first autonomous vehicles were built, VaMP and VITA-2. Computer commands relied on the real time evaluation of image sequences, which made possible the control of the steering wheel, throttle and brakes. The dynamic computer vision based system was tested in heavy traffic in Paris but with a safety driver on board to approve some of the maneuvers (such as overtaking). One year later, an experiment was conducted on German motorways from Munich to Copenhagen, proving that the system was working, except in some really particular situations when the driver had to take over the driving task.

An important move towards autonomous vehicles research was made in the United States when the Intermodal Surface Transportation Efficiency Act of 1991 (ISTEA) was passed by the Congress, The US Department Of Tranportation (USDOT) was asked to demonstrate an automated vehicle and highway system by 1997. The project involved the Federal Highway Administration (FWA), General Motors, Caltrans and UC Berkeley. It led to the Interstate 15 San Diego demonstration of 1997 [9] in which a platoon control demonstration showed vehicles driving with close headways (6.5 meters spacing) and at 96 km/h, and vehicles doing maneuvers to leave the platoon or gain access to it. The technology lay in built-in magnetic detectors along the road. At the same time, the ARGO project aimed at using low-cost video cameras and stereoscopic vision algorithms to sense the environment. Over a thousand miles were covered, almost all of them in fully

automated mode.

2.2.2 Connected vehicles

The recent advances in the fields of mobile broadband and vehicular communication systems have contributed to the development of vehicles endowed with communication capabilities: connected vehicles. Mobile broadband represents the wireless internet access for any kind of portable modems (mobile phones, computers...). The constant progress in terms of mobile phone technology and infrastructure contributed to developing the standards of communication, from the Global System for Mobile Communication (GSM) in 1991, to the Universal Mobile Telecommunication System (UMTS) in 2001 and the recent 4G technology, which is based on the Long Term Evolution (LTE) Advanced standardized by the 3rd Generation Partnership Project (3GPP), which will provide data speeds of 1 GBit/s for static systems, and more than 100 MBit/s for mobile systems. In parallel, the Worldwide Interoperability for Microwave Access (WIMAX) is based on the IEEE (Institute of Electrical and Electronics Engineers) 802.16 standard which was amended in 2005, and theoretically provides data speeds up to 128 MBit/s for mobile systems. Besides, the regular deployment of the IPV6 protocol (replacement of the IPV4 protocol) favors data processing by routers for internet traffic. The communication appears more and more mature to the transportation community, and it is now a question of integrating new channels and new protocols for specific networks such as Vehicular Ad Hoc Networks (VANET) [10]. VANETs are comprised of moving vehicles that act as nodes and wireless routers, and are able to connect and communicate with other vehicles. They integrate several technologies and standards such as WIMAX IEEE 802.16, WIFI IEEE 802.11p, Wireless Access in Vehicular Environments (WAVE) IEEE 1609 or Dedicated Short Range communications (DSRC, a higher level standard), and Bluetooth. DSRC standards were developed in Europe by the European Commitee for Standardisation (ECS) and the International Organization for Standardization (ISO). A spectrum of 30Mhz in the 5.9GHz band was specifically allocated for ITS applications in 2008 by the European Telecommunications Standard Institute (ETSI). In the United States 75MHz of spectrum were allocated in 1999 by the Federal Communications Commission (FCC), while in Japan the formulation of DSRC standards was completed in 2006. The ETSI published this harmonized standard to introduce radio systems for co-operative systems [11], enabling the use of ITS for road safety and traffic management. It must be mentionned that DSRC systems are not totally compatible within Europe

and not compatible between Europe, US and Japan, and therefore standardization is an essential step for interoperability. DSRC are relying on on-board units (OBU) and road side units (RSU) and support a wide range of applications starting from electronic toll management. It was integrated in 1998 as an Electronic Road Pricing system in the city of Singapore with the aim to manage traffic demand by using congestion pricing. Other applications of VANET can be probe vehicle data collection, intersection collision avoidance where warnings and data are communicated between the infrastructure and connected vehicles, the emergency warning system to warn the driver of rapid decelerations ahead, or other types of Advanced Driver Assistance Systems (ADAS). Finally, one can refer to the extensive classification of VANET and DSRC based automotive applications that was made by General Motors to help the performance analysis of designed protocols for each specific class of application [12]. VANETs bring up questions relative to the security, confidence, confidentiality, personalization and intelligence of the information.

As a first step towards connected and cooperative vehicles, ADAS have been developed and brought to the market. ADAS are the first generation of cooperative vehicles: they gather all the systems and subsystems that contribute to assisting the driver, without necessarily providing him with a fully automated system. The Dedicated Road Infrastructure for Vehicle Safety in Europe (DRIVE) program was initiated shortly after the end of the PROMETHEUS project, the most ambitious project of this program being the Generic Intelligent Driver Support (GIDS) project, which had the objective "to determine the requirements and design standards for a class of intelligent driver support systems which will conform with the information requirements and performance capabilities of the individual drivers" [13]. ADAS represent a fundamental interest for their potential contribution in relation to safety, which is the main concern of automotive industry and stakeholders, and possibly to highway capacity, to the robustness to adverse weather conditions and to the assistance of disabled people. They can go from any support to the driver to the override of his driving task, operating through warning, advice or automatic control. For instance, Adaptive Cruise Control (ACC) systems use either a radar or a laser sensor to slow or accelerate depending on the speed and distance to the leading vehicle, and have been widely implemented by car manufacturers.

Cooperative adaptive cruise control Systems (CACC) is an extension to ACC, where vehicle to vehicle communication (DSRC) is added to the ACC system allowing information to be communicated from vehicles ahead in the same lane. This new generation of ACC still requires a standardization ef-

fort across manufacturers, but its implementation has produced promising results [14]. A sophisticated automated parking application (Valet Park4U) where the driver could leave the car park itself and order it to pick him outside the parking via his smartphone was presented by Valeo at the 2012 ITS World Congress in Vienna. Other applications can be emergency brake assist, lane change assistance, lane departure warning system, blind spot detection among others. An exhaustive list of deployed ADAS systems is available in [3]. It should be mentionned that the sometimes poorly designed systems inside vehicles, the excess of information which may cause lack of attention and the excessive compliance that may increase reaction time in case of emergency situations are dangers of those partially automated systems. As a result the natural evolution of ADAS is to flow towards fully automated systems [15]. If those systems have been extensively commercialized, a legal framework is still needed for pushing forward with autonomous driving. The EU financed AutoNet 2030 project (Co-operative Systems in Support of Networked Automated Driving by 2030) which gathers five industrial partners (BroadBit, BaseLabs, Fiat, Volvo, Hitachi Europe) and four research institutions (ARMINES, EPFL, Institute of Communication and Computer Systems, Technical University of Dresden) was launched in 2013, with the goal to bring contributions on the development of efficient decentralized control algorithms and on facing noisy sensing and constrained situations [16].

In conclusion, cooperation can come either from in-vehicle equipement or from communication devices, thereby defining cooperative vehicles: a cooperative vehicle is able to both sense its immediate environment (like an autonomous vehicle) and receive information at a network level (connected vehicle). An autonomous vehicle can move into a congested traffic using cameras, lidars, radars, but does not receive any information outside the scope of its sensing capabilities. Connected vehicles, if they are still subjected to a standardization effort, can bring a broader vision much needed for traffic management purposes and as a result follow a top down approach, where the local behavior is influenced by network information. They may be less needed for safety applications such as collision avoidance or automated parking systems, however, a broader vision will help bring more diverse features as for example in the CACC case. The new generation of ADAS systems, integrating VANETs and new communication standards, are the cooperative systems. It seems that, at least from the European perspective, the cooperative systems are the path to follow towards cooperative vehicles. To our understanding, cooperative vehicles gather potentialities of both autonomous and connected systems and are absolutely needed for traf-

fic flow management. The Google self-driving car is fully autonomous, but at the same time Google Ventures made its biggest ever investment in the taxi brand UBER, with the underlying goal to provide network information services to users (connected taxis). Figure 2.1 tries to express this duality connection/automation, and some of the described systems are classified.

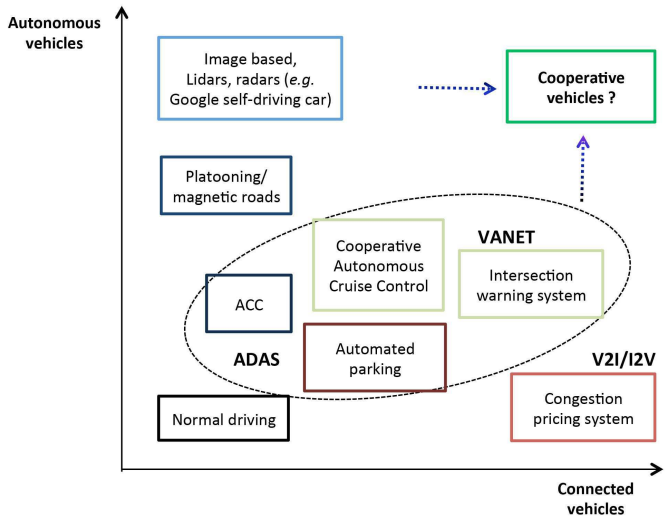

Figure 2.1: Duality in the advent of cooperative vehicles

2.3 Cooperative systems: state of the practices and testbeds for future deployments

2.3.1 State of the practices

Cooperative systems have been the target of many recent research and development projects. In Europe, the Car 2 Car Communication Consortium is a very active organization of 60 members involving 12 major vehicle manufacturers, technology suppliers and academic institutions. The objective of the consortium is to progress towards the standardisation of protocols and interfaces of wireless communication systems. The creation of standards for communication systems, the worldwide harmonization of these standards, the demonstration of safety applications, and the development of strategies and business models to favor the market penetration are among the objectives of the consortium [17]. The consortium is expected to meet its

self-imposed target, which is to introduce V2X (vehicle to vehicle and vehicle to infrastructure) communication applications into the market by 2015. Several studied scenarios include cooperation forward collision warning, precrash sensing and warning, hazard notification, V2V merging assistance and internet access in the vehicle. Before that, two essential projects for the deployment of cooperative systems had been launched in 2006 in the domain of mobile communication: the Cooperative Vehicle-Infrastructure Systems (CVIS) project and the SAFESPOT project. CVIS (budget 38 M€) was established to design a platform for supporting cooperative applications. The Communications Access for Land Mobiles (CALM) standard, which supported all the communication standards, was developed during this four years project co-funded by the European Commission. Applications concerned freight and fleet management at an urban network level and were based on a V2I infrastructure. The SAFESPOT project (budget 41 M€) was also co-funded by the European Commission and lasted for 4 years. It focused on V2V communication standards aligned with the CALM standardisation group, and resulted in the development of the safety margin assistance system, which predicts dangerous situations and communicates this information to the surrounding environment (cars and infrastructure). The implemented and developed technologies included dynamic local road maps and accurate relative positioning (sub-meter scale).

Innovation in automotive transportation may be divided into three groups, the material and manufacturing research, the fuel and electric vehicles research, and the integrated safety and management research. Cooperative systems form part of this last category. Unlike the SAFESPOT and CVIS projects, which focused on the design of integrated platforms for vehicle and infrastructure cooperation, other projects such as PREVENT, interactIVe or CO-DRIVE address the vehicle perspective. The PREVENT project (budget 55 M€) was co-funded by the European Commission and led to three general concepts: the virtual safety belt (integration of complementary safety functions), the time to collision timescale to trigger preventive and active interventions, and the perception-decision-action architecture designed to warn the driver of potential dangers. The interactIVe project massively involved car manufacturers and was launched the same year with the aim to extend the development of ADAS and enhance the perception of the driver, by warning and actively intervening in case of dangerous situations. Emergency assistance, collision avoidance and collision mitigation, Human Machine Interface (HMI) development are the major preocupations of the project that ends in November 2013. The Co-Pilot for an Intelligent road and vehicular communication system (CO-DRIVE) is a french project co-

ordinated by VALEO aiming at delivering a product to guide the driver or perform autonomous actions in the vehicle. The definition of an open architecture interoperable with infrastructure systems, the in-vehicle integration of ITS applications, and the used of standardized messages to exchange data are among the preoccupations of the project.

2.3.2 Field Operational Tests

The euroFOT project focused on the development of Field Operational Tests (FOTs) to perform large scale testing programs for evaluating cooperative systems. The user acceptance, the performance, and the impacts on the safety, efficiency and on the environment are evaluated according to the Field opErational TeSt SupporT Action (FESTA) methodology, see the FESTA handbook [18]. Today, the FOT-Net is an action funded by he European Commission and aims at regrouping international stakeholders to discuss and share the results of the FOTs, as well as promoting the used methodology worldwide. The FOTsis (European Filed Operational Test on Safe, Intelligent and Sustainable Road Operation) [19] is an European field testing program to assess the effectiveness and potential for full deployment of seven road infrastructure cooperative systems technologies: emergency management, safety incident management, intelligent congestion control, dynamic route planning, special vehicle tracking, advanced enforcement, and infrastructure safety assessment. A total of 9 test sites have been selected in Germany, Greece, Portugal and Spain, with the aim at developing FOT from the road operators perspective, *i.e.* connecting the infrastructure mangement systems into the European Communication Architecture developed along the CVIS and SAFESPOT projects. Likewise, the DRIVE C2X project [20] is a testing and methodology project (budget 18.5 M€) to build the foundation for the deployment of cooperative systems in Europe. There is a total of seven test sites, two of them allowing for the test of all functions defined in the DRIVE C2X system, and the others serving for the evaluation of specific functions matching with the project. It concerns safety related functions, traffic efficiency related functions, and selected business and deployment related functions. For instance, the French test site has been built up on open roads around the Versailles Satory test track within the French SCORE@F (Système COopératif Routier Expérimental Français) project, integrating both vehicle to vehicle and vehicle to infrastructure communication. The Swedish test site located in Gothenburg has been collaboratively developed by Volvo trucks and the Swedish Road Administration (SRA) along the CVIS and Safespot projects.

In Japan, the Smartway initiative which started in 2004 is a Field Operational Test for autonomous systems aiming at integrating and developing advanced ITS technology services on the roads such as Vehicle Information and Communication System (VICS) and Electronic Toll Collection (ETC). The provision of internet hot spots along the roads also enabled ITS applications like dynamic route guidance and assisting dafe driving. Besides, the Japanese New Energy and Industrial Technology Development Organization (NEDO) has been promoting the introduction and dissemination of new technologies since 1980, and pays particular attention to the applications of robotics vehicles. For instance, the driverless trucks project [21] evidenced the potential of the autonomous platooning technology, which consists of a combination of lasers, cameras and vehicle control equipment, in terms of fuel saving. Other research and development achievements include the CACC experimental truck system, vehicle models for lateral motion, white line detection technology using laser radar, light projection high-speed vision sensor, among others. Very recently, the IT strategy head office produces a handbook which formulates short, medium and long term vision for ITS deployments with the following guidelines: develop driving assistance technologies by 2014; develop micromobilities and dramatically reduce annual traffic fatalities by 2018; realize the safest, most efficient and more environmentally friendly road transport by 2020; and launch auto pilot systems in the mid 2025.

In the US, the Research and Innovative Technology Administration (RITA) of the USDOT is promoting the development of connected vehicle technology, with particular interest in the design of a technological platform that ensures stable, reliable and interoperable systems and applications. Generally speaking, it seems that the harmonization of the standards and technologies for cooperative vehicles has become a priority. The Virginia connected testbed initiative in Northern Virginia is led by the Virginia Tech Transportation Institute (VTTI). The 2013 launched initiative [22] consists of two testbeds of wireless connected infrastructure and equipped vehicles and aims at investigating a full range of applications from infrastructure repair and maintenance to congestion management. The Connected Vehicle Safety Pilot Model Program conducted by the USDOT and the University of Michigan Transportation Research Institute (UMTRI) is the world's biggest testbed of connected vehicles technology: 3000 vehicles are currently being tested to determine the effectiveness of vehicle to vehicle and vehicle to infrastructure communications to avoid road crashes. Empirical data is being collected for several connected vehicle safety technologies and applications, and will support the National Highway Traffic Safety Administration

(NHTSA) decision on the use of vehicle communications for safety [23]. Some of the goals of the program are to test a real world and multi-modal environment, assess the driver acceptance of those systems, and to develop the interoperability of DSRC technology.

Chapter 3

An overview of traffic models

Traffic models have been proposed, studied and discussed for more than 50 years to estimate, analyze and predict traffic conditions. In this chapter, a brief overview of different approaches in traffic modeling is presented and some specific traffic models used to evaluate ITS technologies are discussed.

Contents

3.1 Traffic modelling: a brief overview

Traffic modeling is essential to understand and investigate the impact of cooperative vehicles on traffic characteristics. As previously discussed, it is imperative for the behavior of a controlled cooperative vehicle to be similar to observable behaviors of normal vehicles to prevent creating abnormal traffic situations. Therefore, mechanisms of normal traffic physics have to be well understood from a mathematical standpoint.

Traffic modeling has progressively become an attractive domain for many researchers from multiple fields since the 30s and the early work of Green-

shields, who proposed fundamental and empirical relations between flow, density and velocity in vehicular traffic [24]. The first theory of traffic flow was then introduced by Lighthill and Whitham [25, 26] and Richards [27]. Decades of collaborative work and a diversity of traffic models followed. For a description of the multitude of modelling oriented works, one can refer to the exhaustive review of Helbing [28], to the classification proposed by Hoogendorn and Bovy [29] and to the flowchart available in a recent dissertation [30]. The field of traffic modelling is usually divided into three categories following the different types of granularities possibly adopted in the models: macroscopic, at the scale of a network and sections; mesoscopic, at the scale of packs and groups of vehicles; and microscopic, at the scale of the vehicle. Macroscopic models mainly refer to first and second order models derived from the Lighthill-Whitham-Richards (LWR) theory, the mesoscopic mainly to gas kinetic models, and the microscopic mainly to car-following and cellular automata models. Multiple works have also been dedicated to the connection between those modeling scales, in which mesoscopics models can be derived from macroscopic ones *via* methods coming from statistical mechanics, and macroscopic models from mesoscopics *via* methods coming from fluid mechanics, see for example the paper of Ni [31] for more details. In addition to this usual classification, Kerner's three-phase qualitative theory has also proven to be a satisfactory framework to understand the complexity of congested patterns [32].

3.1.1 Macroscopic modelling

First order macroscopic models

The nature of traffic is made up of interacting vehicles that can be assimilated to a discrete dynamical system. However, the first attempts to model traffic flow are directly inherited from the fluid mechanics principles. The LWR theory starts with a basic conservation law of vehicles:

$$\partial_t \rho + \partial_x q = 0, \tag{3.1}$$

where ρ is the traffic density and q is the traffic flow. The equation states that the number of vehicles entering in any road section of the time space region is the same number as the number exiting it. A relation between the average speed V, flow and density is naturally written as

$$q = \rho V. \tag{3.2}$$

The closure to the dynamical system is then introduced *via* an equilibrium flow-density function (or equivalently a speed-density relation) known as the

Fundamental Diagram (FD) first introduced by Greenshields [24] in traffic engineering or more generally the flux function for hyperbolic systems of conservation laws [33]:

$$q = q_{eq}(\rho). \tag{3.3}$$

Different forms of the fundamental diagram have been proposed in the literature. The first model came out with Greenshields who gave the relation

$$q_{eq}(\rho) = 4q_{\max}\rho\left(1 - \frac{\rho}{\rho_{\max}}\right)\mathbb{1}_{0\leq\rho\leq\rho_{\max}}, \tag{3.4}$$

where $q_{\max}$ is the maximum flow and $\rho_{\max}$ is the maximum observable density. The Greenshields FD is represented in figure 3.1, where ρ_c is the critical density, and r_1 and r_2 the solutions to equation $q_{eq}(\rho) = q_s$, and q_s an arbitrary flow.

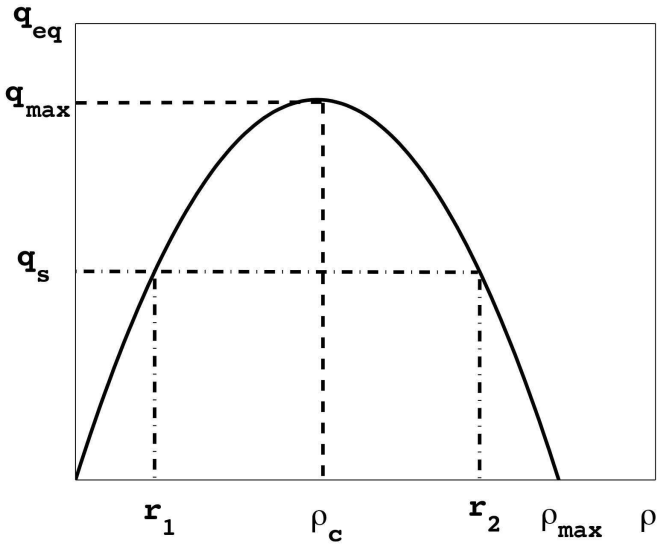

Figure 3.1: Greenshield fundamental diagram

The most popular form of the FD was introduced by Pipes [34] as a piecewise linear (triangular) form. The triangular FD has the advantage of simplifying mathematical and numerical analyses, as developed in the theoretical works of Newell and Daganzo [35, 36, 37]. It is written:

$$q_{eq}(\rho) = \begin{cases} \rho V_{\max} \text{ if } \rho \in [0, \rho_c] \\ \rho_c V_{\max}\dfrac{\rho_{\max} - \rho}{\rho_{\max} - \rho_c} \ \rho \in [\rho_c, \rho_{max}], \end{cases} \tag{3.5}$$

where $V_{\max}$ is the free flow speed. Numerous other forms of the FD may be mentionned, such as the Greenberg [38], Van-Aerde [39], Underwood [40] or Wang and Papageorgiou [41] models. More generally, the reader can refer to the report made by the Traffic Flow Theory and Characteristics Committee of the Transportation Research Board for the celebration of the 75 years of the Greenshields FD [42], which gathered a set of relevant papers regarding historical and recent developments.

Assuming the derivability of q with respect to ρ the equation of the LWR theory has now become a more simple partial differential equation (PDE):

$$\partial_t \rho + q'_{eq}(\rho)\partial_x \rho = 0, \tag{3.6}$$

which immediately allows using the methods of characteristics to solve the PDE [43]. The density remains constant along the characteristics defined by $\partial x/\partial_t = A$, with A being a constant. The slope of the characteristics is therefore equal to $q'_{eq}(\rho)$. The PDE characterized by equation (3.6) with piecewise constant and self-similar (for $x \in \mathbb{R}^n$, $\forall \alpha \in \mathbb{R}$, $f(\alpha x) = f(x)$, see Blandin [44]) initial condition presenting a single discontinuity, is known as the Riemann problem [45]. This initial condition corresponds to the discontinuous profile of density ρ (successively equal to ρ_l and ρ_r) on a stretch of road:

$$\rho(t=0,x) = \begin{cases} \rho_l \text{ if } x < 0 \\ \rho_r \text{ if } x > 0. \end{cases} \tag{3.7}$$

For a FD with constant concavity sign, the unique solution ρ_s of the Riemann problem is defined for $(x,t) \in \mathbb{R}^{\star,+}$ so that:

- if $q'_{eq}(\rho_l) > q'_{eq}(\rho_r)$ the solution exhibits a shock wave

$$\rho_s(x,t) = \begin{cases} \rho_l \text{ if } x < \sigma t \\ \rho_r \text{ if } x > \sigma t, \end{cases} \tag{3.8}$$

  where the shock wave is located at $x = \sigma t$, with σ identified by the Rankine-Hugoniot relation [46]

$$\sigma = \frac{q_{eq}(\rho_l) - q_{eq}(\rho_r)}{\rho_l - \rho_r}; \tag{3.9}$$

- if $q'_{eq}(\rho_l) < q'_{eq}(\rho_r)$ the solution has the form of a rarefaction wave

$$\rho_s(x,t) = \begin{cases} \rho_l \text{ if } x \leq q'_{eq}(\rho_l)t \\ (q'_{eq})^{-1}(\frac{x}{t}) \text{ if } x \in [q'_{eq}(\rho_l)t, q'_{eq}(\rho_r)t] \\ \rho_r \text{ if } x \geq q'_{eq}(\rho_r)t. \end{cases} \tag{3.10}$$

Now that the solution of the Riemann problem has been made explicit for the LWR model, some attention must be given to equation 3.3, where it is assumed that the dynamical system always evolves at an equilibrium state.

Second order macroscopic models

Differently from first order models, second order traffic models aim at describing traffic transition phases and reproducing local instabilities phenomena (such as spontaneous traffic jams), and for that they take into account non-equilibrium states. The general structure of the second order traffic models can be written as:

$$\frac{\partial}{\partial t}U + F(U)\frac{\partial}{\partial x}U = S(U), \tag{3.11}$$

with the quantities

$$U = \begin{pmatrix} \rho \\ V \end{pmatrix}, \tag{3.12}$$

$$F(U) = \begin{pmatrix} V & \rho \\ 0 & V + c(\rho) \end{pmatrix}, \tag{3.13}$$

$$S(U) = \begin{pmatrix} 0 \\ \left(q_{eq}(\rho) - q\right) / \left(\tau\rho\right) \end{pmatrix}, \tag{3.14}$$

where V is the vehicle flow speed, τ is a relaxation time towards the equilibrium and $c(\rho)$ a coefficient which can be seen as the anticipation speed.

Equations (3.11) can also be written for the couple of variables (ρ, q)

$$\frac{\partial \rho}{\partial t} + \frac{\partial q}{\partial x} = 0, \tag{3.15}$$

$$\frac{\partial (q/\rho)}{\partial t} + \left(\frac{q}{\rho} + c(\rho)\right)\frac{\partial (q/\rho)}{\partial x} = \frac{q_{eq}(\rho) - q}{\tau\rho}. \tag{3.16}$$

Note that in the case of a non-homogeneous road, the physical and geometrical parameters may depend on x, then $c(\rho)$, $q_{eq}(\rho)$ and τ are explicitly location-dependent. Among successful models, one can mention the Aw-Rascle [47], Zhang [48], Jiang [49] and De Vuyst-Billot [50] models, which have been developed following Daganzo's critical study [51] of Payne-like models [52]. The quantity $c(\rho)$ is specific for each model, and is defined

such as:

$$\begin{cases} \text{Model 1 (Zhang): } c(\rho) = \rho \dfrac{dV_{eq}}{d\rho} = \rho \dfrac{d\left(q_{eq}/\rho\right)}{d\rho}, \\ \text{Model 2 (Jiang): } c(\rho) = -c_0,\ c_0 > 0, \\ \text{Model 3 (Aw-Rascle): } c(\rho) = -\rho \dfrac{dp}{d\rho} \text{ with } p = \rho^{\gamma},\ \gamma > 0, \\ \text{Model 4 (De Vuyst-Billot): } c(\rho) = -\dfrac{k_0 V}{\rho} = -\dfrac{k_0 q}{\rho^2},\quad k_0 > 0. \end{cases} \tag{3.17}$$

The characteristics are directly related to the eigenvalues of matrice F, the interested reader can refer to [53] for more details. The two characterictics speeds are then written $\lambda_1 = V + c(\rho)$ and $\lambda_2 = V$. The behavior of the model can be studied, and it can be proven that the solutions are bounded in a satisfactory way with respect to traffic physics [47, 54]. The reader can refer to the thesis of Billot [55] for detailed explanations.

3.1.2 Mesoscopic modelling

Another level of representation is the mesoscopic view, an intermediary between the macroscopic -fluid propagation- and microscopic -vehicle to vehicle interaction- scales, where vehicles are observed as groups of particles. Mesoscopic models represent traffic flow as the probability of presence of vehicles at a time t, a position x and a speed V.

First examples of mesoscopic models are the DYNAMIT [56] and DYNASMART [57] models, which track individual vehicle movements from macroscopic principles. Besides, the most popular family of mesoscopic models comes from the kinetic approach which consists in describing the density probability functions of the main traffic variables and their evolution in time. Kinetic models were brought to the field of traffic theory by Priogine and Andrews [58] in the 60s. Those models have the specificity of potentially being integrated from microscopic equations, or being used for the integration or derivation of macroscopic and microscopic models. It is indeed possible to derive macroscopic models from gas kinetic formulations [59, 60, 61] via the method of moments and appropriate closure choices. Within this Boltzmann type family of models introduced by Priogine and Andrews, the evolution in time of the probability $f(V, x, t)$ to have vehicles at position and time (x, t) of speed V is

$$\partial_t f + V \partial_x f = (\partial_t f)_{rel} + (\partial_t f)_{int}, \tag{3.18}$$

where $(\partial_t f)_{rel}$ is a relaxation towards an ideal (or equilibrium) distribution function f^{eq}, which would correspond to a distribution for which there is no interaction between the drivers (low density). The interaction term $(\partial_t f)_{int}$ is based on observed behaviors of drivers such as attraction, repulsion and overtaking. Multiple works have discussed possible improvements of the first proposed model, which does not match real data behaviors, see [28] for a complete literature review.

More recently, Klar and Wegener developed an improved gas kinetic model derived from microscopic equations [62]. By introducing an Enskog-type (inherited from dense gases models) correction to Priogine-like models they obtain

$$\partial_t f + V \partial_x f = \sum_{i=1}^{N} C_i f(V, x, t), \tag{3.19}$$

where N is a given number of traffic situations (*e.g.* the vehicle changes its speed situation if the headway becomes larger than a given threshold) and C_i is an integrated term from the microscopic equations. Finally, a relevant work for this family of models is the one included by Hoogendoorn regarding multi-lane and multi-class gas kinetic models, their derivation to macroscopic equations, and their comparison to Priogine-like models [63].

The relation between macroscopic, mesoscopic and microscopic models has already been emphasized. In this dissertation the main focus is put on the microscopic framework, as communication happens at a microscopic scale. However it must be kept in mind that the evaluation of cooperative systems may be extensible from this work to different modelling scales depending on the application.

3.1.3 Microscopic modelling

The prevalent microscopic approach consists in using car-following models, in which vehicles update their cinematics according to their perception of the leading vehicle behavior. Two main classes of car-following models are available in the literature, the time-continuous and the time discrete car-following models. Time continuous models relate to empirical models that model the acceleration trajectories of vehicles as a continuous function of time whereas time discrete models relate to physical models which try to capture reaction times and stimulus-response mechanisms. More generally, car-following models aim to propose realistic acceleration and speed profiles. They can be collision-free or collision-prone in the sense that collisions between two vehicles (crashes) are prohibited or possible. Regarding the clas-

sification and the assessment of the car-following models, the completeness and orthogonality notions, which have been introduced in the recent book of Treiber and Kesting [64], can be used. The completeness notion regards the capacity of the model to describe all types of car-following situations (approach, traffic lights, free-flow situations), whereas the orthogonality describes the variation of the parameters in relation to the driving cycle; an orthogonal model will have corresponding parameters ranges and driving cycles, and this has an interest in calibration (and eventually in control of vehicles) as it will be presented in chapter 5. In addition to car-following models, cellular automata models are another branch of microscopic models that will be described in the last part of the section.

Time continuous car-following models

The general form of time-continuous car-following models to describe the motion of a vehicle n is a set of coupled ordinary differential equations (ODE)

$$\dot{x}_n = \frac{dx_n}{dt} \tag{3.20}$$

$$\ddot{x}_n = f(\dot{x}_n, \Delta x_n, \Delta \dot{x}_n), \tag{3.21}$$

where f is a general non-linear function, $\dot{x}_n$ is the position of vehicle n, $\dot{x}_n$ its speed, $\ddot{x}_n$ its acceleration, Δx_n the space headway and $\Delta \dot{x}_n$ the relative velocity between vehicles n and $n+1$, where $n+1$ represents the leading vehicle. In the case of no leader, Δx_n is taken as $+\infty$. Starting from this general expression, some car-following models have demonstrated their ability to represent accurately traffic features, namely the Intelligent Driver Model (IDM) [65] and the Optimal Velocity Model (OVM) first developed by Bando *et al.* [66, 67, 68, 69]. Some extensions of this latter model have been proposed. The Optimal Velocity with Relative Velocity model [70, 71], also called the Full Difference Velocity Model, is one example. However, as stated in [64], it needs modification to accurately describe free flow situations. The modified OVRV, which can be called the improved OVM (IOVM) model (see [64]), will be considered here under its most linear form, which is derived from the triangular fundamental diagram. In the OVRV model, the acceleration is updated as follows:

$$\ddot{x}_n = f(\dot{x}_n, \Delta x_n, \Delta \dot{x}_n) = -\frac{1}{\tau}\dot{x}_n + \frac{1}{\tau}V_1(\Delta x_n) + \gamma \Delta \dot{x}_n, \tag{3.22}$$

where τ is a reaction time, γ weights the sensitivity of the perception of

the relative velocity for the driver. V_1 is a non-linear function chosen to be written as in [67]:

$$V_1(\Delta x_n) = \frac{V_{\max}}{2}\Big(\tanh(s \cdot h_c) + \tanh\left(s \cdot (\Delta x_n - h_c)\right)\Big), \tag{3.23}$$

where $V_{\max}$ is a free flow speed, s is a smoothing parameter, h_c is a legal or safe headway measuring a threshold around which the driving behavior is highly contrained by the leader.

The improved OVM model is written as:

$$f(\dot{x}_n, \Delta x_n, \Delta\dot{x}_n) = -\frac{1}{\tau}\dot{x}_n + \frac{1}{\tau}V_2(\Delta x_n) + \frac{\gamma}{\max(1, \frac{\Delta x_n}{V_{\max}T_0})}\Delta\dot{x}_n, \tag{3.24}$$

where V_2 is defined such as:

$$V_2(\Delta x_n) = \min\left(V_{\max}, \frac{\Delta x_n - s_0}{T_0}\right), \tag{3.25}$$

where s_0 is a minimum distance gap and T_0 a time gap. It is noticeable that the coefficient γ of the OVRV model is now weighted by the inverse of the headway. This allows the vehicle not to be impacted if there is a leader braking far away in the road section (*e.g.* case of traffic lights). Those two models are close in their formulation to the Newell's car following model [72] that is described in the next section.

Finally, the IDM model is more intended to describe acceleration patterns of vehicles, and is given by:

$$f(\dot{x}_n, \Delta x_n, \Delta\dot{x}_n) = a\left[1 - (\frac{\dot{x}_n}{V_{\max}})^\delta - \left(\frac{s^\star(\dot{x}_n, \Delta\dot{x}_n)}{\Delta x_n - l}\right)^2\right], \tag{3.26}$$

where

$$s^\star(\dot{x}_n, \Delta\dot{x}_n) = s_1 + \max\left(0, \dot{x}_n T_1 - \frac{\dot{x}_n\Delta\dot{x}_n}{2\sqrt{ab}}\right), \tag{3.27}$$

where l is the length of the vehicle, a is the maximum acceleration, b is the desired deceleration, $V_{\max}$ is the desired speed, s_1 is the minimum net stopped distance from the leader, T_1 is the desired safety time headway, and γ is an acceleration exponent. Note that the IDM model is a collision-free model, contrary to the OVRV and IOVM models.

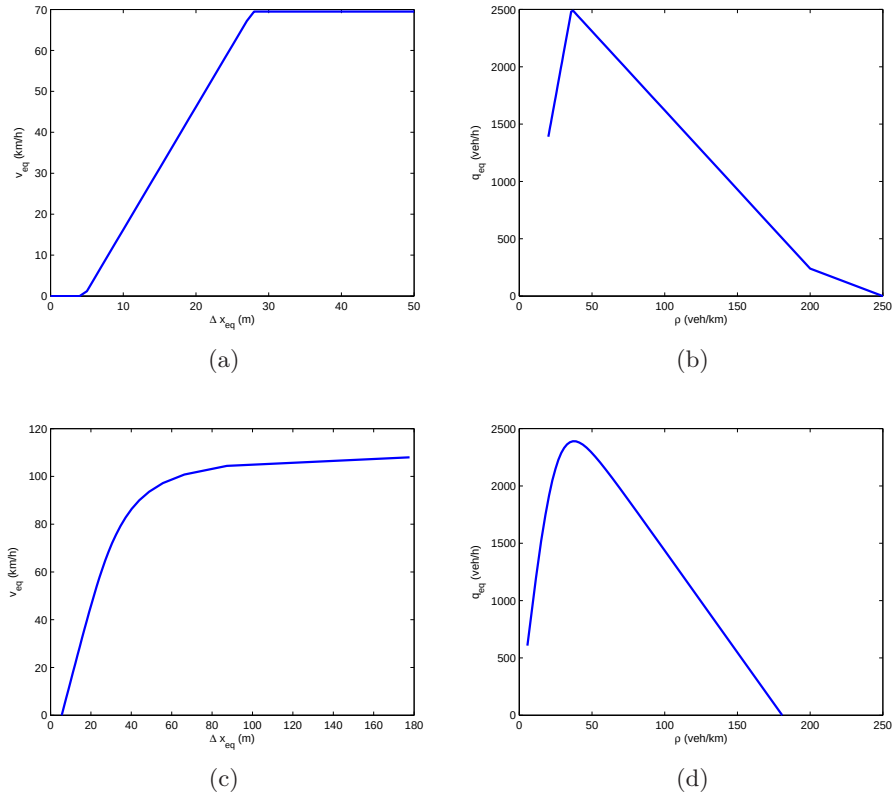

Figure 3.2: Steady-state speed-headway relations and derivated FDs for the: (a), (b) IOVM model; (c), (d) IDM model.

To conclude, the relation between microscopic and macroscopic traffic for the presented car-following laws can be studied in steady-state conditions, when the speed of the leader is equal to the speed of the follower. Figure 3.2 displays the steady state speed-headway and flow-density relations, with the calibrated parameters values taken as the mean value of the calibrated set of parameters that will be presented in section 5.3 and summarized in table 6.1. Note that the calibrated parameters are only valid for one functional point in the flow-density region, *i.e.* the flow and density values for which the calibration was performed. These steady-state relations can play an important role when calibrating microscopic data from macroscopic data such as loop detectors [73]. It will also be evidenced that the steady-state relations play an important role with respect to linear stability analyses

(section 4.3).

Time discrete models

Differently to continuous car-following models, time discrete models refer to delay differential equations. Historically, a first class of car-following models was developed by the General Motors Laboratory, in which Greenshields, Pipes [34] and Greenberg [74] were notably working. The Pipes model, or GM-1 model, is the first stimulus response model and is written as

$$\ddot{x}_n(t+\tau) = \alpha \cdot [\dot{x}_{n+1}(t) - \dot{x}_n(t)] \tag{3.28}$$

where τ is the reaction time of the driver, and α is the driver sensitivity factor to the speed differential, which is considered to be the stimulus. Experiments conducted on the GM test track les to an estimation of 1.5 s for the average driver reaction time, and 0.37 s^{-1} for the sensitivity factor [75]. The final version of the GM models, known as GM-5, is written as:

$$\ddot{x}_n(t+\tau) = \frac{\alpha(l,m)(\dot{x}_n(t+\tau))^m}{\Delta x_n(t)^l} \cdot [\dot{x}_{n+1}(t) - \dot{x}_n(t)]. \tag{3.29}$$

Note that this last model, with $l = 1$ and $m = 0$, is the microscopic form of the macroscopic Greenberg model, as stated in his paper [74]. The acceleration formulation of the Van Aerde car-following model [76, 77] also offers a sophisticated form of the sensitity factor:

$$\ddot{x}_n(t+\tau) = \frac{V_{\max} - \dot{x}_n(t+\tau)}{\alpha_3(V_{\max} - 2\dot{x}_n(t+\tau)) - \alpha_1 + \tilde{\Delta x}_n(t)} \cdot [\dot{x}_{n+1}(t) - \dot{x}_n(t)], \tag{3.30}$$

where parameters α_1 and α_3 are those defined in the original formulation of the Van Aerde model $\Delta x_n(t) = \alpha_1 + \alpha_3 \dot{x}_n(t+\tau) + \alpha_2/(V_{\max} - \dot{x}_n(t+\tau))$, and $\tilde{\Delta x}$ is the predicted headway computed as the headway at the previous time step plus the travel distance obtained by integrating the acceleration value. The predicted headway term allows large simulation time steps (0.5 s) to be considered in practice [78, 77]. Finally, the RPA car-following model [77] generalizes this class of models, with specifications on acceleration and collision avoidance constraints.

Other forms of time delayed car-following model are the ones proposed by Newell [72, 79] and defined as

$$\dot{x}_n(t+\tau) = \dot{x}_n \left(1 - \exp^{-\frac{\lambda}{\dot{x}_n}(\Delta x_n - l)}\right), \tag{3.31}$$

for the non linear form, and defined as

$$x_n(t+\tau) = x_{n+1}(t) - d \tag{3.32}$$

for the linear form, where d is a safe distance the driver of vehicle n aims to preserve. Actually, the IOVM model of equation 3.24 with $\gamma = 0$ and $T_0 = \tau$ is the Newell's car following model with an improved Euler numerical scheme [80] for updating speeds and a simple Euler scheme for updating positions. There, it corresponds to the triangular FD and the shock wave speed can be easily obtained as $\sigma = -1/\tau$. This simplified theory is well suited to describe traffic flow behavior but fails to integrate heterogeneities such as lane changing behaviors [81].

Finally, the Gipps car-following model belongs to the same class of time discrete car-following models. A simplified version of this model is written as

$$\ddot{x}_n = \min\left(\dot{x}_n + a\Delta t, V_{\max}, V_{\text{safe}}(\Delta x_n, \dot{x}_{n+1})\right), \tag{3.33}$$

where a is the acceleration of the vehicle if it has not reached the desired speed $V_{\max}$ or the safe speed V_{safe}. The safe speed is the speed that is computed considering the breaking distance of the leader and the stopping distance of the vehicle which includes a reaction time Δt, and is calculated according to the following equation

$$\Delta x_n = s_0 + V_{\text{safe}}\Delta t + \frac{V_{\text{safe}}^2}{2b} - \frac{\dot{x}_{n+1}}{2b}, \tag{3.34}$$

where b is a constant deceleration at which the braking maneuvers are executed. The Gipps model has the advantage of being an easy to implement collision-free model, however, its main drawback lies in the computed unrealistic acceleration profiles [64].

Rule-based modeling

Rule-based modeling is an approach that uses a set of rules to create a behavior. When the set of rules appears much simpler than the described behavior, rule based modeling can be particularly effective. In traffic, cellular automata models may be mentioned first, as they provide simple evolution rules to describe microscopic phenomena. A cellular automaton is a set of n cells that can take a finite number of traffic states. The evolution in time is discrete and at each time step rules are applied to determine the new system state. The well-known Nagel-Schreckenberg [82] splits the rules into 4 possibilities:

- Acceleration: if $\dot{x}_n < V_{\max}$ and there is enough space the speed (the unit of which is the number of cells/time step) is increased by +1, then $\dot{x}_n \leftarrow \dot{x}_n + 1$.
- Deceleration: if another vehicle is at a distance $\Delta x_n < \dot{x}_n$, then $\dot{x}_n \leftarrow \Delta x_n - 1$.
- Randomization: the speed is decreased by 1 given a random probability p.
- Motion: vehicles move forward.

Other types of rule-based models include neuro fuzzy rule-based models [83], which combine neural networks and fuzzy logic, or psycho-physical vehicle models, which try to capture and model the human components of behavior [84].

3.2 Traffic models for cooperative vehicles

The diversity of traffic models facilitates dealing with different modelling scales, and different potential applications in the fields of estimation, prediction and control. The progressive advent of cooperative vehicles raises concerns as to the capacity of traffic modeling tools to investigate the effect of those not-yet deployed systems. The idea of this dissertation is the following: while tools from the seventy years of research in traffic theory are fundamental and must not be disregarded, new applications and inspirations such as the self-organization paradigm are of interest. Cooperative vehicles should behave "like"the non-cooperative vehicles to not perturb the organization of traffic flow, but they should behave "differently"to increase traffic flow homogeneity. It is important to understand and to reproduce traffic phenomena as well as the variability of drivers' behaviors in simulation; however, self-organization is about the emergence of a certain order, and this order (or organization) should be directly inspired by models describing the living.

In this work the choice was to focus on the microscopic level, as the cooperation in communication deals with microscopic interactions, and as data brings more and more insights on microscopic behaviors. Attempts to address this issue from the macroscopic level has been proposed in recent works: in [60], Ngoduy *et al.* derived a multi-class gas kinetic model from the gas kinetic theory and applied the method of moments to derive the

macroscopic equations of cooperative traffic flow. Assuming a linear relation between the desired velocity and the information value, it is shown through numerical simulations that equipped vehicles can have a traffic flow stabilizing effect as well as a jam suppression effect. In [85], the same method of moments is applied to derive a macroscopic model to support the CACC framework, whose benefits over the ACC framework are highlighted in terms of linear and non-linear stability. Very recent works regard a platoon-based generalized force model [86] and a multi-anticipative macroscopic model [87], also derived from the gas kinetic theory.

The rest of the section details some existing microscopic models that have increased levels of cooperation, and whose ideas contribute to the outcomes of this dissertation. Three examples are described: the microscopic ACC model, which has been implemented for autonomous cruise control systems; the multi-anticipation framework, used in microscopic traffic, which can be applied to the CACC framework; and the flocking model of birds motion, which describes homogeneous group behavior. Understanding the accomplishments and limitations of these three models enables their ideas to be integrated and organized for utilization in the development of a cooperative modelling framework.

3.2.1 The ACC model

The first level of cooperation concerns the Autonomous Cruise Control system: the ACC is an embedded automated system that controls the longitudinal behavior of a vehicle based on the sensed headway and speed of its leader. One issue regarding its road implementation lies in the discontinuities coming from lane changes, as the vehicle only reacts to a leader which may suddenly change over time. The ACC model was developed by Kesting *et al.* [88] in response to the difficulties of the IDM to simulate discontinuities in traffic. Indeed as a collision-free model the IDM model makes the vehicle overreact, and a relaxation reaction would be more appropriate than the sudden reaction induced by the IDM model. This realistic reaction is modeled via the Constant-Acceleration Heuristic model (CAH). Normally, the acceleration of the vehicle n is defined in the CAH model as:

$$a_{\mathrm{CAH},n} = \begin{cases} \dfrac{\dot{x}_n^2 a_{n+1}}{\dot{x}_{n+1}^2 - 2\dot{x}_n a_{n+1}} \text{ if } \dot{x}_{n+1}(\dot{x}_n - \dot{x}_{n+1}) \leq -2\dot{x}_n a_{n+1}, \\ a_{n+1} - \dfrac{(\dot{x}_n - \dot{x}_{n+1})^2 \mathcal{H}(\dot{x}_n - \dot{x}_{n+1})}{2\Delta_{x_n}} \text{ otherwise,} \end{cases} \tag{3.35}$$

where $\mathcal{H}$ is the Heavyside function and $a_{n+1} = \min(\ddot{x}_n, a_{\max})$ is the effective acceleration, $a_{\max}$ being the maximum acceleration parameter. A series of physical considerations on the critical deceleration values, see [88, 64], lead to the following form for the ACC acceleration model:

$$a_{\mathrm{ACC},n} = \begin{cases} a_{\mathrm{IDM},n} \text{ if } a_{\mathrm{IDM},n} \geq a_{\mathrm{CAH},n}, \\ (1-c)a_{\mathrm{IDM},n} + c\left[a_{\mathrm{CAH},n} + b\tanh\left(\dfrac{a_{\mathrm{IDM},n} - a_{\mathrm{CAH},n}}{b}\right)\right] \text{ oth.}, \end{cases} \tag{3.36}$$

b being the comfortable deceleration of the IDM model, and c a "coolness factor". This model brings a satisfactory framework to control the ACC systems and has been used on public highways [64]. Although the main core of the dissertation will limit the discussion to the IDM model, further studies could be performed with the ACC model when investigating discontinuities induced by lane changing maneuvres.

3.2.2 Multi-anticipation framework

The second level of cooperation is the multi-anticipation framework, in which drivers or vehicles deal with information from multiple downstream and/or upstream vehicles. More specifically, multi-anticipation can refer to driving behavior that include driver responses to multiple vehicles ahead, as it has been observed in empirical analyses [89], but also to a cooperative traffic flow where the microscopic state of vehicles is shared through communication devices, *e.g.* the CACC framework. It becomes apparent that multi-anticipation increases the stability domain of traffic flow, as it will be confirmed in section 4.3, helps stabilize the evolution of the speed of the propagation of disturbances, and improves platoon stability [90, 70].

The most common form of dealing with multi-anticipation is to consider that vehicle n updates its acceleration by taking into account the information, *i.e.* headways and relative velocities, from multiple leaders (n to $n + m_f$), which, for acceleration time continuous models, gives

$$\ddot{x}_n = f(\dot{x}_n, \Delta x_n, \Delta x_{n+1} ..., \Delta x_{n+m_f}, \Delta v_n, \Delta v_{n+1} ..., \Delta v_{n+m_f}), \tag{3.37}$$

where $n + m_f$ is the index of the last forward vehicle for which the headway and relative velocity with its leader are considered in the car-following law. The idea is then to integrate all the information with weighting coefficients:

$$\ddot{x}_n = f(\dot{x}_n, \sum_{j=0}^{m_f} a_j \Delta x_{n+j}, \sum_{j=0}^{m_f} b_j \Delta \dot{x}_{n+j}), \tag{3.38}$$

where $(a_j)_{0\leq j\leq m_f}$ and $(b_j)_{0\leq j\leq m_f}$ are coefficients of cooperation supposed to define the importance of the interaction between a vehicle n and its preceding vehicles (n+1 to n+m+1) within a given spatial neighborhood. These coefficients are critical as they weight the importance of each vehicle in the cooperative law. Several weighting windows can be chosen, and the optimality of the window can be discussed, see section 4.5. This form of multi-anticipation appears well suited to the CACC framework, as the coefficients of cooperation can be controlled based on the traffic situation.

A more human form of multi-anticipation is introduced in [91] as the Human Driver Model (HDM). This applies to cases where a driver detects further vehicles ahead of him and react to all of them with the same behavioral function, based on his perception of their speeds and distances. The acceleration is written as a sum of a free flow term and an anticipated interaction term:

$$\ddot{x}_n = a_n^{\text{free}} + \sum_{j=1}^{m_f} a_{n,n+j}^{\text{int}}, \tag{3.39}$$

where

$$a_{n,n+j} = f(\dot{x}_n, (x_{n+j} - x_n) - j \cdot l, (\dot{x}_{n+j} - \dot{x}_n)). \tag{3.40}$$

Here the multi-anticipation law follows a parameter-free approach. Simulations allow concluding that the reaction times and estimation errors of the drivers are compensated by temporal and spatial anticipation of the drivers. The proposed multi-anticipation law corresponds to a more human form of multi-anticipation, very close to the supposed realistic mechanisms of driving.

3.2.3 Flocking framework

A third level of cooperation happens when all particles or vehicles of a group interact to create a coordinated or homogeneous movement. Scientists have been discussing for decades the movements of birds, fish, insects, and land animals respectively calling their emerging organized group motion flocking, schooling, swarming, and herding [92, 93]. In 1986, the BOIDS computer model was introduced by Reynolds [94], in which a basic flocking model was designed following three rules: separation to avoid local flockmates, alignment to head towards the average direction of flockmates, and cohesion to move towards the average position of flockmates. More recently, the flocking framework discussed by Reza Olfati-Saber [95] brings a deeper insight on a perfect behavior: a model of birds movement is described for navigation in

dispersed or cohesive groups, and for obstacle avoidance. He defines free-flocking as a motion where each particle or agent i updates its acceleration according to

$$\ddot{x}_i = f_i^g + f_i^d + f_i^\gamma, \tag{3.41}$$

where $f_i^g = -\nabla_i V(x)$ is a gradient based term of the collective potential function V of the flock defined as the sum of the flock pairwise potentials, f_i^d is a velocity alignment term that acts as a damping force, and f_i^γ is a group objective feedback.

In his paper, it is shown through Lyapunov stability analysis that the convergence of a cohesive flock towards an equilibrium state with limited collisions is possible for a symmetric communication graph given that the initial structural energy of the dynamical system is lower than a threshold value. The dynamics is split up into translational and structural dynamics, with the main objective to determine the stability of equilibrium states of the structural dynamics. It is demonstrated using Lasalle's invariance principle [96] that the linear control term added to the cooperative law is fundamental to obtain a cohesive group motion. If the positions of particles or agents i are written x_i in $\mathbb{R}^2$, $i \in \mathbb{R}^+$, the acceleration expression which ensures the cohesion of the flock and the convergence towards an equilibrium state is written

$$\ddot{x}_i = \sum_{j \in N_i} \Phi(||x_j - x_i||_\sigma \mathbf{n}_{ij}) + \sum_{j \in N_i} a_{ij}(x)(\dot{x}_j - \dot{x}_j) + u_i^\gamma(x_i, \dot{x}_i), \tag{3.42}$$

where $\mathbf{n}_{ij}$ is a vector connecting the particle x_i and x_j, N_i is the set of neighbors in the flock, Φ is an attractive repulsive action function which cancels itself at the relative distance equilibrium (the pairwise potential function is its integrand), $a_{ij}(x)$ is the matrix of the adjacency values which are computed based on proximity considerations, and u_i^γ a linear control term based on the behavior of a dynamic γ agent (or controller), defined such as $u_i^\gamma = -c_1(x_i - x_\gamma) - c_2(\dot{x}_i - \dot{x}_\gamma)$. The equilibrium state is defined by the minimum of the aggregate potential function, which is the sum of the collective potential function and the moment of inertia weighted by coefficient c_1.

This third level of cooperation draws a controlled framework to obtain the formation of perfect cohesive structures of particles, which can be seen as the ultimate goal in any traffic organization. The future developments will include notions from the three presented levels of cooperation, starting from the multi-anticipative framework in chapter 4.

Chapter 4

Stability analyses of cooperative time continuous car-following models

The objective of this chapter is to build a mathematical framework to assess the conditions for apperance of shock waves under cooperative and non-cooperative traffic. Phantom traffic jams designate the spontaneous congestion appearances on regular road stretches, and are often the cause of safety infringements and hazardous situations. They are classified as non-recurrent events, in contrast with recurrent events that refer to insufficient capacity and an overly high demand [5]. Cooperative car-following models relate to car-following models taking into account information from multiple vehicles in the form of forward and backward (*i.e.* bilateral) multi-anticipation. This form of cooperation is made possible via communication systems and can, for instance, be supported by the CACC framework [97].

Time continous car-following models are empirical models that describe vehicle motion as a set of ODE. They were chosen as testbed for the analyses of this dissertation, as they have been proved to accurately reproduce traffic flow mechanisms and features, see section 3.1.3. Besides, their continuous formulation facilitates the integration of the almost continuous communication exchanges, which can happen at a much lower time step than the driver reaction time. Their main drawback, in comparison with the RPA class of car-following models [77], lies in their difficulty to capture the physical characteristics of the vehicle. However, recent analyses of the IDM model have shown that the model is relevant to describe driving cycles [98].

One focus of stability analyses in traffic consist in determining conditions

for the stability of the vehicles trajectories under small perturbations such as braking, lane-changing, or even acceleration maneuvers. First, a review of their developments in the field of traffic theory is presented. Stability analyses are then conducted for the time-continuous class of car-following models over the entire wave number spectrum. The necessary and sufficient condition (NSC) for linear stability for non multi-anticipative traffic and an instability condition for multi-anticipative traffic are presented. This is closely related to previous work performed by Wilson and Ward [99]. However, here it is extended further as the wavelength value for stability is given as NSC. A chart based on the partial derivative values at the equilibrium state of the dynamical system describes the stability thresholds for bilateral multi-anticipative traffic at long wavelengths. The potential of an added linear control term to the car-following law is discussed in terms of stability. The third subsection brings an insight on how to characterize shock wave structures for bigger perturbations under multi-anticipative and non multi-anticipative traffic. Next to the instability frontier, a Korteweg De Vries (KdV) development is found and gives the amplitude and speed as well as the shock wave equation relevant to understand the evolution of a stop-and-go wave in time and space. The analysis goes further than previous studies as it presents a generic way of deriving stability domains and soliton equations for both non multi-anticipative and multi-anticipative traffic. Any time continuous car-following model has a KdV development, and the extension to bilateral multi-anticipative traffic is made. A closure term valid for open boundaries is introduced. The general solutions of the KdV equation are then discussed. They allow to give a simple condition to know the sign of the soliton amplitude, which corresponds to the leading edge of the travelling wave, and providing the value of the soliton saturation amplitude. Finally, the importance of the window that weights coefficients of cooperation in the multi-anticipative car-following law is analyzed by the mean of the graphical root locus method. The root locus analysis evidences the necessity of a trade-off between stability at short and long wavelengths when choosing the weighting window.

Contents

4.1 Stability analyses: state of the art

Stability analyses have been widely used and developed to assess the stability of dynamical systems since the seminal works of Poincaré and later by Lyapunov in the end of the 19th century, in which the first geometric approach to analyze the stability of solutions of a dynamical system was proposed. Researchers then focused their attention on the study of non-linear oscillators, which played an important role in the invention of radio, laser and radar technologies. In 1963, Lorenz evidenced the potential chaotic behavior of systems with his Lorenz attractor [100], in which a deterministic dynamical system can exhibit complex aperiodic behaviors highly dependent on initial conditions. Four years later, the concepts of fractal theory were raised by Mandelbrot [101].

Stability analyses concern the study of solutions and trajectories of a dynamical system for small perturbations in the initial conditions. In traffic, the response of drivers to a stimulus such as a sudden braking or acceleration may cause disturbances that propagate in the traffic flow. There, the goal is to determine conditions on the dynamical system properties for which the trajectories at a microscopic level or the traffic state at a macroscopic level remain stable under some introduced perturbation. In the case of propagation of those perturbations, the equation of the perturbation growth can be studied. Indeed, it appears fundamental to determine whether a dense traffic is likely to fall into congestion and how this congestion is going to spread. The study of the introduction of a perturbation in a steady state traffic flow requires the system to describe non-equilibrium traffic states, which is not compatible with first order macroscopic models. Stability analyses can be conducted on second order macroscopic models by calculating the characteristic speeds and expanding the solution of the system around the wavefront [102]. The same technique was used to study the behavior of a macroscopic ACC model with a Constant Time Headway policy (CTH) [103]. The analysis can be performed in Fourier mode and it can be showed that instabilities are always long-wavelength instabilities for the class of models described in equation (3.17) [64]. For other works on macroscopic models stability analyses, the interested reader can refer to [104, 47].

The microscopic car-following models are well suited for linear stability analyses, which consist in obtaining conditions on the model parameters for the propagation of a small perturbation. Bando *et al.* [66] introduced the Optimal Velocity Model (OVM) with its linear stability analysis. If linear stability analyses were regularly performed for each specific car-following model, in their recent paper [99] Wilson and Ward described a general framework to investigate the linear string stability of car-following models, which designates the study of perturbation propagation in a platoon of vehicles following a slightly perturbed leader. They show that, again, the instability is always of the long-wavelength type for the time continuous class of car-following models. They claim that car-following models are unnecessarily complicated, as an understanding of their mathematical properties is much needed for their use and calibration. This attempt at generalization was initiated in a previous paper [105]. Besides, the linear stability analyses of the iterated maps class of car-following models are more complicated and do not lead to the same result [106, 64], as they are subject to instabilities for short wavelength. Very recently, a classification of the instabilities found in traffic was made by Treiber and Kesting and the equation for the perturbation growth was determined [64, 107]. Local instabilities refer to the

most severe level of traffic flow instabilities when the first following vehicle undergoes a persistent perturbed motion, whereas string instabilities refer to the propagation of the perturbation in a platoon of vehicles. A flow can therefore be locally stable but string unstable. Convective string instability is less strong than string instability as it describes a perturbation that only propagates in one direction of the traffic flow (convective dowsntream instability or convective upstream instability). A flow can therefore be string unstable but not convectively string unstable. A flow is absolute stable where no such convective instabilities appear. For small perturbations, the flow is locally unstable, string unstable, convectively string unstable or absolute stable. However, it is empirically observable that the "vast majority of all instabilities of highway traffic flow is of the convective type" [64].

In contrast, few papers address non-linear stability analyses, when for larger perturbations the first order Taylor expansion around the steady state is not an acceptable assumption anymore. However the traffic community agrees that such analyses are much needed to characterize wave profiles and explain the capacity drop phenomenom [99, 108]. In fact, there is always a domain where the traffic flow is linearly string stable but string unstable for bigger perturbations: this is called the string metastable domain. Kerner was probably the first to introduce the idea in his three phase traffic theory [109], in which he explains that a meta stable traffic is evidenced at the transition between free flow and synchronized flow. A way of handling non-linear studies lies in the derivation of a KdV equation by the mean of the reductive perturbation method [110]. The KdV equation belongs to a particular type of partial differential equations for which the inverse scattering transform allows finding exact solutions [111, 112, 113] such as solitary-waves (solitons) which maintain their shape and speed in time. This special shape of waves is due to a compensation effect between dispersive and non-linear effects [114]. The KdV equation was firstly introduced as an equation governing the evolution of weakly non-linear water waves [115]. It has also been brought to traffic modelling, more precisely to study the OVM model in weakly non-linear regimes ([116], [117]). Finally, in a very recent paper [118], a Lyapunov function was found for the OVRV model, helping verify that the Lyapunov stability is less strict than the string stability.

4.2 Mathematical framework for analyzing cooperative car-following models

4.2.1 Cooperation as a bilateral multi-anticipation

In a cooperative setting, a vehicle should adjust its speed/acceleration using information from multiple vehicles ahead and behind. A vehicle reacts to multiple leaders as a form of anticipation of future conditions, and reacts to multiple followers to increase traffic homogeneity. Here, a multi-anticipative approach is described in section 3.2.2 as a framework of the vehicles cooperation. Every single vehicle updates its acceleration at the same time step based on its leaders and followers within a predetermined range called interaction range. For the sake of simplicity, no noise such as sensors errors or communication latency is considered, as the first aim is to highlight the potential benefits of cooperation between vehicles.

Let r be the interaction range between vehicles, so that the spatial neighborhood of a vehicle i is defined as follows:

$$N_i = \{j \in \Omega \setminus \{i\} : |x_j - x_i| \leq r\}, \tag{4.1}$$

where x_i is the position of vehicle i and Ω the set of vehicles in the road section. r represents the interaction range, which means that beyond that distance from vehicle i no vehicle information can be considered in the multi-anticipative law, and it will be seen in chapter 6 that a limited number of vehicles should be considered. The interaction range is therefore lower than the radio range which is typically of the order of 300 meters for single-hop broadcasting (without information forwarding) [119].

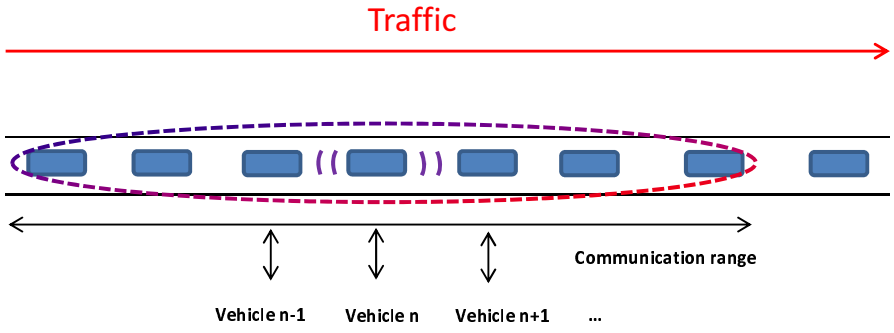

Figure 4.1: Cooperative traffic: a vehicle updates its speed as a function of multiple leaders and followers in a given interaction range of magnitude r.

As illustrated in figure 4.1, the car-following model (3.37) should be rewritten as:

$$\begin{aligned}\ddot{x}_n =& f(\dot{x}_n, \Delta x_{n-m_b}..., \Delta x_n, \Delta x_{n+1}..., \Delta x_{n+m_f}, \\ & \Delta v_{n-m_b}..., \Delta v_n, \Delta v_{n+1}..., \Delta v_{n+m_f}),\end{aligned} \tag{4.2}$$

where $m_b + m_f = |N_n|$ is the fixed-in-time number of vehicles within the interaction range of vehicle n, and f the function representing the car-following model.

In this section, it is assumed that m_b and m_f does not depend on n, the number of cooperative leaders and followers being fixed. Therefore, a cooperative vehicle will update its acceleration as a function of its current velocity and the knowledge of the speed and headways of its leaders and followers within the interaction range following

$$\ddot{x}_n = f(\dot{x}_n, \sum_{j=-m_b}^{m_f} a_j \Delta x_{n+j}, \sum_{j=-m_b}^{m_f} b_j \Delta \dot{x}_{n+j}), \tag{4.3}$$

where $(a_j)_{-m_b \leq j \leq m_f}$ and $(b_j)_{-m_b \leq j \leq m_f}$ are the coefficients of cooperation defining the importance of the interaction between a vehicle n and its surrounding vehicles ($n - m_b$ to $n + m_f$) within its interaction range. Note that the number of backward and forward information data points, *i.e.* the number of considered couples $(\Delta x_j, \Delta v_j)$ in the multi-anticipative car-following law, differs from m_b and m_f as vehicle n counts as one information data point. If m' and m are respectively the number of backward and forward information data points, this gives

$$m' = m_b, \tag{4.4}$$

$$m = m_f + 1. \tag{4.5}$$

Several weighting windows can be chosen, see section 4.5 for a discussion. Without loss of generality and for the sake of clarity only, the weights are chosen such as $(a_j)_{-m_b \leq j \leq m_f} = (b_j)_{-m_b \leq j \leq m_f}$. For continuity purposes between cooperative and non-cooperative traffic, it is set:

$$\sum_{j=-m_b}^{m_f} a_j = 1. \tag{4.6}$$

This normalization ensures that in the case of an equilibrium flow ($\Delta x_j = \Delta x_{eq},\ \dot{x}_j = \dot{x}_{eq},\ \forall j$), equation (3.20) is obtained again. Then the cooperative model (4.3) includes the non-cooperative model as a particular case with $m_b = m_f = 0$.

Now that the multi-anticipative car-following model has been defined, the introduction of a perturbation into a steady-state traffic is the first step towards linear and non-linear stability analyses.

4.2.2 Introduction of a perturbation

To get more compact expressions the notation $\sum_j = \sum_{j=-m_b}^{m_f}$ is used, the arguments of f (respectively $\dot{x}_n,\ \sum_j a_j \Delta x_{n+j},\ \sum_j a_j \Delta \dot{x}_{n+j}$) form the vector u_n, the equilibrium regime being characterized by vector $u_{eq,n} = u_{eq} = (\dot{x}_{eq}, \Delta x_{eq}, 0)\ \forall n$, with $f(u_{eq}) = 0$.

A small position perturbation $y_n(t)$ around an equilibrium state u_{eq} is written:

$$\begin{aligned} x_n(t) &= x_{neq}(t) + y_n(t), \\ \dot{x}_n(t) &= \dot{x}_{eq} + \dot{y}_n(t), \\ \Delta x_n(t) &= \Delta x_{eq}(t) + \Delta y_n(t), \\ \Delta \dot{x}_n(t) &= \Delta \dot{y}_n(t). \end{aligned}$$

A perturbation $\bar{u}_n(t)$ around the equilibrium state is therefore introduced as follows:

$$u_n(t) = u_{eq} + \bar{u}_n(t), \tag{4.7}$$

with

$$\bar{u}_n(t) = {}^t\left(\dot{y}_n, \sum_j a_j \Delta y_{n+j}, \sum_j a_j \Delta \dot{y}_{n+j}\right)(t). \tag{4.8}$$

For linear and weakly non-linear analysis, the developments are limited to the second order:

$$f\left(u_{eq} + \bar{u}_n\right) = f\left(u_{eq}\right) + {}^tJ u_n + \frac{1}{2}{}^t u_n H u_n, \tag{4.9}$$

where J and H are the Jacobian and Hessian taken at the equilibrium point u_{eq}. Their components will be noted $f_i,\ i = 1, 2, 3$ for the Jacobian and $f_{ij},\ i, j = 1, 2, 3$ for the Hessian, being respectively the first and second partial derivatives computed for $u_n = u_{eq}$. For future developments, (4.9) is extended by using $\Delta \ddot{y}_n = (\ddot{y}_{n+1} - \ddot{y}_n)$, which leads to:

$$\Delta \ddot{y}_n = {}^tJ(u_{n+1} - u_n) + \frac{1}{2}{}^t(u_{n+1} + u_n) H (u_{n+1} - u_n), \tag{4.10}$$

where the last term follows the symmetry property of the Hessian.

Definition of linear string instability and non-linear instability

Before going any further, the mathematical definitions of linear string instability and non-linear instability are specified.

A traffic flow is linearly string unstable if

$$\lim_{t\to\infty} \max_{N} x_N(t) > 0, \forall y_n(0) > 0 \tag{4.11}$$

where N is the set of vehicles on the road, and non-linearly unstable if $\exists\, Y > 0$ so that

$$\lim_{t\to\infty} \max_{N} x_N(t) = \begin{cases} Y_0 > 0 & \text{if } y_n(0) > Y \\ 0 & \text{if } y_n(0) \in [0, Y], \end{cases} \tag{4.12}$$

where Y_0 is a positive real number.

4.3 Linear string stability analysis and discussion

For the linear string stability analysis, the proposed approach is similar to the one of Wilson and Ward ([99]) as the objective is to evaluate the NSC for stability, *i.e.* for all wave-numbers k. Most approaches only dealt with small perturbation and long waves, and only gave an instability condition for long wavelengths. Wilson [105] also showed that the stability type is explained by the behavior near $k = 0$. Such an assumption is not always true in the cooperative multi-anticipative case as a stable behavior near $k = 0$ could result in an unstable flow for a larger wave-number, for a particular set of weighting coefficients, see section 4.5. In this work an emphasis is put on the stability threshold k_z, which was not clearly specified in [99] (but probably could have been easily specified), and on the potential of forward and bilateral multi-anticipation, and linear control terms.

The linearization aims at keeping the first order terms of equation (4.10). This gives:

$$\begin{aligned} \Delta\ddot{y}_n =& {}^{t}J\,(u_{n+1} - u_n) \\ =& f_1 \Delta\dot{y}_n + f_2 \sum_j a_j \,(\Delta y_{n+j+1} - \Delta y_{n+j}) \\ &+ f_3 \sum_j a_j \,(\Delta\dot{y}_{n+j+1} - \Delta\dot{y}_{n+j})\,. \end{aligned} \tag{4.13}$$

The perturbation is written into Fourier mode:

$$\Delta y_n(t) = Y_0 e^{i(kn - \omega t)}, \tag{4.14}$$

where k is the wave-number ($0 \leq k \leq \pi$), n the vehicle number and ω the wave angular frequency. For further analysis, $z = -i\omega$ is set.

Physical meaning of the dispersion relation roots

Consider the harmonic form (4.14) for $y_n(t)$ and a solution $z(k) = z_r(k) + iz_i(k)$ for a given wave number k, $y_n(t)$ is then written

$$y_n(t) = e^{z_r(k)t} e^{ik(tz_i(k)/k+n)}. \tag{4.15}$$

The definition of linear string stability (or asymptotic stability) can be applied to a perturbation written in Fourier mode. A dynamic system is stable if and only if $\forall k \in]-\pi, \pi], z_r(k) < 0$, *i.e.* the perturbation exponentially decays in time.

The imaginary part $z_i(k)$ also has an important meaning, related to the wave phase velocity. It is clear from the second factor of (4.15) that $k/z_i(k)$ is the time interval needed for the wave to move from vehicle n to vehicle $n - \text{sign}\,(k/z_i(k))$. The propagation propagates upstream if $k/z_i(k) > 0$ and downstream if $k/z_i(k) < 0$. If Δ_{eq} is the steady-state headway around which the linearisation is performed, a phase velocity can be associated:

$$V_\phi(k) = -\Delta_{eq} \frac{z_i(k)}{k}. \tag{4.16}$$

According to the definition of y_n, (equation 4.7), this velocity is relative to the moving frame of the equilibrium regime. The absolute velocity of the wave relatively to the road is then $V_\phi(k) + V_{eq}$.

4.3.1 Non-cooperative case

In the non multi-anticipative case, by integrating equation (4.14) into (4.13), the dispersion relation is being reduced to

$$z^2 - z\left(f_1 + f_3\left(e^{ik} - 1\right)\right) - f_2\left(e^{ik} - 1\right) = 0. \tag{4.17}$$

The $k-$dependence of the real parts z_{r1} and z_{r2} of the dispersion equation roots is displayed in figures 4.2a and 4.2b, respectively in a stable example and an unstable one.

The wave-number k evolves in $[0, \pi]$. For $k = 0$ the dispersion equation gives solutions $z_1 = 0$ and $z_2 = f_1 < 0$. For $k = \pi$, the real parts of the roots are negative since the coefficients of the dispersion equation are positive. As the dispersion relation is a continuous function of k, it means that the real

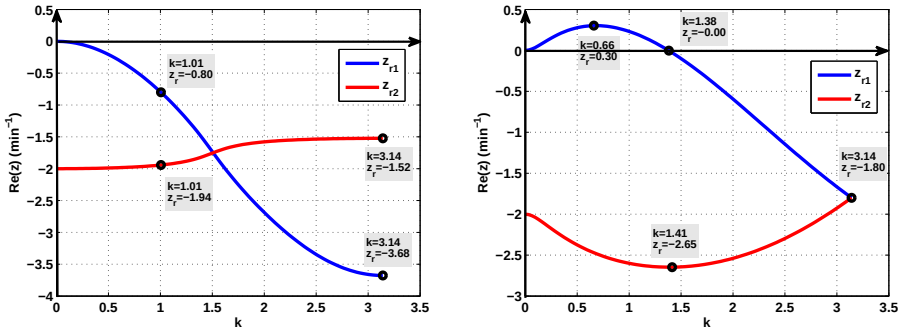

(a) (b)

Figure 4.2: Real parts of the dispersion equation solutions in (a) stable case with $f_2/f_1^2 = 0.7$, $f_3/f_1 = -0.8$, (b) unstable case with $f_2/f_1^2 = 2$, $f_3/f_1 = -0.4$.

part of the roots have to cross the k axis to become positive and in that case the dynamical system would be unstable. For example, it is clear in figures 4.2a and 4.2b that the behavior near $k = 0$ may explain the behavior over the whole k spectrum.

Therefore, the existence of k_z values such that $z_r(k_z) = 0$ should be investigated. The explicit expression of the stability threshold k_z will be given as well as the condition for its existence.

Starting from the dispersion relation (4.17), and separating complex numbers into real and imaginary parts, the following relations can be obtained:

$$z_r^2 - z_i^2 - z_r f_1 - z_r f_3 c_k + z_r f_3 + z_i f_3 s_k - f_2 c_k + f_2 = 0, \tag{4.18}$$

$$2 z_i z_r - z_r f_3 s_k - z_i f_1 - z_i f_3 c_k + z_i f_3 - f_2 s_k = 0, \tag{4.19}$$

where z_i is the imaginary part of the root, and $c_k = \cos(k_z)$, $s_k = \sin(k_z)$. $z_r = 0$ is set, and z_i is expressed in k from equation (4.19) and then used in (4.18). In order to get an equation in c_k the relation $s_k^2 = 1 - c_k^2$ is used, getting the second order equation:

$$f_2 (c_k - 1) \left(c_k \left(f_2 + 2 f_3^2 - f_3 f_1 \right) - f_1^2 - 2 f_3^2 + 3 f_1 f_3 + f_2 \right) = 0. \tag{4.20}$$

The first solution $c_k = 1$ gives the already known point $k = 0$. The other solution is written

$$c_k = \frac{f_1^2 + 2f_3^2 - 3f_1f_3 - f_2}{f_2 + 2f_3^2 - f_3f_1}. \tag{4.21}$$

The condition $|c_k| \leq 1$ gives that the condition of existence of a $k_z > 0$ such that $z_r(k_z) = 0$, leading to an unstable dynamical system, is

$$f_1^2 - 2f_2 - 2f_1f_3 < 0, \tag{4.22}$$

which is the same instability condition as in (4.44) for large wavelengths and without multi-anticipation. Finally, when (4.22) is statisfied, the stability threshold value k_z is given by (see figure 4.2b)

$$k_z = \arccos\left(\frac{f_1^2 + 2f_3^2 - 3f_1f_3 - f_2}{f_2 + 2f_3^2 - f_3f_1}\right). \tag{4.23}$$

4.3.2 Bilateral non-cooperative case

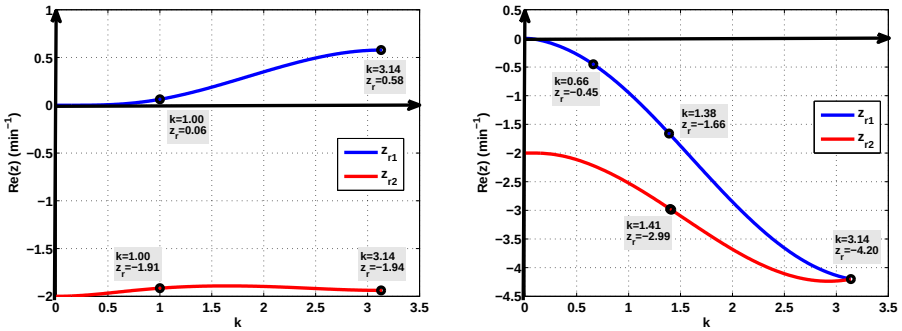

(a) (b)

Figure 4.3: Real parts of the dispersion equation solutions in (a) unstable case of figure 4.2b with bilateral cooperation $a_{-1} = 0.6$, (b) with bilateral cooperation $a_{-1} = -1.5$.

When bilateral traffic is introduced, the vehicle reacts to its leader and its follower, respectively with weigthing coefficients a_0 and a_{-1}. This is the same as having a driver who is constantly looking at his rear-view mirror. For bilateral non-cooperative and cooperative analyses, one should rely on graphical analyses, see section 4.5.5, as there is no analytical solution. It can be observed in figures 4.3a and 4.3b that there is a stabilizing effect if the

coefficient a_{-1} is negative and a destabilizing effect when it is positive. Indeed, the real parts of the roots become negative with bilateral cooperation, which converts the unstable dynamical system into a stable one.

4.3.3 Cooperative case

A study over the entire k domain is not feasible for multi-anticipative traffic. Indeed, the multi-anticipative law (equation 4.3) leads to high degree polynomial terms in the dispersion relation. Consequently the analytical study is only made in the neighborhood of $k = 0$. After some developments, the dispersion relation is given

$$z^2 - z\left(f_1 + f_3\left(e^{ik} - 1\right)\sum_j a_j e^{ijk}\right) - f_2\left(e^{ik} - 1\right)\sum_j a_j e^{ijk} = 0. \tag{4.24}$$

which, after non-dimensionalization, corresponds to,

$$\nu^2 - \nu(K\eta - 1) - \gamma K = 0, \tag{4.25}$$

with

$$\nu = -\frac{z}{f_1}, \tag{4.26}$$

$$K = (e^{ik} - 1)\sum_j a_j e^{ijk}, \tag{4.27}$$

$$\gamma = \frac{f_2}{f_1^2}, \tag{4.28}$$

$$\eta = -\frac{f_3}{f_1}. \tag{4.29}$$

Roots of the equation are:

$$\nu_1 = \frac{1}{2}(K\eta - 1 - \sqrt{D}), \tag{4.30}$$

$$\nu_2 = \frac{1}{2}(K\eta - 1 + \sqrt{D}), \tag{4.31}$$

with $D = (K\eta - 1)^2 + 4\gamma K$.

Expanding the limited developments up to the second order, one can get

$$K = ik + (ik)^2\left(\frac{1}{2} + \sum_j j a_j\right), \tag{4.32}$$

and

$$\sqrt{D} = 1 + ik(2\gamma - \eta) + (ik)^2 \left(\frac{1}{2}\eta^2 - \eta \left(\frac{1}{2} + \sum_{j=0}^{m} j a_j \right) + 2\gamma \left(\frac{1}{2} + \sum_{j} j a_j \right) - \frac{(4\gamma - 2\eta)^2}{8} \right). \tag{4.33}$$

For $k = 0$, $\nu_1 = -1$ and $\nu_2 = 0$. The behavior of ν_2 is therefore of interest, and

$$\nu_2 = ik(\gamma) + (ik)^2 (\gamma(\frac{1}{2} + \sum_{j} a_j) - \gamma^2 + \gamma\eta). \tag{4.34}$$

Note that the coefficients weighting the relative velocity information do not have an effect on the linear condition for stability, although this is not the case anymore for non-linear analysis. The necessary condition for stability is written

$$\frac{1}{2} + \sum_{j} j a_j - \gamma + \eta \geq 0, \tag{4.35}$$

which gives the following instability condition at long wavelengths, *i.e.* near $k = 0$ ([99]):

$$f_1^2 \left(\frac{1}{2} + \sum_{j} j a_j \right) - f_2 - f_1 f_3 < 0. \tag{4.36}$$

4.3.4 Long wavelength linear stability

A phase chart can be produced regarding long wavelength linear stability for bilateral multi-anticipative traffic. Strating with equation 4.44, and defining the dimensionless parameters:

$$\begin{aligned} P_1 &= \frac{f_1}{\sqrt{f_2}}, \\ P_3 &= \frac{f_3}{\sqrt{f_2}}, \\ A_c &= \frac{1}{2} + \sum_{j} j a_j. \end{aligned} \tag{4.37}$$

Note that $P_1 < 0$ due to the condition on f_1. P_1 and P_3 relate to the traffic model, while A_c is a parameter related to the cooperation (number of

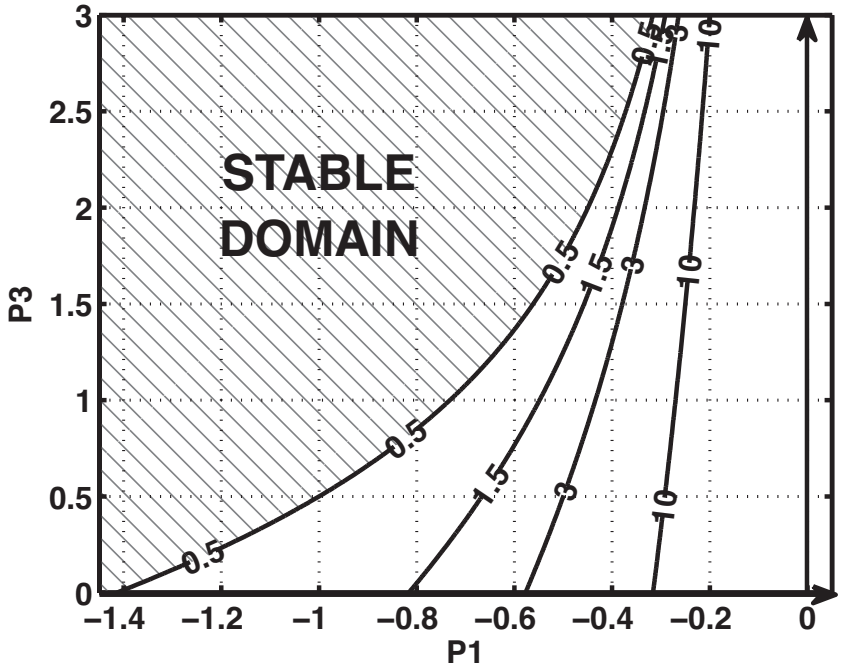

Figure 4.4: Contour of A_c values: traffic is string unstable on the right side of the instability frontier.

involved vehicles and coefficients of cooperation). The instability condition can be expressed in the following way:

$$A_c < \frac{1 + P_1 P_3}{P_1^2}. \tag{4.38}$$

This gives the instability region in the (P_1, P_3) plane, which is, for constant A_c, on the right side of the boundary curve $A_c = (1 + P_1 P_3)/P_1^2$, see figure 4.4. It can be observed that this region is reduced when A_c increases, the $A_c = 0.5$ curve corresponding to the non cooperative case.

This graph can be seen as a generic phase diagram that can be useful for physical interpretation. After estimating the car following parameters, and therefore the P_1 and P_3 values, the A_c value (and the numbers of cooperative vehicles) needed to move traffic into the stability region can be obtained.

4.3.5 Effect of an added linear control

It can be interesting to investigate the influence of an added linear control term on the car-following law. Such an investigation is of fundamental importance in the flocking framework (see section 3.2.3), and is presumed to have a stabilization effect. The objective could consist in heading towards a desired equilibrium state $(\Delta x_d, \dot{x}_d)$, given the set of parameters of the car-following model. It could be the closest state to verify the stability condition in a non-cooperative traffic (if there is a mixed traffic of cooperative and non-cooperative vehicles it seems more reasonable to use the non-cooperative condition as target).

Function f of equation (4.3) now includes linear terms and becomes f_c so that

$$f_c = f + g, \tag{4.39}$$

where

$$g(\dot{x}_n, \sum_j a_j \Delta x_{n+j}, \sum_j a_j \Delta \dot{x}_{n+j}) = -c_1(\dot{x}_n - \dot{x}_d) + c_2(\sum_j a_j \Delta x_{n+j} - \Delta x_d), \tag{4.40}$$

where c_1 and c_2 are proportional gains, with $c_1 > 0$ and $c_2 > 0$ (physical sense). By analogy,

$$f_{c1} = f_1 - c_1, \tag{4.41}$$
$$f_{c2} = f_2 + c_2, \tag{4.42}$$
$$f_{c3} = f_3, \tag{4.43}$$

where $(f_{ci})_{1\leq i\leq 3}$ are the first order partial derivatives of f_c. By analogy and replacing $(f_i)_{1\leq i\leq 3}$ by $(f_{ci})_{1\leq i\leq 3}$, the instability condition 4.44 is written

$$(f_1 - c_1)^2 \left(\frac{1}{2} + \sum_j j a_j\right) - f_2 - f_1 f_3 - c_2 + c_1 f_3 < 0, \tag{4.44}$$

which allows to conclude that the linear control terms bring string stability if

$$A_c c_1^2 + (f_3 - 2 f_1 A_c) c_1 - c_2 > 0. \tag{4.45}$$

Following equation (4.45), figure 4.5 exhibits the domain of the gains (c_1, c_2) that brings string stability for different values of A_c. The added linear control brings string stability in the (c_1, c_2) domain on the right side of the curves.

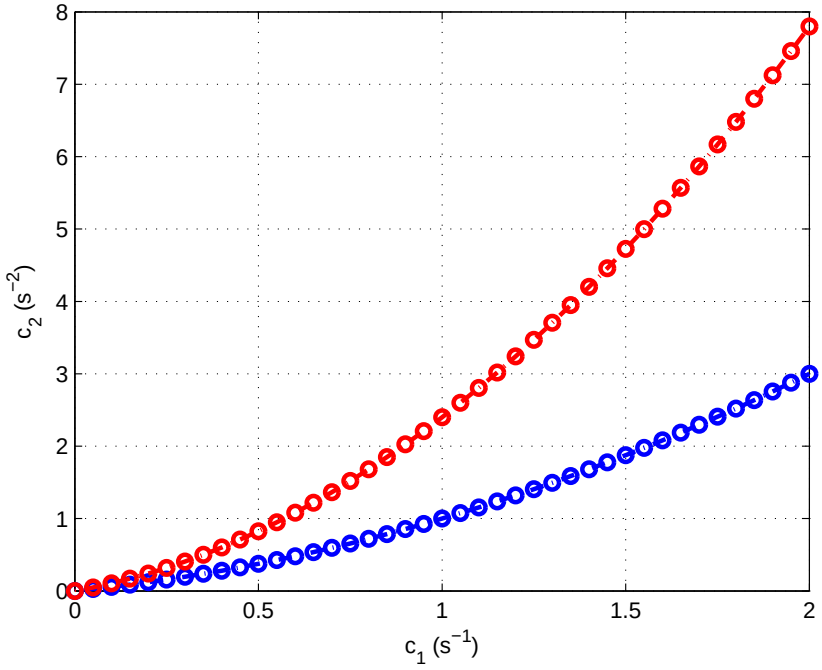

Figure 4.5: Domain of validity of (4.45) for $f_1 = -0.2$ and $f_3 = 0.3$.

Finally, the effect of an added linear control term can be examined in the light of figure 4.4, and is represented in figures 4.6a and 4.6b. The operating starting point corresponds to (a) an unstable dynamical system and to (b) a stable dynamical system with nil control gains. Let $P1_c$ and $P3_c$ be defined by analogy with equations (4.37) with partial derivatives $(f_{ci})_{1\leq i\leq 3}$. In the $(P1_c, P3_c)$ diagram, the increase of gains c_1 and c_2 respectively cause a more unstable or less stable system for increasing c_1 and a more stable or less unstable system for increasing c_2. It is therefore observed that the c_2 term does not have a positive impact on string stability, however, this might be different from a control perspective. Note that a negative c_2 gain would lead to instabilities as well, as it opposes traffic physics.

4.4 Weakly non-linear stability analyses

In the previous section, linear string stability analyses have been refined for bilateral multi-anticipative time continuous car-following models with

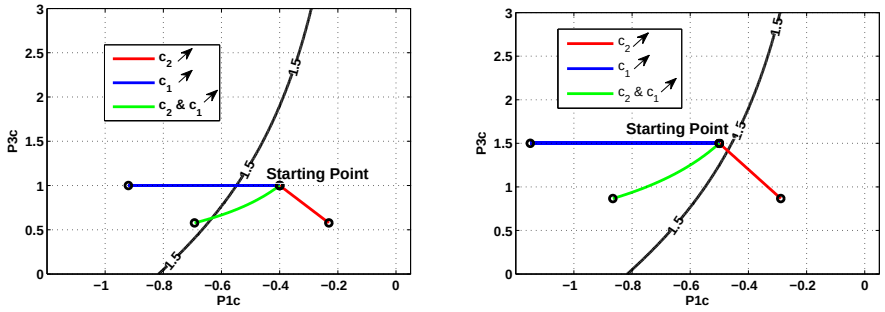

Figure 4.6: Variation of control gains c_1 and c_2 to turn the (a) unstable, (b) stable, dynamical system (represented by starting point P) into (a) a stable, (b) an unstable system for $A_c = 1.5$.

and without added linear control terms. In this section, weakly non-linear stability analyses, which designate analyses for slightly bigger sizes of initial perturbations, are performed for the time continuous class of bilateral multi-anticipative car-following models, which allows a new complete framework to be built for the study of wave propagation. A KdV development is found near the neutral string stability surface, *i.e.* the surface that separates string unstable and string stable traffic in the domain of the partial derivatives of function f.

As stated before, the idea of deriving the KdV equation was first introduced by Muramatsu and Nagatani for the OVM [116], and developed by Ge *et al.* [90, 117] in later studies. These developments are here generalized for the class of continuous car following models, and extended to bilateral multi-anticipative traffic. Physics and traffic related results are discussed.

4.4.1 Problem statement and basic relations

The formation of solitons can happen in the weakly non-linear regime only if some relations between the wavelength, the amplitude and propagation distance of the wave are satisfied. The reductive perturbation method is a multi-scale analysis that consists in the introduction of a small perturbation parameter ϵ to get the right scaling between variables [120].

Starting from equation (4.10), the following notations are introduced to

shorten the mathematical developments and improve clarity:

$$\bar{u}_{n+1} + \bar{u}_n = \begin{pmatrix} \dot{y}_{n+1} + \dot{y}_n \\ \sum_j a_j(\Delta y_{n+j+1} + \Delta y_{n+j}) \\ \sum_j a_j(\Delta \dot{y}_{n+j+1} + \Delta \dot{y}_{n+j}) \end{pmatrix}, \tag{4.46}$$

and

$$\bar{u}_{n+1} - \bar{u}_n = \begin{pmatrix} \Delta \dot{y}_n \\ \sum_j a_j(\Delta y_{n+j+1} - \Delta y_{n+j}) \\ \sum_j a_j(\Delta \dot{y}_{n+j+1} - \Delta \dot{y}_{n+j}) \end{pmatrix}. \tag{4.47}$$

The neutral string stability surface is described by the equation $h(f_1, f_2, f_3) = f_2 + f_1 f_3 - f_1^2 \left(\frac{1}{2} + \sum_j j a_j\right) = 0$. The small scaling parameter ϵ is introduced by setting:

$$h(f_1, f_2, f_3) = \epsilon^2. \tag{4.48}$$

This ensures that h evolves at the vicinity of the neutral string stability surface (for small ϵ), *i.e.* in the weakly non-linear regime. Then, new quantities have to be defined: the slow space and time variables X and T and the perturbation R. From the dispersion equation (4.17) and equation (4.48) the scaling between variables X, T and R is chosen such that (see [116])

$$\begin{aligned} X &= \epsilon(n + b \cdot t), & (4.49)\\ T &= \epsilon^3 t, & (4.50)\\ \Delta y_n &= \epsilon^2 R(X_n, T), & (4.51) \end{aligned}$$

where b is an arbitrary constant that will be specified later. From equations (4.46,4.47, 4.49-4.51), two basic operations are needed: the time derivation and the shift of j vehicles from the current position. From equations (4.49-4.51)

$$\partial_t = \epsilon \left(b\partial_X + \epsilon^2 \partial_T\right), \tag{4.52}$$

and

$$\begin{aligned} R\left(X_{n+j}, T\right) &= R\left(X_n + j\epsilon, T\right) \\ &= \sum_{k=0}^{k_M} \frac{(j\epsilon)^k}{k!} \partial_X^k R(X_n, T), \end{aligned} \tag{4.53}$$

k_M being the chosen upper order for the limited development of $R\left(X_{n+j}, T\right)$, being $k_M = \infty$ for the Taylor series.

4.4.2 Boundary conditions

The boundary conditions of the section must be specified, and allow the term $\dot{y}_{n+1} + \dot{y}_n$ of equation (4.46) to be expressed as a function of $\Delta\dot{y}_{n+i},\ i \geq 0$. Perturbations are introduced to an equilibrium traffic regime characterized by a velocity $\dot{x}_{eq}$ and a headway Δx_{eq} so that $f(\dot{x}_{eq}, \Delta x_{eq}, 0) = 0$. This regime is established maintaining the following boundary conditions: at the entrance, vehicles enter with speed $\dot{x}_{eq}$ and are separated by distance Δx_{eq}; at the exit, the front vehicle loses its leader and gains the equilibrium speed $\dot{x}_{eq}$, meaning that $\dot{y} = 0$. Using these conditions, it is possible to get an expression for the term $\dot{y}_n + \dot{y}_{n+1}$ which appears in (4.46):

$$\begin{aligned} \dot{x}_n &= -\Delta\dot{x}_n + \dot{x}_{n+1} = -\Delta\dot{x}_n - \Delta\dot{x}_{n+1} + \dot{x}_{n+2} \\ &= ... = -\textstyle\sum_{i=0}^{M_n-1} \Delta\dot{x}_{n+i} + \dot{x}_{eq}, \end{aligned} \tag{4.54}$$

where M_n is the total number of vehicles ahead of vehicle n. Since $\dot{x}_n = \dot{x}_{eq} + \dot{y}_n$ and $\forall j,\ \Delta\dot{x}_j = \Delta\dot{y}_j$, it can be rewritten:

$$\dot{y}_n = -\sum_{i=0}^{M_n-1} \Delta\dot{y}_{n+i}, \tag{4.55}$$

which leads to:

$$\begin{aligned} \dot{y}_n + \dot{y}_{n+1} &= -\textstyle\sum_{i=0}^{M_n-1} \Delta\dot{y}_{n+i} - \sum_{i=0}^{M_{n+1}-1} \Delta\dot{y}_{n+1+i} \\ &= -2\textstyle\sum_{i=1}^{M_n-1} \Delta\dot{y}_{n+i} - \Delta\dot{y}_n. \end{aligned} \tag{4.56}$$

4.4.3 Derivation of the partial differential equation in relation to R (or Δy_n)

In this section, the mathematical developments will lead to a KdV equation in R, which is directly related to the perturbation headway Δy_n according to equation (4.51). Based on equations (4.49-4.56) the following relations

can be derived

$$\Delta\ddot{y}_n = \epsilon^4 \left(b\partial_X + \epsilon^2\partial_T\right)^2 R, \tag{4.57}$$

$$\dot{y}_n + \dot{y}_{n+1} = -\epsilon^3(b\partial_X + \epsilon^2\partial_T) \times \left[2\sum_{k=0}^{k_M}\epsilon^k \sum_{l=1}^{M_n-1} l^k \frac{\partial_X^k}{k!} + 1\right] R, \tag{4.58}$$

$$\sum_j a_j \left(\Delta y_{n+j+1} + \Delta y_{n+j}\right) = \epsilon^2 \sum_{k=0}^{k_M} \epsilon^k K_k R, \tag{4.59}$$

$$\sum_j a_j \left(\Delta \dot{y}_{n+j+1} + \Delta \dot{y}_{n+j}\right) = \epsilon^3 \left(b\partial_X + \epsilon^2\partial_T\right) \sum_{k=0}^{k_M} \epsilon^k K_k R, \tag{4.60}$$

$$\sum_j a_j \left(\Delta y_{n+j+1} - \Delta y_{n+j}\right) = \epsilon^3 \sum_{k=0}^{k_M} \epsilon^k L_k R, \tag{4.61}$$

$$\sum_j a_j \left(\Delta \dot{y}_{n+j+1} - \Delta \dot{y}_{n+j}\right) = \epsilon^4 \left(b\partial_X + \epsilon^2\partial_T\right) \sum_{k=0}^{k_M} \epsilon^k L_k R, \tag{4.62}$$

with

$$L_k = \sum_j a_j \frac{(j+1)^{k+1} - j^{k+1}}{(k+1)!}\partial_X^{k+1}, \tag{4.63}$$

$$K_k = \sum_j a_j \frac{(j+1)^{k} + j^{k}}{(k)!}\partial_X^{k}. \tag{4.64}$$

Equation (4.10) is then rewritten under matrix form:

$$\begin{aligned} 0 = & -\epsilon^4 \left(b\partial_X + \epsilon^2\partial_T\right)^2 R \\ & + {}^t\begin{pmatrix} f_1 \\ f_2 \\ f_3 \end{pmatrix} \begin{pmatrix} \epsilon^3 \left(b\partial_X + \epsilon^2\partial_T\right) R \\ \epsilon^3 \sum_{k=0}^{k_M} \epsilon^k L_k R \\ \epsilon^4 \left(b\partial_X + \epsilon^2\partial_T\right) \sum_{k=0}^{k_M} \epsilon^k L_k R \end{pmatrix} \\ & + \frac{1}{2}\, {}^t\begin{pmatrix} \epsilon^3(b\partial_X + \epsilon^2\partial_T)\left(-2\sum_{k=0}^{k_M}\epsilon^k \sum_{l=1}^{M_n-1} l^k \frac{\partial_X^k}{k!} - 1\right) R \\ \epsilon^2 \sum_{k=0}^{k_M} \epsilon^k K_k R \\ \epsilon^3 \left(b\partial_X + \epsilon^2\partial_T\right) \sum_{k=0}^{k_M} \epsilon^k K_k R \end{pmatrix} \\ & \cdot \begin{pmatrix} f_{11} & f_{12} & f_{13} \\ f_{21} & f_{22} & f_{23} \\ f_{31} & f_{32} & f_{33} \end{pmatrix} \begin{pmatrix} \epsilon^3 \left(b\partial_X + \epsilon^2\partial_T\right) R \\ \epsilon^3 \sum_{k=0}^{k_M} \epsilon^k L_k R \\ \epsilon^4 \left(b\partial_X + \epsilon^2\partial_T\right) \sum_{k=0}^{k_M} \epsilon^k L_k R \end{pmatrix}. \end{aligned} \tag{4.65}$$

The above equation is presented so that the leading order in ϵ explicitely appears in front of each expression. The successive terms of given order ν in ϵ can then be extracted by simple inspection. Note that the minimum order is 3, and that the non-linear last term has no contribution for orders lower than 5.

Then, after writing

$$0 = \epsilon^3 T_3 + \epsilon^4 T_4 + \epsilon^5 T_5 + \epsilon^6 T_6 + o(\epsilon^6), \tag{4.66}$$

the expressions of the $T_k,\ k \in \{3, ..., 6\}$ terms can then be straightforwardly obtained by simple identification and using relations (4.63) and (4.64):

- Term T_3:

$$T_3 = (bf_1 + f_2)\,\partial_X R. \tag{4.67}$$

  In order to remove this term, b is chosen as $b = -f_2/f_1$. The b value will be used in all the following T_k terms.

- Term T_4:

$$T_4 = \frac{f_2}{f_1^2}\left[f_1^2\left(1/2 + \sum_j j a_j\right) - f_2 - f_1 f_3\right]\partial_X^2 R. \tag{4.68}$$

  However, relation (4.48) defines the close proximity to the neutral string stability surface, so that the term within the bracket is equal to ϵ^2. Then the term T_4 is of order ϵ^6 and can be discarded at this stage.

- Term T_5:

$$\begin{aligned} T_5 =& f_1 \partial_T R + \left[f_2 \sum_j a_j \frac{3j^2 + 3j + 1}{6}\right. \\ & \left. - \frac{f_3 f_2}{f_1}(\frac{1}{2} + \sum_j j a_j)\right]\partial_X^3 R + \\ & \left[-f_{12}\frac{f_2}{f_1} + f_{22}\right] R \partial_X R. \end{aligned} \tag{4.69}$$

- Term T_6:

$$\begin{aligned}
T_6 =&\partial_{XT}R\Big(2\frac{f_2}{f_1}+f_3\Big)\\
&+\partial_X^4R\Big(f_2\sum_j a_j\frac{(j+1)^4-j^4}{4!}\\
&-\frac{f_3f_2}{f_1}\sum_j a_j\frac{3j^2+3j+1}{6}\Big)\\
&+(\partial_XR)^2\Big(\frac{1}{2}\frac{f_2}{f_1}(1+2S_0)(-f_{11}\frac{f_2}{f_1}+f_{12})\\
&-f_{21}\frac{f_2}{f_1}\sum_j a_j(2j+1)+\frac{1}{2}f_{22}\sum_j a_j(2j+1)\\
&+f_{31}\frac{f_2^2}{f_1^2}-f_{32}\frac{f_2}{f_1}\Big)\\
&+R(\partial_X^2R)\Big(f_{22}\sum_j a_j(j+\frac{1}{2})-f_{23}\frac{f_2}{f_1}\Big)\\
&+\partial_X^2R\left(\frac{f_2}{f_1^2}\right),
\end{aligned}\tag{4.70}$$

  where $S_{k_M}=\sum_{k=0}^{k_M}\epsilon^k\sum_{l=1}^{M_n-1}l^k\frac{\partial_X^k}{k!}$, and ∂_X^2R is coming from the T_4 term.

The first term to consider is T_5. Its cancellation leads to the KdV type equation ([114, 115])

$$C_1\partial_X^3R+C_2R\partial_XR+C_3\partial_TR=0,\tag{4.71}$$

with

$$C_1=f_2\sum_j a_j\frac{3j^2+3j+1}{6}-\frac{f_3f_2}{f_1}(\frac{1}{2}+\sum_j ja_j),\tag{4.72}$$

$$C_2=-f_{12}\frac{f_2}{f_1}+f_{22},\tag{4.73}$$

$$C_3=f_1.\tag{4.74}$$

Sign of C_1 and simplification of T_6

In this subsection the sign of C_1 is investigated and term T_6 is simplified for further developments.

Since $f_1 < 0$, $C_3 < 0$. Note that $C_1 > 0$ in case of monolateral cooperation. In the bilateral case, C_1 should be rewritten in a more suitable way for physical interpretation. First $\sum_j a_j(3j^2+3j+1) = 1 + 3\sum_j a_j j(j+1)$, the a_j coefficients being normalized. The sum can be presented combining the coefficients by pairs, *i.e.* a_j with $a_{-(j+1)}$, giving:

$$\sum_j a_j j(j+1) = \sum_{j=0}^{m} j\,(j+1)\left(a_j + a_{-(j+1)}\right) \tag{4.75}$$

C_1 is then the sum of two terms $C_1 = C_{11} + C_{12}$ with:

$$C_{11} = \frac{1}{2}\sum_{j=0}^{m} j\,(j+1)\left(a_j + a_{-(j+1)}\right), \tag{4.76}$$

$$C_{12} = \frac{1}{6} - \frac{f_3 f_2}{f_1}(\frac{1}{2} + \sum_j j a_j). \tag{4.77}$$

Consequently $C_{12} > 0$, indeed $f_1 < 0$ and $ja_j \geq 0$, j and a_j always being of the same sign. Regarding the C_{11} term, one can consider that, in realistic traffic flow situations, for a given driver behavior the downstream conditions are more important than the upstream ones. It is then realistic to assume, and this is in accordance with the continuity condition (equation 4.6), that $a_j \geq |a_{-(j+1)}|$, $\forall j$. Therefore, from now on it will be considered that $C_1 > 0$.

Besides, the term T_6 could be rewritten as

$$\begin{aligned}
T_6 =& \partial_X^4 R\Big(-\frac{C_1}{C_3}(2\frac{f_2}{f_1} + f_3) + f_2 \sum_j a_j \frac{(j+1)^4 - j^4}{4!} \\
&- \frac{f_3 f_2}{f_1}\sum_j a_j \frac{3j^2+3j+1}{6}\Big) \\
&+ (\partial_X R)^2\Big(\frac{1}{2}\frac{f_2}{f_1}(1+2S_0)(-f_{11}\frac{f_2}{f_1} + f_{12}) \\
&- f_{21}\frac{f_2}{f_1}\sum_{j=0}^{m} a_j(2j+1) + f_{31}\frac{f_2^2}{f_1^2}\Big) \\
&+ (\partial_X^2 R^2)\frac{1}{2}\Big(f_{22}\sum_j a_j(j+\frac{1}{2}) - f_{23}\frac{f_2}{f_1} - \frac{C_2}{C_3}(2\frac{f_2}{f_1} + f_3)\Big) \\
&+ \partial_X^2 R\left(\frac{f_2}{f_1^2}\right),
\end{aligned} \tag{4.78}$$

where (4.71) is used for simplification purposes.

4.4.4 Solution of the KdV equation and speed/amplitude relationship

In order to get the standard KdV equation, a change of variables is used, where R', X' and T' are defined as follows: $R = \frac{C_1^{\frac{1}{3}}}{C_2} R'$, $X = C_1^{\frac{1}{3}} X'$ and $T = C_3 T'$.

With these new variables, the following KdV equation is obtained: $\partial^3_{X'} R' + R' \partial_{X'} R' + \partial'_T R' = 0$, the solution of which R'_0 is known as

$$R'_0(X', T') = A \operatorname{sech}^2 \left[\sqrt{\frac{A}{12}} (X' - \frac{A}{3} T') \right], \ A > 0. \tag{4.79}$$

Going back to the (R, X, T) variables, the expression of the generated soliton in traffic flow is

$$R_0(X, T) = \frac{C_1^{\frac{1}{3}}}{C_2} A \operatorname{sech}^2 \left[\sqrt{\frac{A}{12} \frac{1}{C_1^{\frac{2}{3}}}} (X - \frac{A}{3} \frac{C_1^{\frac{1}{3}}}{C_3} T) \right]. \tag{4.80}$$

Using expression (4.51), the expression of the created physical wave Δy_n can now be given:

$$\Delta y_n = \operatorname{sgn}(C_2) \mathbf{A} \operatorname{sech}^2 \left[\sqrt{\frac{|C_2| \, \mathbf{A}}{12 C_1}} \, (n - \alpha_s t) \right], \tag{4.81}$$

where $\operatorname{sgn}(C_2)$ indicates the sign of C_2, and with:

$$\mathbf{A} = \epsilon^2 A \frac{C_1^{\frac{1}{3}}}{|C_2|}, \tag{4.82}$$

$$\alpha_s = \frac{3 f_2 + \mathbf{A} |C_2|}{3 f_1}. \tag{4.83}$$

Two important remarks that characterize the soliton wave can be made at this stage. First, the soliton amplitude has the same sign as C_2. It means that the leading edge of the travelling wave in Δy_n is positive or negative based on the C_2 sign, which has a direct link with the acceleration regime of the wave. Secondly, the propagation term $(n - \alpha_s t)$ appears in the argument of function sech^2. This means that the wave propagates upstream (relatively to the equilibrium flow) since $\alpha_s < 0$. The time interval Δt_1 needed to pass from vehicle n to vehicle $(n-1)$ is:

$$\Delta t_1 = -\frac{1}{\alpha_s}. \tag{4.84}$$

Considering that the traffic flow evolves close to the equilibrium characterized by the headway Δx_{eq}, the velocity v_s of the traveling wave can be given as

$$v_s = \alpha_s \Delta x_{eq}, \tag{4.85}$$

which gives the following relation between the velocity and amplitude:

$$|v_s| = \left| \frac{3f_2 + \mathbf{A}|C_2|}{3f_1} \right| \Delta x_{eq}. \tag{4.86}$$

4.4.5 Amplitude of the modified KdV equation

The amplitude A of the perturbation is a free parameter, so the perturbation term T_6 must be used to select an unique solution among the family of solitons [114]. There is a unique solution if the orthogonality condition is verified [121]. The orthogonality condition of the modified KdV (mKdV) solution is written, where $B'(R'_0)$ is the perturbation term in $O(\epsilon)$, *i.e.* the T_6 term:

$$(R'_0, B'(R'_0)) = \int_{-\infty}^{+\infty} R'_0 B'(R'_0)' dX' = 0. \tag{4.87}$$

The T_6 term should be rewritten as

$$\begin{aligned} T_6 =& \frac{1}{C_2}[m_1 \partial^4_{X'} R' + m_2 (\partial_{X'} R')^2 \\ &+ m_3 \partial^2_{X'} R'^2 + m_4 \partial^2_{X'} R'], \end{aligned} \tag{4.88}$$

where

$$\begin{aligned} m_1 =& \frac{1}{C_1}\Big(- \frac{C_1}{C_3}(2\frac{f_2}{f_1} + f_3) + f_2 \sum_{j=0}^{m} a_j \frac{(j+1)^4 - j^4}{4!} \\ &- \frac{f_3 f_2}{f_1} \sum_j a_j \frac{3j^2 + 3j + 1}{6} \Big), \end{aligned} \tag{4.89}$$

$$\begin{aligned} m_2 =& \frac{1}{C_2}\Big(\frac{1}{2}\frac{f_2}{f_1}(1 + 2S_0)(-f_{11}\frac{f_2}{f_1} + f_{12}) \\ &- f_{21}\frac{f_2}{f_1} \sum_j a_j (2j+1) + f_{31}\frac{f_2^2}{f_1^2} \Big), \end{aligned} \tag{4.90}$$

$$m_3 = \frac{1}{2C_2}\Big(f_{22} \sum_j a_j (j + \frac{1}{2}) - f_{23}\frac{f_2}{f_1} - \frac{C_2}{C_3}(2\frac{f_2}{f_1} + f_3) \Big), \tag{4.91}$$

$$m_4 = \frac{1}{C_1^{\frac{1}{3}}} \left(\frac{f_2}{f_1^2} \right). \tag{4.92}$$

Performing the integration gives the amplitude, and therefore the unique equation of the soliton, derived at the vicinity of the neutral string stability surface. After some developments and changes of variables, the following equations are obtained:

$$\int_{-\infty}^{+\infty} R'_0 \frac{\partial^4 R'_0}{\partial X'^4} dX' = \frac{16A^3}{63}\sqrt{\frac{A}{12}}, \tag{4.93}$$

$$\int_{-\infty}^{+\infty} R'_0 (\frac{\partial R'_0}{\partial X'})^2 dX' = \frac{64A^3}{105}\sqrt{\frac{A}{12}}, \tag{4.94}$$

$$\int_{-\infty}^{+\infty} R'_0 \frac{\partial^2 {R'_0}^2}{\partial X'^2} dX' = \frac{-128A^3}{105}\sqrt{\frac{A}{12}}, \tag{4.95}$$

$$\int_{-\infty}^{+\infty} R'_0 \frac{\partial^2 R'_0}{\partial X'^2} dX' = \frac{-16A^2}{15}\sqrt{\frac{A}{12}}, \tag{4.96}$$

and finally

$$A = m_4 \frac{16}{15}\left[m_1 \frac{16}{63} + m_2 \frac{64}{105} - m_3 \frac{128}{105}\right]^{-1}. \tag{4.97}$$

Here, Muramatsu and Nagatani's approach (see [116]) has been extended to time continuous car following models for both multi-anticipative and non multi-anticipative cases. A systematic way of deriving the KdV equation has been presented by applying the reductive perturbation method. A closure term was introduced, (see. section 4.4.2), which allowed to deal with all the terms of the Taylor's developments. The equation of the soliton was given in (4.81), as well as the velocity and amplitude of the wave, in (4.85) and (4.82). A simple condition for the sign of the leading edge of the travelling wave amplitude was also introduced, in (4.81). All these theoretical results will be validated in section 6.2 based on simulation experiments.

4.5 Root-locus analyses of cooperative car following laws

This section presents a complementary approach to the previous developments. The root locus method is a graphical tool to investigate linear string

stability for all wavelengthes when the analytical developments are not possible. This allows the strategies of multi-anticipation to be assessed, specifically regarding the windows of the coefficients of cooperation. A safety margin method for the stability at short wavelength is introduced, and the potential inputs of bilateral multi-anticipation and added linear control terms conclude the discussion.

4.5.1 Root locus representation

The stability of a dynamical system is directly related to the location of the roots of the dispersion relation on the complex plane. The root locus method of Evans is a powerful graphical tool extensively used in the Control Theory field ([122], [123]). The root locus is the path of the roots traced out in the complex plane as k evolves, where the real part of the roots is represented on the xaxis, and the imaginary part of the roots is represented on the yaxis. As seen in section 4.3.1, a linear string stable traffic is equivalent to negative real parts of the roots.

It is frequently necessary to adjust one or more parameters of the system in order to obtain suitable root locations. Therefore it is useful to determine how the roots of the dispersion relation evolve on the complex plane as those parameters vary. In this section the efficiency of the method to adjust the weighting coefficients of the cooperative car-following law is attested. For the sake of simplicity, the forward multi-anticipative strategy will be the main core of the analysis, however the symmetry of forward/backward multi-anticipation and the previous observations made in section 4.3.2 enable to apply the same methodology, as discussed in section 4.5.5.

Equivalent formulation of multi-anticipative law

Here an equivalence between two forms of multi-anticipation is made, as it will help interpret further developments. Instead of the forward multi-anticipation law (3.37), relative differences to an active vehicle n can be used. Indeed, one can write

$$\ddot{x}_n = f(\dot{x}_n, \sum_{j=0}^{m_f} a'_j \Delta_T x_{n+j}, \sum_{j=0}^{m_f} a'_j \Delta_T \dot{x}_{n+j}), \tag{4.98}$$

where $\Delta_T x_{n+j} = x_{n+j+1} - x_n = \sum_{l=0}^{j} \Delta x_{n+l}$, and similarly for relative speeds.

The two models (3.37, 3.38) are equivalent provided that coefficients verify the relations

$$a_j = \sum_{l=j}^{m_f} a'_l, \tag{4.99}$$

also written as:

$$a'_{m_f} = a_{m_f}, \tag{4.100}$$

$$a'_j = a_{j+1} - a_j \ for\ 0 \leq j < m_f. \tag{4.101}$$

This corresponds to the following normalization:

$$\sum_{j=0}^{m_f} a_j = \sum_{j=0}^{m_f} (j+1) a'_j, \tag{4.102}$$

$$\sum_{j=0}^{m_f} a'_j = a_0. \tag{4.103}$$

A necessary condition for stability, see equation 4.35, is then

$$\eta - \gamma + 1/2 + \sum_{j=0}^{m_f} j\alpha_j = \eta - \gamma + \frac{1}{2} + \frac{1}{2} \sum_{j=0}^{m_f} j \cdot (j+1) a'_j \geq 0. \tag{4.104}$$

Following this necessary condition to linear string stability, the NSC for linear string stability is that the whole root locus lies in the stability region, *i.e.* the whole root locus presents negative real parts (there is no crossing point with the imaginary axis). It has not been possible to find general analytical expressions for the condition of existence of such points and their corresponding k values. However the root locus method remains an efficient graphical tool for the analysis, as it is discussed in the next subsections.

4.5.2 Stabilization *vs* destabilization by drivers cooperation

Stabilization

For the determination of the a_j coefficients a cosine type window is used. Although the choice of the coefficients window will be discussed later, particularly in section 4.5.4, it can be mentioned that a cosine window gives more weight to the first leader, and therefore acts on traffic flow in a smoother way than other windows. r is the interaction range, m_f is the integer part

of $(r/\Delta x_{eq})$, *i.e.* $m = \lfloor (r/\Delta x_{eq}) \rfloor$, then:

$$A_j = 1/2 \left(1 + \cos\left(\pi \frac{j \Delta x_{eq}}{r}\right)\right), \; j = 0 \ldots, m \tag{4.105}$$

$$a_j = \frac{A_j}{\sum_{l=0}^{m_f} A_l}, \tag{4.106}$$

where a_j are non-negative coefficients. The above second relation is a normalisation relation such that $\sum_j a_j = 1$. The number of cooperative vehicles increases with r, increasing by one every Δx_{eq}. Values of those coefficients decrease with the distance to the current vehicle, which seems to be a realistic choice as more importance is given to close vehicles. The values of

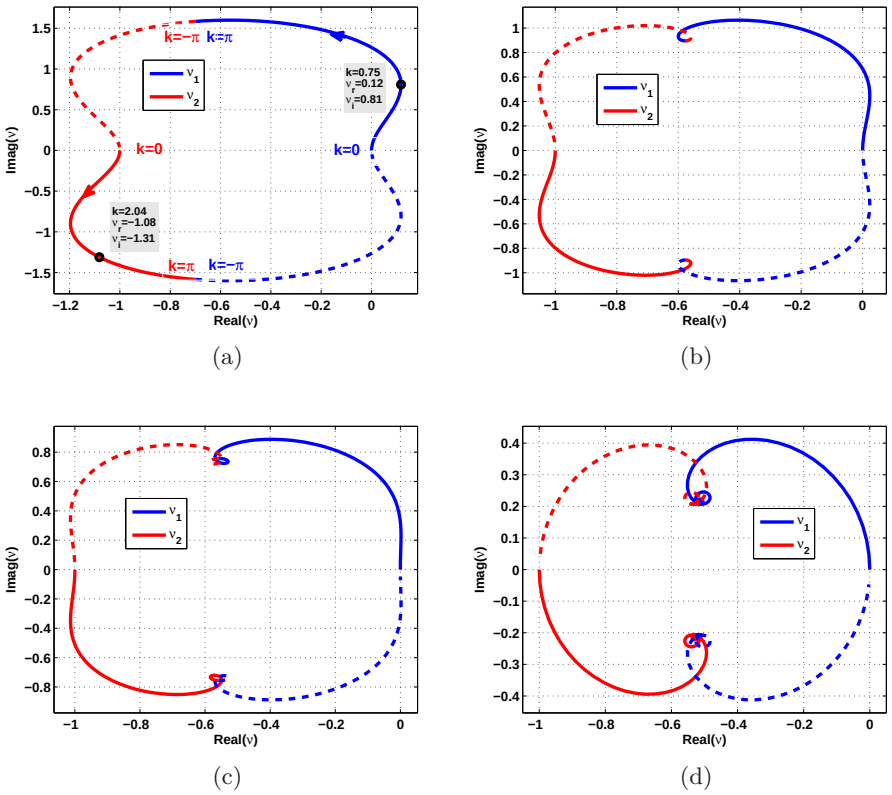

Figure 4.7: Root locus analysis for stabilizing forward multi-anticipation, for (a) $m = 1$, (b) $m = 3$, (c) $m = 4$, (d) $m = 6$

$\gamma = 1.5$ and $\eta = 0.2$ are chosen, which comes out as unstable in the non-

cooperative case, see figure 4.7a where a crossing of the imaginary axis is observable. Figures 4.7a, 4.7b, 4.7c and 4.7d show the obtained results while increasing the interaction range, the number of information data points respectively being $m = 1$, 3, 4, and 6, where $m = m_f + 1$, see (4.4). The stabilization effect due to the increasing number of integrated cooperative vehicles in the car-following law is clearly observed, as in the last figure the whole root locus lies in the stability region.

Destabilization

In the previous subsection, the stabilization of an unstable system by drivers cooperation has been exhibited, using realistic a_j coefficients. However, unstabilization can be obtained through irrelevant choice of the a_j. In order to show this undesirable effect let us take the exemple of the non-cooperative stable system with $\eta = 0.2$ and $\gamma = 0.4$, see figure 4.8a. Coefficients a_j are those of the previous cosine window, but in the reverse order, *i.e.*:

$$A_{m_f-j+1} = 1/2\left(1+\cos\left(\pi\frac{j\Delta x_{eq}}{r}\right)\right),\ j = 0\ldots,m_f \quad (4.107)$$

$$a_j = \frac{A_j}{\sum_{j=0}^{m_f} A_j} \quad (4.108)$$

The a_j coefficients increase with the vehicle number. The result is shown figure 4.8b where $m = 3$. A large part of the root locus lies in the instability region, and intersection points with the imaginary axis are visible, therefore the system is unstable. Actually it appears that the long wavelength instability is preserved while for short wavelengths the real parts are brought in the positive region, causing linear string instabilities.

Besides, the root locus shows that condition (4.35) is only a necessary condition. It cannot be infered from this condition that the system is stable over the whole spectrum. It can be observed that the system is more stable around $k = 0$ than for the non-cooperative one, since the negative coefficient of k^2 in the development in k is greater in absolute value, see 4.32, however instabilities appear in medium and small wavelengths.

When the a'_j are used as the cooperative coefficients, an interpretation of the destabilization can be easily given. Indeed, since the a_j values are increasing with j, their values being 0.003, 0.27, 0.73, it follows from relation (4.101) that $a'_j < 0$ for $j < m_f$ and $a'_{m_f} = a_{m_f}$. In this case the values are -0.26, -0.46, 0.73. Due to the negative sign of the two first a'_j coefficients, this means that, in fact, a driver will react in an opposite manner to perturbations of the two leading drivers dynamics, which explains

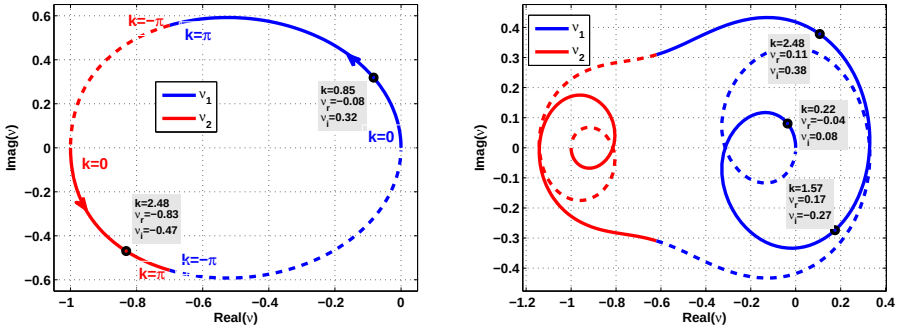

(a) (b)

Figure 4.8: Root locus analysis for destabilizing forward multi-anticipation, for (a) $m = 1$, (b) $m = 3$

the eventual occurence of instabilities. Therefore negative coefficients a'_j, *i.e.* decreasing a_j coefficients with j, correspond to non-realistic behavior. Finally, and this is an important conjecture, from numerical considerations it can be assumed that instabilities are always of the long wavelength type given that coefficients a_j decrease with j.

4.5.3 Collapse of the roots and influence on the wave phase velocity

Several other windows can be tested, such as the exponential window or the window with equal a'_j coefficients. The interested reader can refer to [124] for the study of the exponential window. A simple choice can consist in setting the a'_j all equal, *i.e.* $a'_j = \beta$, $\forall j$. This corresponds to a linear decrease of coefficients a_j with j. Due to the normalisation relation (4.103), the following relation is derived:

$$a'_j = \beta = \frac{2}{(m+1)(m+2)}, \ \forall j. \tag{4.109}$$

Consequently, using relation (4.101), coefficients a_j are:

$$a_j = a'_j (m + 1 - j) \tag{4.110}$$

which shows a linear decreasing dependance in j.

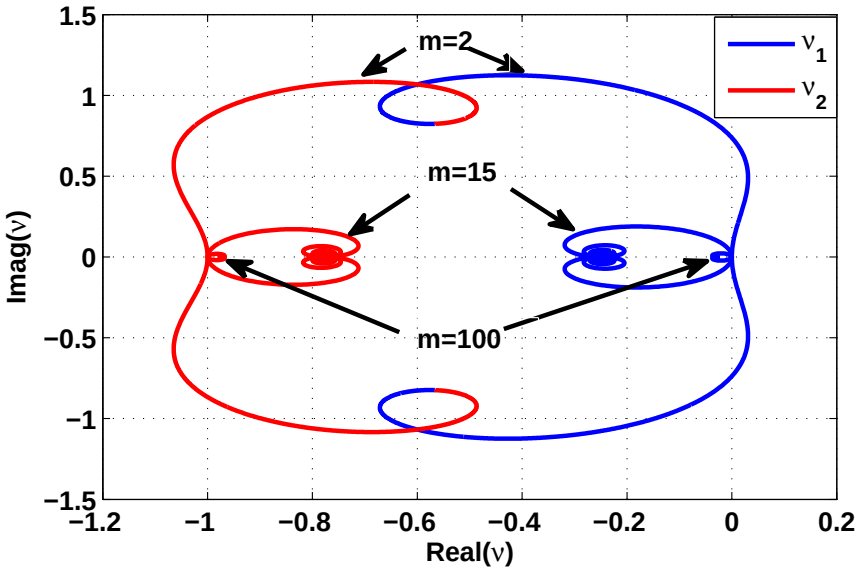

Figure 4.9: Collapse of the roots for increasing m

Since $\sum_{j=1}^{m} \beta \exp(ijk) = \beta \exp(ik)\left(\exp(ikm) - 1\right) / \left(\exp(ik) - 1\right)$ (relation 4.27), this leads to the following expression for K:

$$K = \frac{2}{m+2}\left(\frac{e^{ik(m+1)/2}}{m}\frac{\sin(km/2)}{\sin(k/2)} - 1\right) \tag{4.111}$$

It is now straightforward that $|K|$ decreases to 0 when m increases, *i.e.* with an increasing number of cooperative vehicles. As m increases, a first order limited development gives the roots ν_i

$$\begin{aligned} \nu_1 &= \gamma K, \\ \nu_2 &= -1 + (\eta - \gamma) K. \end{aligned}$$

In this strategy, increasing the number of cooperative vehicles enforces the stability. As an example, let us take the previous unstable non-cooperative system, see figure 4.7a. Figure 4.9 shows the transformation of the root locus with increasing m, clearly reproducing a stabilisation effect in relation with a collapse of the roots. Besides, figure 4.10 also gives information on the damping (exponential decay rate) and the wave phase velocity for a given wave number k, this system being a very unstable non-cooperative one with parameters $\eta = 0.2$ and $\gamma = 1.5$. For the same wave number $k = 0.30$, when

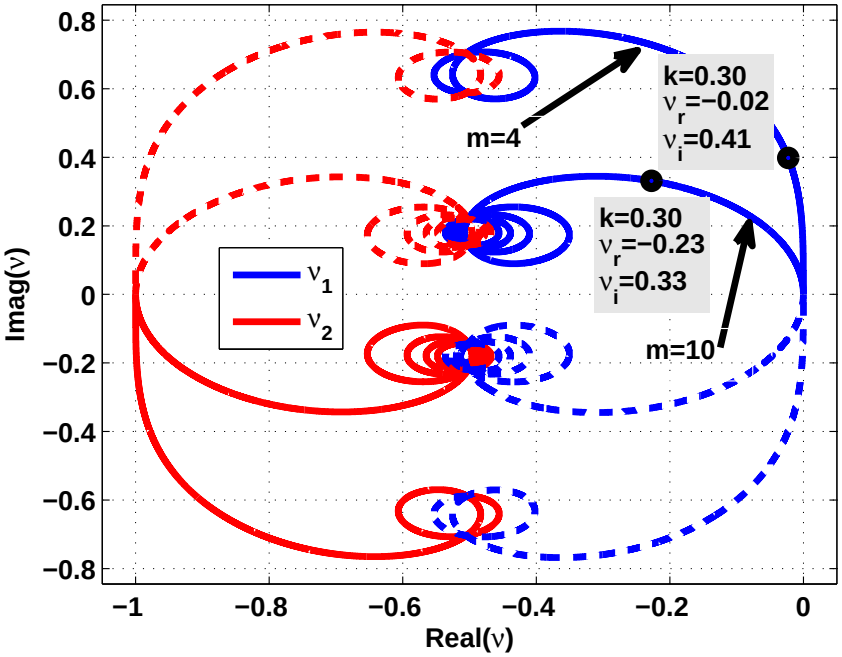

Figure 4.10: Evolution of the damping rate and wave phase velocity with respect to cooperation

m increases from 4 to 10, it can be read that the phase velocity, see equation (4.16), is reduced by about 20% while the exponential decay rate is ten time larger.

4.5.4 Safety margin method

The first criterion to design a cooperative strategy regards linear string stability. To achieve it, the stability at long wavelengths should be increased, which means maximizing the expression $Q_M = \sum_{j=0}^{m_f} j a_j$, with $\sum_{j=0}^{m_f} a_j = 1$, $a_j > 0$, and at the same time short wavelength instabilities should be avoided. Indeed, $Q_M =$ is maximum when $a_{m_f} = 1$, $a_j = 0$, $j < m_f$. Figure 4.8b shows the destabilizing effect of this strategy on the previous stable non-cooperative system, figure 4.8a. By comparison with figure 4.8a, it is observed that the behavior is better at $k = 0$ but fails at shorter wavelengths. These features show there is a balance between the performances at short and long wavelengths, and that a trade-off should be found.

Following this remark, the trade-off would be to locate the root locus sufficiently far from the instability region. However, it is known that the point $k = 0$ is on the imaginary axis. It has been noticed that the root locus is made of several loops, see figure 4.9, each of them possessing a right-most point, which is a maximum of the real part ν_r of the roots. Let ν_{Mr} be the maximum value of these maxima, different to the one for $k = 0$. S_D is the positive distance, called safety margin, from the imaginary axis to the right most point of the root locus loops (with the exception of the $k = 0$ loop, which cannot be avoided). As the behavior near $k = 0$ should also be optimized, the solution is to maximize Q_M with $\sum_{j=0}^{m_f} a_j = 1,\ a_j > 0$, with the constraint $\nu_{Mr} \leq -S_D$: this is the safety margin method.

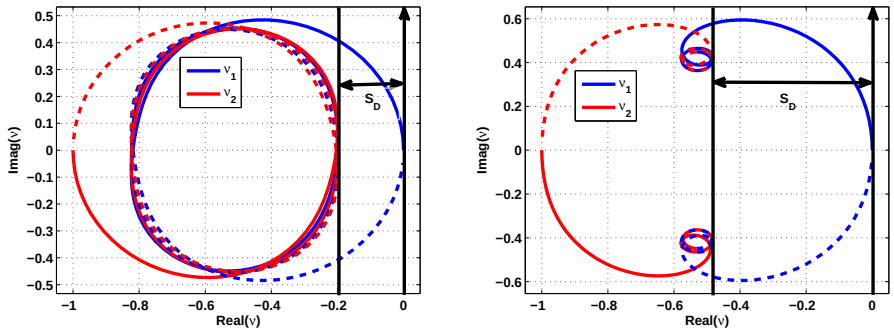

(a) (b)

Figure 4.11: Different weighting windows with corresponding safety margin S_D (a) $S_D = 0.2$, (b) $S_D = 0.5$

Figures 4.11a and 4.11b show the results of the safety margin method for $\gamma = 1.5,\ \eta = 0.2$, which is an unstable non-cooperative system, $m = 6$, and respectively for $S_D = 0.2$ and $S_D = 0.5$, and corresponding coefficients $(a_j)_{0\leq j\leq 5} = (0.29, 0.26, 0.20, 0.14, 0.087, 0.022)$ and $(a_j)_{0\leq j\leq 5} = (0.21, 0.19, 0.18, 0.16, 0.14, 0.12)$. One can observe that, as S_D decreases, coefficients corresponding to high j increase, meaning that long wavelengths stability is being given priority to. At the same time, the decrease of low j coefficients has the effect to bring the short wavelengths part of the root locus closer to the instability region.

It is now possible to conclude over the safety margin method. An identification of the traffic conditions is necessary prior to determining the safety margin S_D. An appropriate traffic model should describe real time traffic in an accurate way, but uncertainties subsist. The model is represented by the

function f (4.3), which is supposed to be calibrated in order to determine the model parameters along with their uncertainties, as it will be presented in section 5. More precisely, with respect to linear string stability, the modelling uncertainties are included in the coefficients η and γ of the dispersion relation (4.25). The values of these coefficients depend on the car following model form and parameters, but also on the equilibrium traffic regime around which the linearisation is performed. Therefore, these coefficients may vary a lot, which, as a consequence, triggers the migration of the root locus. The S_D value must then be chosen large enough so that no crossing of the root locus in the instability region occurs when these coefficients vary but also not too large in order to keep acceptable stability performances at long wavelengths. Given all these considerations, the equality of the a'_j coefficients of relation (4.109), or the cosine window of relation (7.6) are appropriate choices.

4.5.5 Extension to bilateral cooperation and to added linear control terms

To conclude this section, a short discussion regarding bilateral multi anticipation is provided. The case of the very unstable system is taken, with $\gamma = 1.5$ and $\eta = 0.02$, and $m = 3$. The variable is now the number of information data points for backward cooperation, *i.e.* $m' = m_b$. The weighting window is chosen such as $(a'_j)_{0\leq j\leq 2} = \beta$, which gives $(a_j)_{0\leq j\leq 2} = (0.5, 0.33, 0.17)$ for a normalized window. However, in the bilateral case, the forward window is normalized to 2 whereas the backward window is normalized to -1, again with $(a'_j)_{-m'\leq j\leq 0} = -\beta$. This is due to the needs of having negative coefficients for negative j, see 4.3.2 for an explanation. Figures 4.12a, 4.12b, 4.12c, 4.12d, display the root locus with respectively $m' = 0 \cdots 3$. If the same mechanisms as in forward multi-anticipation are observable, this raises the potential importance of bilateral traffic in terms of string stability.

For the tuning of the a_j coefficients, the safety margin methodology described in the previous section 4.5.4 applies. The unstable behavior at long wavelength is eliminated as soon as a backward information is considered, otherwise 3 vehicles are needed to start decreasing the safety margin.

Finally, the impact of an added linear control term can be investigated, and an example of root locus is traced with $\gamma = 1.5$ and $\eta = 0.02$, $f_3 = 0.05$, m=3, m'=1, which was observable in figure 4.12b for nil control terms, and varying control gains c_1 and c_2. Figures 4.13a, 4.13b display the rootlocus for $c_1 = 0$, $c_2 = 1.5$ and $c_1 = 2.0$, $c_2 = 1.5$, which allows to discuss two

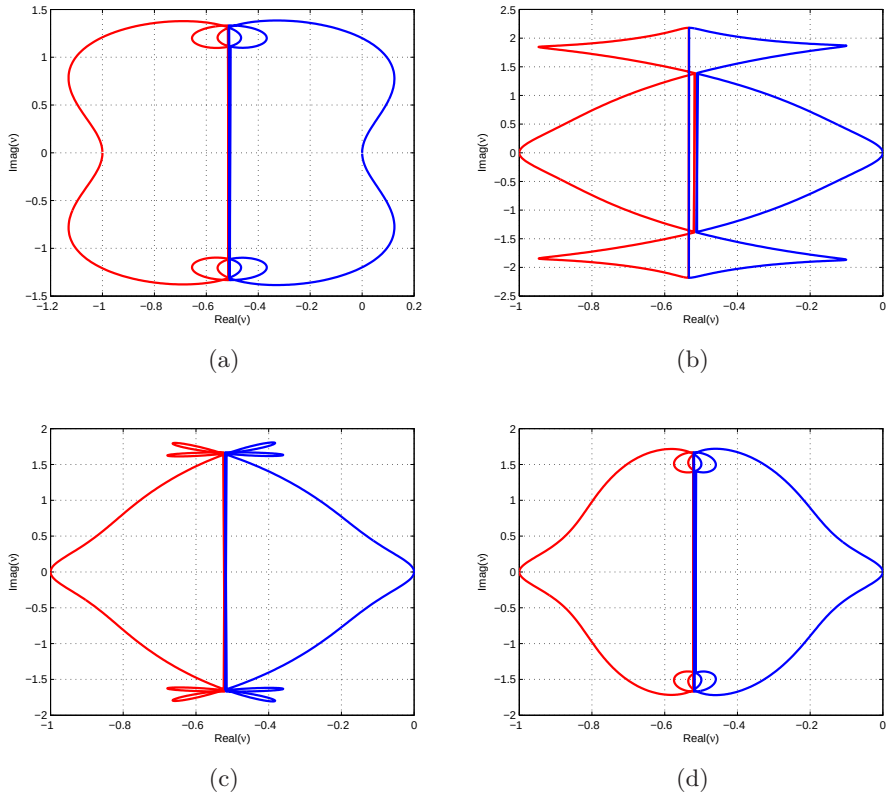

Figure 4.12: Influence of bilateral multi-anticipation, (a) m'=0, (b) m'=1, (c), m'=2, (d) m'=3

observations. First, an increase of the term c_2 does not have a positive influence on short wavelength stability as the safety margin of figure 4.13a ($S_D = 0.12$) is smaller than the one of figure 4.12b ($S_D = 0.08$). Secondly, the term c_1 has a positive influence on both short and long wavelength stability, as the safety margin is being increased by a factor 3 ($S_D = 0.24$) and as the exponential decay rate is also being increased in a significant way at the vicinity of $k = 0$. The influence of c_2 appears negative in terms of stability but could be relevant for control purposes, for instance if the goal is to obtain a homogenous traffic with identical headways. Overall, the observations made in section 4.3.5 are being confirmed by the root locus analysis.

In conclusion, the root locus analysis is a powerful tool to address long

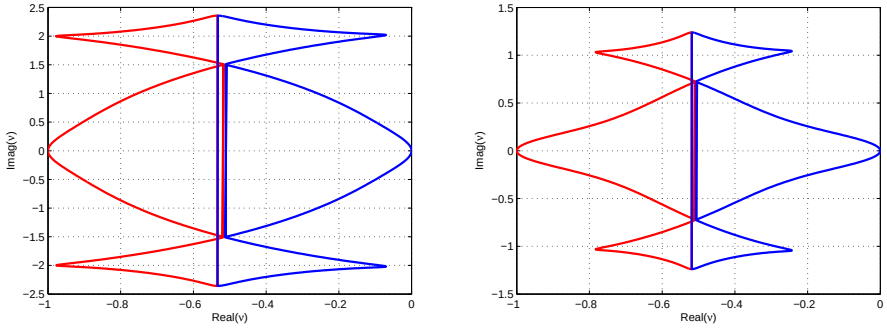

(a) (b)

Figure 4.13: Influence of bilateral multi-anticipation m=3 and m'=1; (a) $c_1 = 0$, $c_2 = 1.5$, (b) $c_1 = 2.0$, $c_2 = 1.5$

wavelength and short wavelentgh instabilities for both forward and bilateral multi-anticipation. If the behavior near $k = 0$ is analytically obtainable through limited developments, the root locus provides a relevant insight on the short wavelength instability, and the safety margin method allows dealing with uncertainties on the model parameters, here embodied by η and γ.

Chapter 5

Car-following parameters identification based on a NGSIM trajectory dataset

Drivers behave in different ways and this is one cause of traffic disturbances. Therefore a key objective for simulation tools is to accurately reproduce this variability, in particular at a microscopic level for car-following models. It has been emphasized that cooperative vehicles should be able to train normal drivers while adopting very similar behaviors as they are more aware of their surrounding environment. The knowledge of the variability of the drivers' behaviors and their reproducibility in simulation are fundamental steps towards assessing the potential of the cooperative vehicles. Those results have to be robust, and can be used for simulation purposes, see chapter 6 and as a basis for agent-based modelling, see chapter 7.

From the data collection to the sampling of realistic behaviors, a chain of key issues must be addressed. In this chapter, data filtering, robustness of calibration, correlation between parameters and sampling techniques of acceleration time continuous car-following models are discussed. With respect to calibration, its robustness is systematically investigated with an objective function that allows to obtain confidence regions around the minimum. Then, the correlation between sets of calibrated parameters and the joint distributions sampling techniques validity are discussed. This validates the needs of adapted calibration and sampling techniques in order to obtain realistic sets of car-following parameters, later used for simulation purposes.

Contents

5.1 From data filtering to sampling of realistic parameters

Among the vehicles trajectories data sources, the Next Generation SIMulation (NGSIM) datasets are the most commonly used [125]. However, it is agreed that, in case of NGSIM data, data correction is a mandatory step, prior to the calibration process, which must follow established rules. A various range of averaging and smoothing techniques can be applied, see [126, 127]. For a review of vehicle data correction techniques, see previous work from Punzo *et al.* [128], Marzack and Buisson [129], and Rakha *et al.* [130]. Assuming the need for data correction, NGSIM trajectory datasets have been extensively studied for calibration purposes in the literature: the methodology of the car-following parameters estimation was discussed in several papers [131, 132, 133, 134], while the estimation of lane changing dynamics was the main preoccupation in [135, 136, 137].

The calibration methodology of car-following models is an active topic within the traffic theory community and most of the initiatives are synthetized in the recent COST action TU0903: the Methods and tools for supporting the Use caLIbration and validaTIon of Traffic simUlation moDEls (MULTITUDE) project [138]. In any calibration procedure, the model to be calibrated, dataset, measure of perfomance (MoP), goodness of fit (GoF) and optimization procedure have to be successively chosen. In [133],

combinations of various optimization algorithms, measure of performances and goodness of fit functions were compared in the light of various performance indicators, which underlined the necessity to correctly bind the parameters space and to limit the calibration to the most sensitive parameters when possible. A recent paper from Treiber and Kesting [98] stated that the robustness of the calibration and parameter orthogonality -when each parameter range corresponds to a driving action- should be relevant criteria to assess the quality of models. Then, once the calibration methodology has been specified, one may be interested in sampling realistic driving behaviors from the calibrated leader-follower trajectories. In that respect, Kim and Mahmassani [134] considered multivariate normal distributions to estimate the correlation between parameters, in order to sample realistic car-following behaviors. Amer *et al.* [139] used cascaded regression and the Cholesky decomposition to capture interaction between the model parameters of a proposed driver decision logit model at signalized interesections.

When calibrating a car-following model, the leader-follower couple must be seen as a dynamical system with the behavior of the leader as input and the resulting motion of the follower as output. Model parameters identification has been extensively studied, some classical references are the books of Ljung and Landau [140, 141]. Assuming that the parameter identification constitutes an observable problem, the methods are all based on the optimization of a criterion involving the comparison between the model and the system outputs (coming up from the same inputs). Then the main issues deal with the choice of the fitting criterion and the most suitable inputs. A simple parameters fitting is not very meaningful. If robust and consistent results are desired, as for any physical quantity, uncertainties or confidence intervals must be given for the fitted parameters. The classical approach is then to maximize the likelihood (or, equivalently, to minimize the negative of the log-likelihood function). In the Gaussian case, this leads to chi-square minimization (see Eadie *et al.* [142], or F.James [143] or chap. 7 of [144]).

Previous and recent works express the need of a methodological framework for car-following parameters analysis and sampling from empirical trajectory data. The sampled sets of parameters could then be used as simulation tools inputs. The main contributions of this chapter are: a complete methodological chain going from empirical trajectory data to realistic sampling of car-following parameters; a robust calibration procedure performed for each leader-follower couple; a full parameters' dependence/correlation analysis by means of complementary Pearson, Kendall, Spearman tests, and multi-dimensional Principal Component Analysis, showing that results are consistent with the parameters physical meanings and previous studies; a

non-parametric Kernel density estimation given the fact that the Gaussian assumption does not apply for all marginal distributions; a comparison of different sampling methods, where correlation-based bootstrap, multivariate normal estimation, multivariate Kernel density estimation as well as more refined combinations are tested.

It is therefore aimed to successively achieve calibration, estimation and sampling of three previously studied time continuous car-following models: the IDM [65], the OVRV [71], and the IOVM [64]. All the numerical experiments are conducted on a NGSIM trajectory dataset. The dataset is the 45 minutes time frame observation (7:50 am to 8:35 am) on a stretch of the Hollywood Freeway (US 101) located in Los Angeles, California. The dataset was collected on June 15th, 2005. The stretch consists of five lanes and includes one on-ramp and one off-ramp. The following study focuses on the car-following behaviors of the two leftmost lanes, that is, those lying farthest from the on- and off- ramps, in order to maximize the fraction of pure car-following situations.

5.2 Data filtering

To record the vehicles trajectories, synchronized video cameras were installed on top of buildings next to the highways. Post processing of images provided vehicle positions every tenth of a second. Then the velocity and acceleration information were numerically derived from the tracked positions.

One characteristic of the NGSIM data concerns its treatment errors when tracking positions from images. When looking at the velocity and acceleration distributions, some spikes are observed, which would mean that vehicles are more likely to evolve at certain values of velocities, sometimes jumping from one value to another. This unrealistic information is certainly due to approximation errors following the time-space discretization of positions. Those spikes are clearly observable in figures 5.1a and 5.1b. Filtering techniques aim at reducing those noises which can have damaging consequences on the accuracy of calibration results.

The outliers leading to unrealistic acceleration and jerk values as well as the random disturbances (potentially coming from the image treatment) both need to be removed. Punzo *et al.* [145] proposed a multi-step procedure to get rid of all the possible biased trajectories in the first I80 dataset sample -which has since been updated. They successively apply a spline interpolation to remove the main outliers, a low-pass filter to cut the high frecuency responses, a polynomial interpolation to remove the residual un-

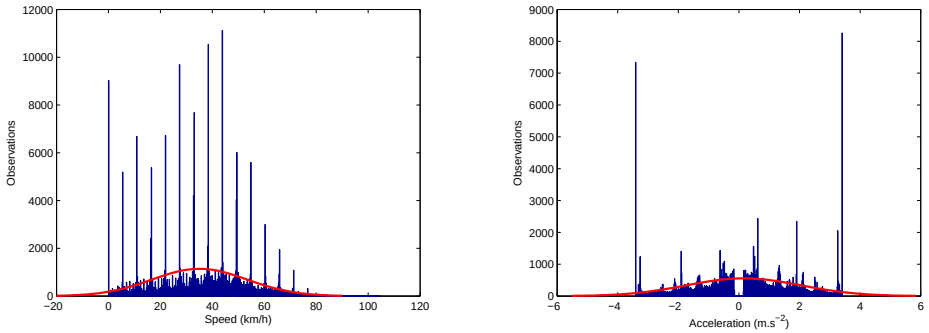

(a) (b)

Figure 5.1: Observed spikes in the non corrected US101 dataset, most left lane: (a) Speed distribution, (b) Acceleration distribution (filtered at |0.2| m.s^{-2}) over a 15 minutes time frame (7:50 a.m.-8:05 a.m.).

physical accelerations, and again a low-pass filter. As no such outliers were observed in the most recent updated online version of the US101 dataset, a simple low pass filter was selected to remove the main inconsistencies. Other robust filtering techniques can be relevant alternatives, particularly for online filtering of noisy trajectories with presence of outliers [130].

Here the study has been performed for the speed filtering as the time series of the followers speeds will serve as the measure of performance (MoP) in the model calibration. Note that other MoPs can be used, see [145] for a discussion. A low-pass Butterworth filter (cutting frequency $f_c = 0.07$ Hz, order $n = 4$) is used and compared with the exponential moving average filter used by Kesting *et al.* [131] (a smoothing window of 10 time steps was chosen, accordingly to their paper). It is observed that the Butterworth filter helps keep more variation in the speed profile (figure 5.2) while reducing the spikes in the satisfactory way, see figures 5.3a and 5.3b. The gain and the impulsive response (figure 5.4a and figure 5.4b) show that the Butterworth low-pass filter high frequencies in a more drastic way than the exponential filter. Note that for the Butterworth filter, in order to annul the phase angle, the discrete signal has to be filtered along forward and backward directions, which as a consequence double the order of the filter. Such spikes are unfortunate as they are likely to introduce bias in the calibration process, however they cannot be totally removed, as a more drastic filter will cause a loss of information.

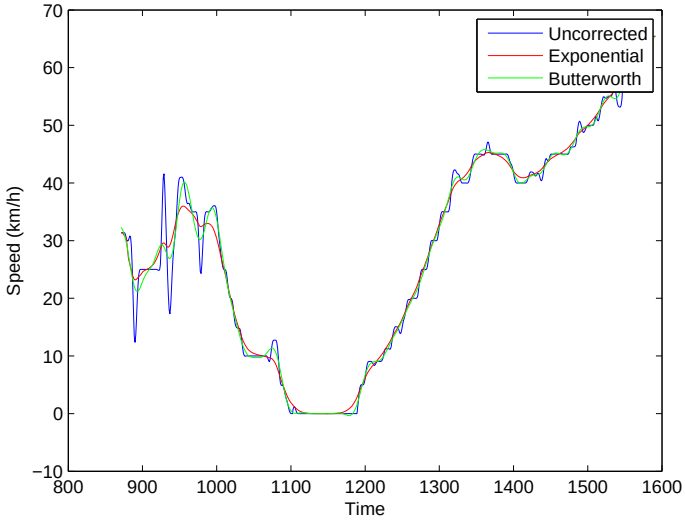

Figure 5.2: Vehicle speed trajectory

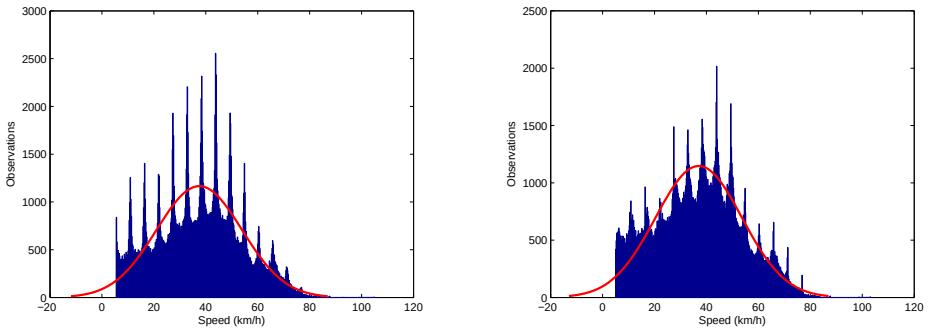

(a) (b)

Figure 5.3: Speed distributions (filtered > 5 km/h): (a) Butterworth filter; (b) Exponential filter.

5.3 Calibration and robustness

5.3.1 Choices for the calibration procedure

Note that for all the acceleration time continuous car-following models 5 parameters have to be calibrated. The Measure of Performance is chosen to

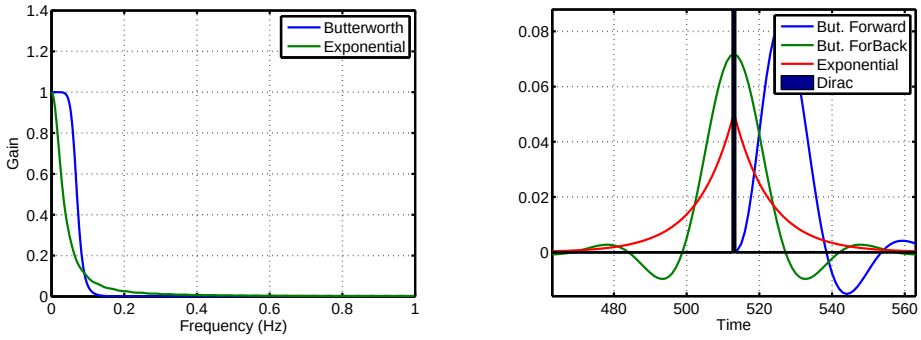

(a) (b)

Figure 5.4: Comparison between filters: (a) gain for the forward backward low-pass Butterworth filter and the exponential filter; (b) impulse response for the forward Butterworth filter, the forward backward Butterworth filter, the exponential filter.

be the time series of the follower's speed, as in [145]. The Goodness of Fit is picked as a χ^2-function such as in [144]

$$\chi^2 = \sum_{i,j}(x_i - y_i(a))\Gamma_{ij}^{-1}(x_j - y_j(a)), \tag{5.1}$$

where x is the vector of observations (speed for each time step) and $y(a)$ the speed computed with the set of fitted values a, Γ is the error covariance matrix. Γ is set to be diagonal if there is independance between the measurement errors, and its diagonal is chosen to be equal to the standard deviation of the difference between filtered and non-filtered speeds. A specific advantage of this MoP (and it is also the case for a negative log-likelihood function) resides in its statistical interpretation. If a hypercontour is drawn such that $\chi^2 = \chi^2_{\text{min}} + \text{UP}$, where UP is the distance of the minimum χ^2_{min}, there is for example a probability of 90% that two parameters simultaneously take values within a contour with $up = 4.61$ (see [144] and table 5.1).

Then, a genetic algorithm with penalty function [131] (in case of collision or unrealistic deceleration/acceleration, the average of realistic acceleration values being selected as $-7.5 < \ddot{x} < 3.5$ m/s^2) is used, with the maximum number of generations set to 130. The bounds of the parameters were fixed after some testing experiments, and in accordance to values in the litterature [64]. Note that other optimization procedures could also be selected, such as the downhill simplex method [133], which is a gradient-free uncon-

	Confidence level for UP values				
Number of parameters	50%	70%	90%	95%	99%
1	0.46	1.07	2.70	3.84	6.63
2	1.39	2.41	4.61	5.99	9.21

Table 5.1: Table of UP for multi-parameter confidence regions

strained optimization technique, or the OptQuest Multistart method, which combines a gradient based local Non-Linear Programming (NLP) solver with scatter search global optimization [146].

5.3.2 On the robustness of calibration: an example

In any calibration procedure the choice of suitable inputs (here leading vehicles) is critical. For example, the steady-state calibration of car-following models, *i.e.* when leaders and followers have similar speeds, can be relevant as the identified parameters are highly correlated to the macroscopic traffic variables [147]. Besides, inputs have to sufficiently excite the system in order to be informative, *i.e.* highly perturbated with rapid variations (see Ljung, Landau [140, 141]). However in this case, the inputs, *i.e.* the trajectories of leaders, are those available in the dataset, a lot of them with a relatively smooth behavior corresponding to a non perturbed traffic. More leaders with aggressive behaviors would have been better adapted to an efficient parameter identification. More precisely, in a schematic description, a population of too soft drivers providing non perturbed traffic situations results in very poor parameter identification conditions, except for the free-flow speed. Highly perturbed drivers trajectories are needed and in order to illustrate this effect, two leader-follower couples were generated for a duration of $T_2 = 20$s. The leading vehicles were generated as seen in figure 5.5, and the following vehicles generated through the IOVM model with the set of parameters $\tau = 2.0$ s, $V_{\max} = 50.0$ km/h, $\gamma = 0.5$ s^{-1}, $s_0 = 3.0$ m, $T_0 = 1.0$ s. A noise $v = 0.1$ km/h was added to the leader's trajectory to test the robustness of the estimation to a measurement noise. Figure 5.6a, 5.6b, 5.6c, 5.6d displays the contour of χ^2 for the two different leader trajectories used as references.

The results clearly show that the original parameters have been efficiently identified in the second case (highly perturbed leader), and very poorly -even wrongly- in the first (soft leader). It also shows that the addition of a noise completely changes the calibration result in the case of a soft

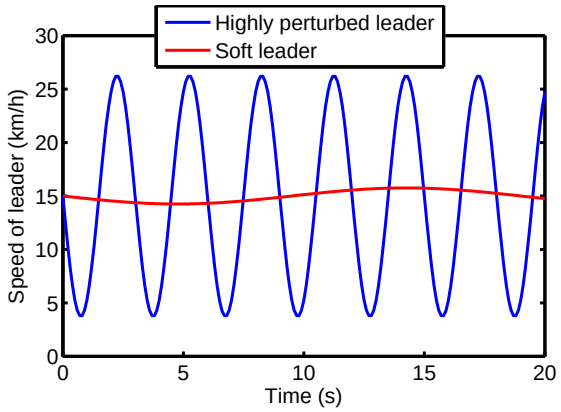

Figure 5.5: Soft and highly perturbed leading vehicles

leader. One can easily understand that in the extreme case of a very soft leader with almost constant velocity, no parameter identification can be performed. It must be mentioned that, for efficient identification experiments, the extensively used inputs are Pseudo Random Binary Sequences (PRBS) (see [140, 141]), which are more perturbed than the sinus functions used in figure 5.5 but less realistic in the traffic context. There is a consequence of this discussion on the relevancy of inputs: in the dataset population, leader-follower couples with too soft leaders have to be removed as they could lead to wrong calibrated parameters. Therefore, in our analysis, leader-follower couples with leader's speed standard deviation lower than a given threshold have been filtered from the population. Note that for this specific dataset, it is argued that this filtering choice does not perturb the estimate of the free-flow speeds, as vehicles were observed to adopt periods of constrained free-flow and periods and stop and go waves along their trajectories.

5.3.3 Calibration results

The calibration was performed on the two leftmost lanes, which were subject to stop and go waves. There were 445 vehicles for the leftmost lane and 559 vehicles for the second leftmost lane. As specified in the above discussion, the leaders speed standard deviations above 11.0 km/h were selected, which represent 594 vehicles in total so 59% of the trajectories. If any of the calibrated parameter reached the 1% around its predefined boundary, no physical minimum was found and the calibrated set was discarded. When the generations reached the maximum set number of generations (130), the set was discarded as well. Results for the two lanes were then merged, which

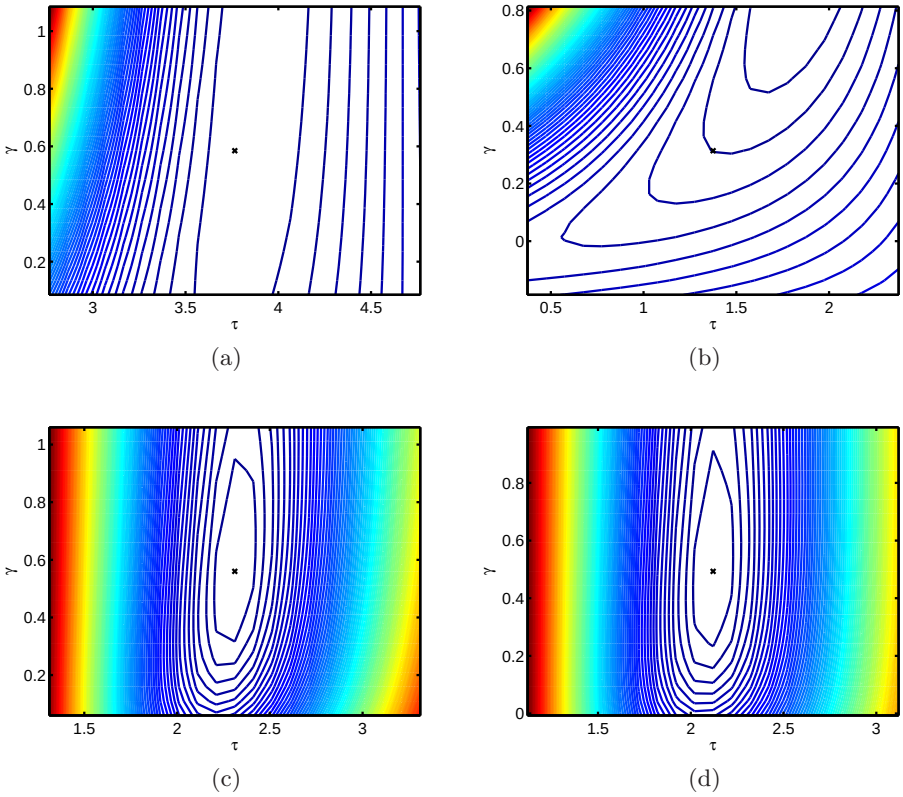

Figure 5.6: Contour of χ^2 values for the IOVM parameter identification around the found minimum (black cross at the center of each figure) for: (a) soft leader without added noise, (b) soft leader with added noise; (c) highly perturbed leader without noise, (d) highly perturbed leader with noise.

gave a total of 417 sets of parameters for the IOVM, 403 for the OVRV and 374 for the IDM model. This is due to the strong non-linear behavior of the IDM model. As for the goodness of fit values, the three models gave very comparable results, the IOVM and IDM model being slightly better.

The statistical meaning of the χ^2 fitness function has its importance to assess the robustness of the calibration, as introduced in section 5.3.1. For example, if UP is set equal to 1 and the contour curve is drawn, the probability that the true value of one parameter lies within the contour is 68.3%, and this corresponds to the probability of a normally-distributed parameter lying within one standard deviation of its mean. In case of two

parameters, the probability that parameter one and parameter two simultaneously take on values within the one standard deviation likelihood contour is 39.3%, see [144]. Following these considerations, one concept appears to be essential. The calibration should be reproducible, meaning that different comparable minima should not exist. Indeed, if different sets of parameters correspond to the same driving behavior, the model is not orthogonal in the sense of Kesting and Treiber [64, 98]. A flat minimum for a couple of parameters means that different values are admissible to describe the same driving behavior. The found minimum should not be flat, so that the estimation can be called as robust.

Figures 5.7, 5.8, 5.9 display the contour curves of UP values (see section 5.3.1) for a calibrated follower with a leader's standard deviation of 20.8 km/h, for all the possible parameters couples of the three calibrated models. The contour curves of UP values are chosen as the second line of table 5.1 (for two parameters), and then from 20 to 250 with a step of 10. As a result, the probability that two parameters simultaneously take on values within the area of the first contour (1.39 standard deviations) is 50%, whereas the probability that two parameters simultaneously take on values within the area of the fifth contour (9.21 standard deviations) is 99%. Therefore an empty space inside the first contour reveals a flat minimum, and proper ellipsoids allow to identify regions of confidence. It appears that for this calibrated follower, the most robust minimum are found for the OVRV and IDM models. More generally, although the IDM and OVRV model exhibit more non-linearities and consequently require more refined optimization techniques to identify their minima, they are shown to reveal steeper contours around it. This is due to the form of the models that are close to driving situations in comparison with the IOVM model which was first derived from the triangular fundamental diagram, see section 3.1.3. Note that, as specified earlier, the OVRV is not a complete model as it fails to describe free-flow situations [64], however this work only focuses on dense traffic.

Following these calibration considerations, the distributions of the calibrated parameters are displayed in figure 5.10, with Gaussian and Kernel fitting approximations, which are detailed in the next section. It is noticeable that the shapes of the calibrated distributions are rather balanced, with only parameter s_1 of the IDM model that is concentrated on the boundary, which is normal as it represents the minimum gap tolerated in a dense traffic. Parameters a, T_1, T_0 and h_c present the most normally distributed parameters. From these distributions, one would like to sample sets of parameters to be able to simulate a realistic traffic that include drivers behavior variability.

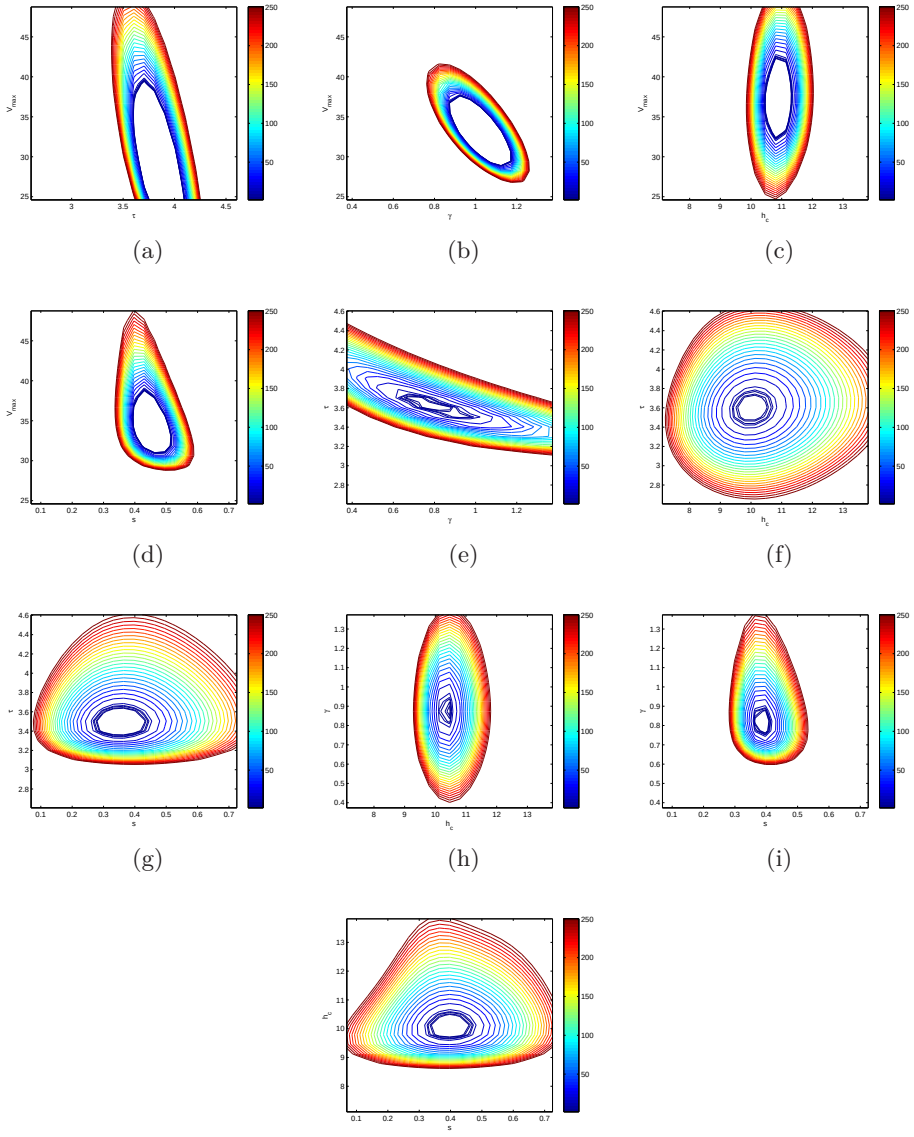

Figure 5.7: Contour of UP values for the OVRV parameter identification for parameter couples (a) $(V_{\max}, \tau)$, (b) $(V_{\max}, \gamma)$, (c) $(V_{\max}, h_c)$, (d) $(V_{\max}, s)$, (e) (τ, γ), (f) (τ, h_c), (g) (τ, s), (h) (γ, h_c), (i) (γ, s), (j) (h_c, s).

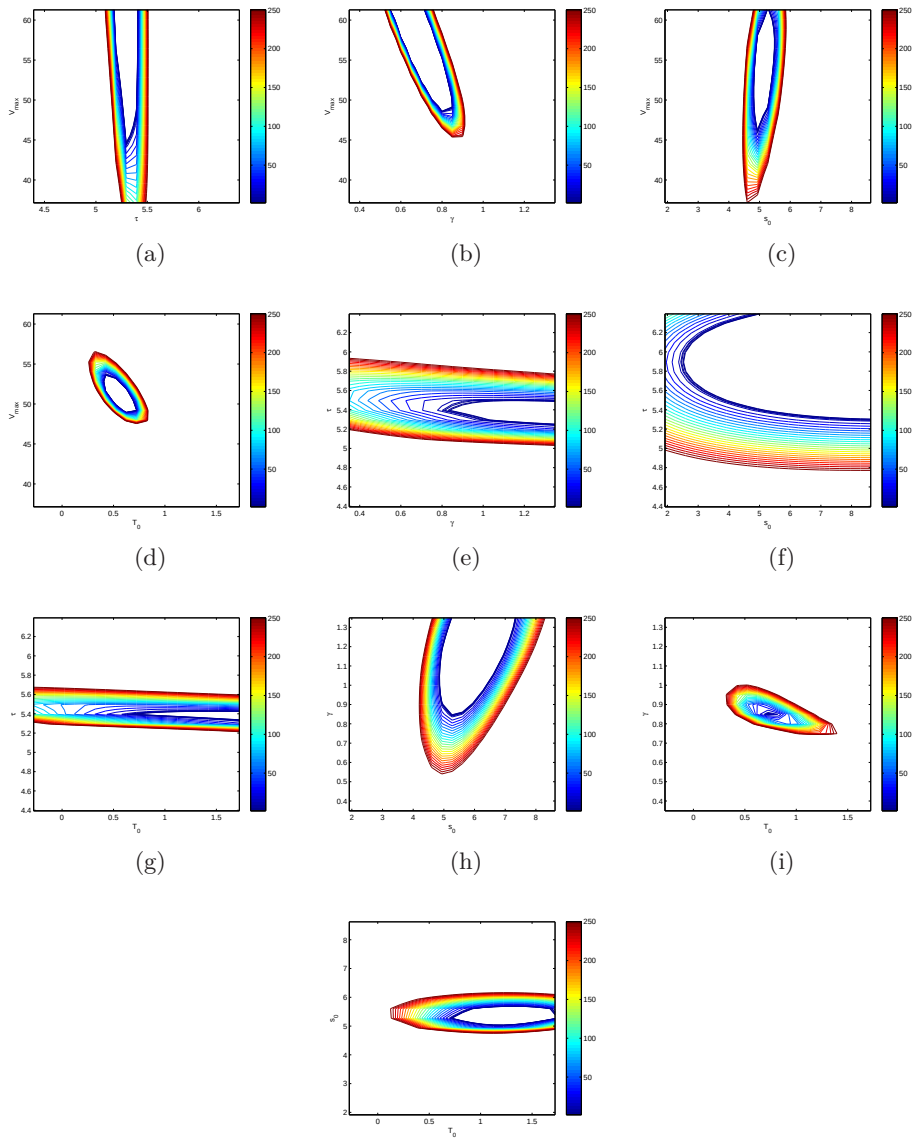

Figure 5.8: Contour of UP values for the IOVM parameter identification for parameter couples (a) $(V_{\max}, \tau)$, (b) $(V_{\max}, \gamma)$, (c) $(V_{\max}, s_0)$, (d) $(V_{\max}, T_0)$, (e) (τ, γ), (f) (τ, s_0), (g) (τ, T_0), (h) (γ, s_0), (i) (γ, T_0), (j) (s_0, T_0).

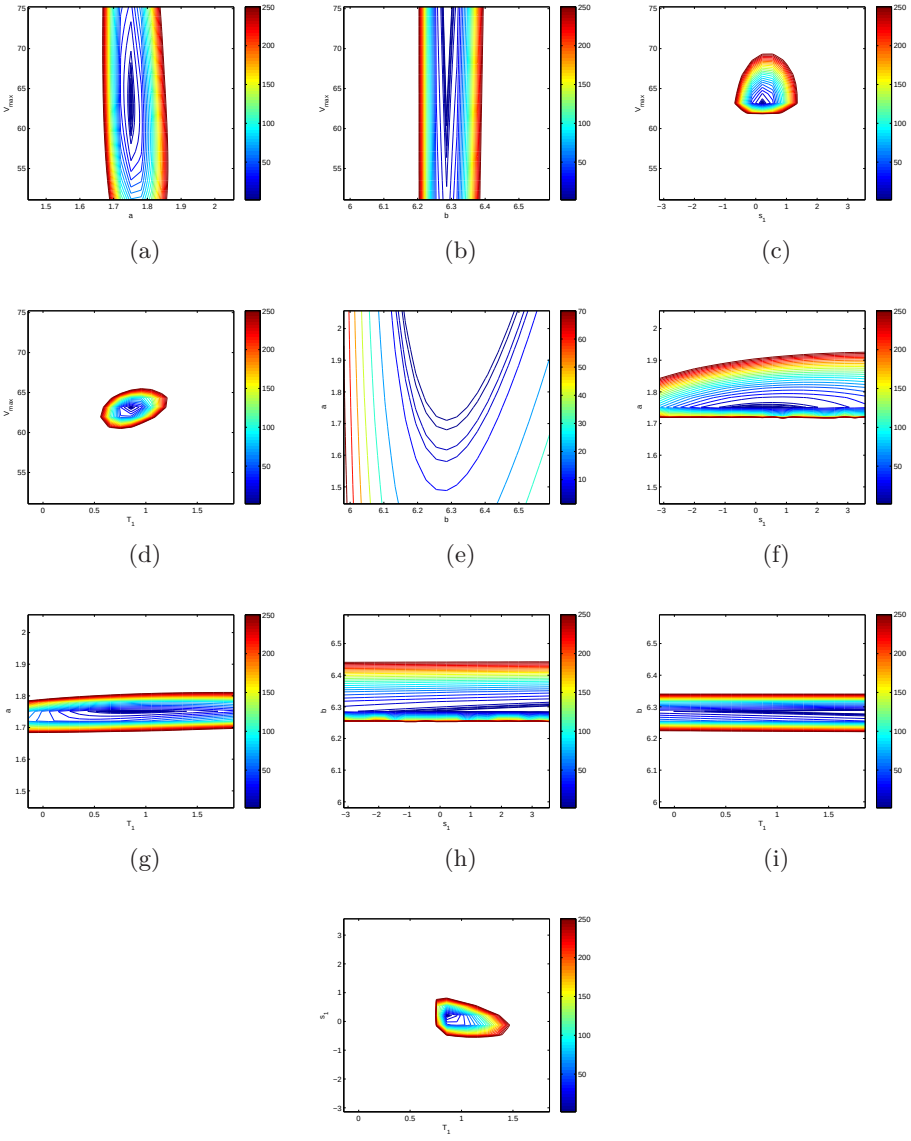

Figure 5.9: Contour of UP values for the IDM parameter identification for parameter couples (a) $(V_{\max}, a)$, (b) $(V_{\max}, b)$, (c) $(V_{\max}, s_1)$, (d) $(V_{\max}, T_1)$, (e) (a, b), (f) (a, s_1), (g) (τ, T_1), (h) (b, s_1), (i) (b, T_1), (j) (s_1, T_1).

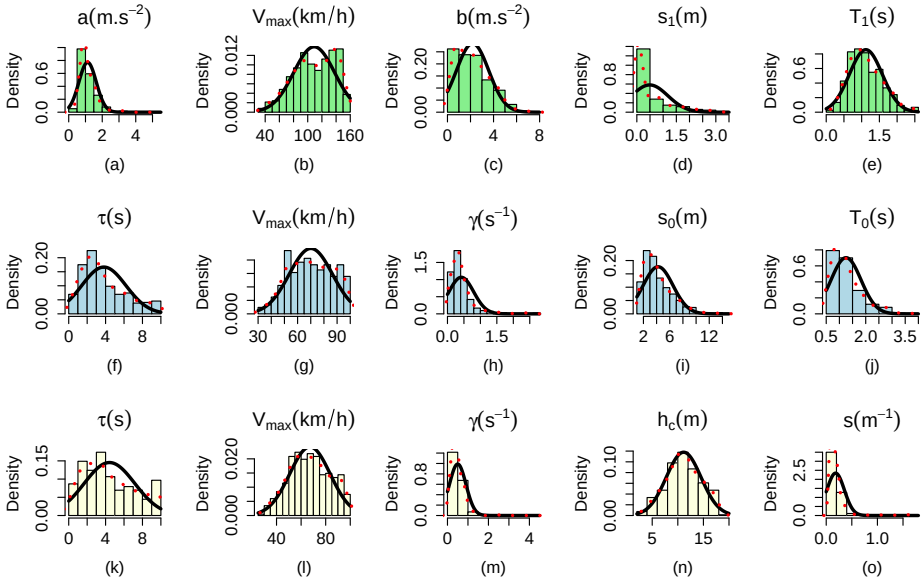

Figure 5.10: Parameters Distribution for the (a),(b),(c),(d),(e) IDM model; (f),(g),(h),(i),(j) IOVM model; (k),(l),(m),(n),(o) OVRM model

This first relates to statistical analyses of those distributions.

5.4 Statistical analysis of parameters distribution

In this subsection, the parameter structures are analyzed and some dependence patterns among parameters are highlighted in both quantitative and qualitative ways. The datasets used for this analysis are the parameters resulting of the calibration of the three models as described above. Thus, for the OVRV, IOVM and IDM models, there are samples of about 400 parameters sets (400 rows of 5 parameters). The goal is to understand the correlation between these parameters as well as their dependence and mutual influence through multidimensional analyses. Regarding the analysis of parameters' distribution, the proposed work is inspired by the work by Kim and Mahmassani [134]. Alternative methods are proposed for identified methodological points in order to address some unresolved issues in previous research efforts.

5.4.1 Parameters dependencies

After calibrating car-following models and with the perspective of sampling realistic sets of parameters, the dependency issue between different parameters has to be tackled. These dependencies can be explained by physical considerations (causalities) or in a more simple way by statistical correlations. It is expected that considering the correlation structure while sampling from parameter vectors will reduce the error and the generation of unrealistic vehicles behavior. The dependency issue has been extensively studied and different measures can be used. The default measure (as used in [134]) is the Bravais Pearson correlation coefficient written for a couple of random variables X_i and X_j as

$$r_{ij} = \frac{E(X_i X_j) - E(X_i)E(X_j)}{\sqrt{Var(X_i)Var(X_j)}.} \tag{5.2}$$

Its weakness lies in the linearity and Gaussian assumptions. One criticism lies in the fact that the more data is available, the easier a link between variables can be identified. In addition to the Pearson test, the Kendall's τ and the Spearman ρ tests consist in testing a correlation between paired samples, using Pearson's product moment correlation coefficient. Actually, the three tests are tests of no correlation (null hypothesis) and the rejection of the null hypothesis allows concluding on a statistically significant correlation between two distributions. The Pearson correlation method remains an acceptable first step to conclude over some links between parameters. The two used additional methods are more often used if the data does not necessarily come from a bivariate normal distribution and are less sensitive to extreme values [148, 149].

The concepts of concordance and discordance enable a better understanding of two major alternatives to the Pearson's coefficient: the Kendall's τ and the Spearman ρ. Between two random variable couples (X_1, Y_1) and (X_2, Y_2), independent and identically distributed, concordance and discordance are the probabilities $P\big((X_1 - X_2)(Y_1 - Y_2) > 0\big)$ and $P\big((X_1 - X_2)(Y_1 - Y_2) < 0\big)$. In other words, these are the probabilities to simultaneously obtain:

- For the concordance: $(X_1 < X_2)$ and $(Y_1 < Y_2)$ OR $(X_1 > X_2)$ and $(Y_1 > Y_2)$,
- For the discordance: $(X_1 < X_2)$ and $(Y_1 > Y_2)$ OR $(X_1 > X_2)$ and $(Y_1 < Y_2)$.

These criteria can model non-elliptic distribution dependencies and are generally more robust [148]. For two random variables X_i and X_j, Spearman's ρ is given by :

$$\begin{aligned}\rho(X_i, X_j) &= 3P\big((X_i - \bar{X}_i)(X_j - X'_j) > 0\big) \\ &\quad -P\big((X_i - \bar{X}_i)(X_j - X'_j) < 0\big),\end{aligned} \tag{5.3}$$

where (X_i, X_j), $(\bar{X}_i, \bar{X}_j)$, (X'_i, X'_j) are independent duplicates. Finally one can see that Spearman's ρ is a rank-based measure of the correlation [150]. Kendall's τ is defined as

$$\begin{aligned}\rho(X_i, X_j) &= P\big((X_i - \bar{X}_i)(X_j - \bar{X}_j) > 0\big) \\ &\quad -P\big((X_i - \bar{X}_i)(X_j - \bar{X}_j) < 0\big),\end{aligned} \tag{5.4}$$

where (X_i, X_j) is again an independent copy of $(\bar{X}_i, \bar{X}_j)$. Thus, Kendall's τ represents the difference between concordance and discordance.

	a	$V_{\max}$	b	T_1	s_1
a	1.000	-0.105	0.304	-0.011	0.092
	1.000	-0.050	0.246	-0.061	0.044
	1.000	-0.075	0.353	-0.088	0.064
$V_{\max}$	-0.105	1.000	0.015	-0.046	0.051
	-0.050	1.00	0.008	-0.034	0.043
	-0.07	1.000	0.011	-0.048	0.067
b	0.304	0.015	1.000	-0.090	0.164
	0.246	0.008	1.000	-0.069	0.091
	0.353	0.011	1.000	-0.105	0.138
T_1	-0.011	-0.046	-0.090	1.000	- 0.061
	-0.06	-0.034	-0.069	1.000	-0.093
	-0.088	-0.048	-0.105	1.000	-0.134
s_1	0.092	0.051	0.164	-0.061	1.000
	0.044	0.043	0.091	-0.093	1.000
	0.064	0.067	0.138	-0.134	1.000

Table 5.2: IDM model. Pearson's correlation coefficients (white lines), Kendall's τ coefficients (light gray lines), Spearman's ρ coefficients (dark grey lines).

The results can now be presented for the three models. The quantitative values of table 5.2 enable a first conclusion: variables are very dependent

on the criterion used and conclusions may vary significantly. The presentation of these three alternatives enables a first comparison with Kim and Mahmassani's methodology [134]. One can focus (for example) on the association between a, the maximum acceleration, and $s1$, a minimum net stopped distance from the leader in the IDM model. In [134], there is a Pearson correlation value of 0.169 and a statistical test leads to a significant correlation between the two parameters at a significance level 0.01. The problem is that this conclusion strongly depends on the used correlation concept and on the dataset in general. In this case, the two parameters are not significantly correlated. With Pearson coefficient, which was used by the previous authors, the statistical test is very close to rejecting the null hypothesis with a p value of 0.07. In this study a different but close conclusion is drawn. However, with Kendall and Spearman methods, which are more robust and non parametric, correlations values are usually smaller and hypothesis tests lead to different results. In table 5.2, it can be observed that Pearson's method can lead to different conclusions by comparison with the two other methods that generally agree with each other. The main conclusion for this introductive analysis is that correlation exists, can be statistically significant, but strongly depends on the measure of association. Actually, this first step is necessary to put in evidence the correlation but not sufficient. Nevertheless, a non rejection of the correlation hypothesis for the three methods (Pearson, Kendall and Spearman) is a good indicator of a significant link within a couple of parameters. With respect to the IDM model, results show that a and b (maximum acceleration and comfortable deceleration) as well as b and $s1$, are correlated. These conclusions are physically well sounded as the parameters seem influenced by aggressive or cautious driving styles. Kendall and Spearman's methods underline relevant links between $T1$, a desired safety time headway, and $s1$, which also corresponds to a degree of aggressiveness.

The results are then presented for the two other models with the Kendall's method, first the correlations coefficients, then the results of the statistical test (gray cases in table 5.3).

Regarding the OVRV model, see table 5.3, a correlation between s, a smoothing coefficient, and all the other parameters is evidenced. This is due to the strong influence of s which operates as a scaling factor in the partial derivative f_2, and therefore has a major influence on traffic physics. As for the other parameters, it appears that h_c, a critical headway for constrained behavior, is correlated with τ, a perception reaction time. Moreover, h_c is also correlated with γ, a sensitivity to the relative velocity. These two associations are physically consistent since one could expect a positive

	τ	$V_{\max}$	γ	h_c	s
τ	1.000	-0.013	0.036	0.083	0.119
$V_{\max}$	-0.013	1.000	-0.011	0.060	-0.303
γ	0.036	-0.011	1.000	-0.110	0.168
h_c	0.083	0.060	-0.110	1.000	-0.108
s	0.119	-0.303	0.168	-0.108	1.000

	τ	$V_{\max}$	γ	$s0$	T_0
τ	1.000	0.007	0.140	0.008	-0.003
$V_{\max}$	0.007	1.000	-0.006	-0.094	-0.062
γ	0.1409	-0.006	1.000	-0.068	-0.230
s_0	0.008	-0.094	-0.068	1.000	0.013
T_0	-0.003	-0.062	-0.230	0.013	1.000

Table 5.3: OVRV and IOVM models. Kendall's τ. Correlation values and statistical tests.

correlation between reaction time and a safe headway as well as a negative correlation between a safe headway and a sensitivity to the relative velocity. With respect to the IOVM model, a positive correlation between τ and γ implies their tendency to describe sensitive *vs* aggressive driving behaviours. This particular aspect is confirmed by the relationships between γ, s_0 and T_0. Note that in general, and for the three models, the relations between parameters tend to highlight and oppose aggressive and cautious behaviors, reactive and smooth behaviors.

While these correlation coefficients (of parameters) provide direct quantitative measures, the use of multidimensional analyses can help confirm qualitative aspects and better interpret these results.

5.4.2 Multi-dimensional analysis

Following the ideas of Kim and Mahmassani, multi-dimensional analyses are carried out in order to observe in a qualitative way which variables contribute to the different axes in a factorised representation of the original dataset. Results from a Principal Component Analysis (PCA) [151, 152] are presented. Its principle is to create from linear combinations of existing variables new principal components which are linearly uncorrelated variables, and the two first components of which should account for as much variability as possible

(high variances). PCA is in fact an orthogonal linear transformation which aims at maximizing the variance scores on the principal components.

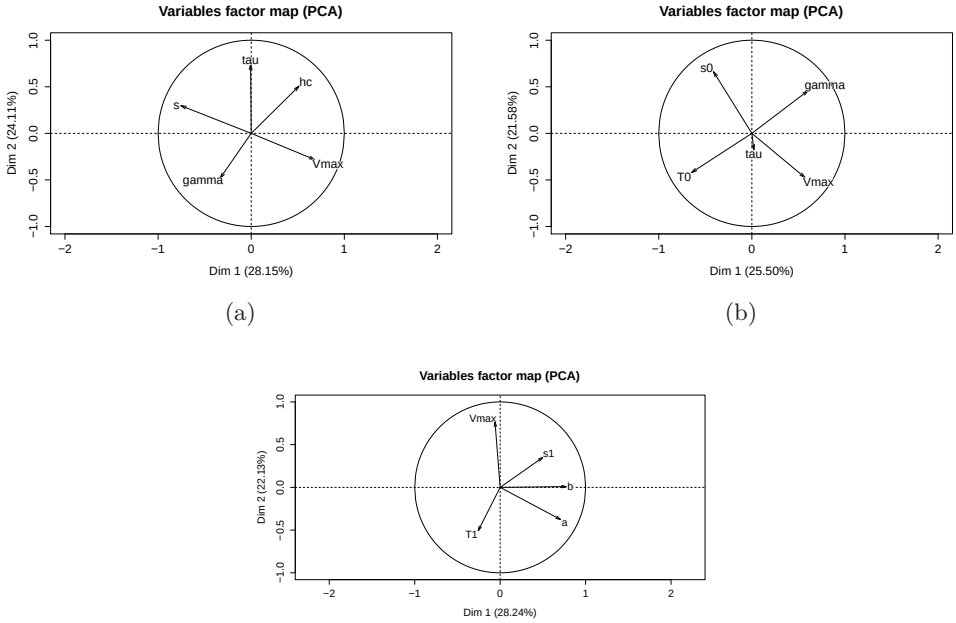

(a) (b) (c)

Figure 5.11: Principal Component Analysis for the (a) IDM, (b) IOVM, (c) OVRV model.

By keeping the first two factors or principal components, the variable points can be displayed on the circle of correlation corresponding to the PCA, see figure 5.11. To each variable is associated a point for which the coordinate on a factorial axis represents a measure of the correlation between the variable and the factor. By projection onto the factorial space, points of the variables are part of a circle of radius 1 called the circle of correlations. The closer the points are to the extremity of the circle, the best they are represented on the factorial plan. Hence only well-represented variables can be interpreted. For OVRV and IOVM models, a comparable structure is visible and the variables s, γ, h_c, $V_{\max}$ (OVRV) and s_0,γ, T_0,$V_{\max}$ (IOVM) are well represented by the two first factors. As for the IDM, the representation is satisfactory as well. With respect to the association between variables, the measure of interest is the angle between two variables, which cosine is equal to the linear correlation coefficient. Thus, if two points are

close, they are highly positively correlated whereas two opposed points are highly negatively correlated. If an angle is equal to 90 degrees, then there is no linear correlation between the two variables. It is now possible to make interpretations about the parameter structures that confirm the previous quantitative analysis:

- IDM : s_1, a, b contribute to the first axis by opposition with T_1, highlighting the relation between a and b. On the second axis, there is a contrast between $V_{\max}$ and T_1. The analysis highlights a clear opposition between aggressive and cautious driving behaviours. There is a negative correlation between s_1 and T_1. These conclusions are consistent with Kim and Mahmassani's conclusions.

- OVRV : there is a form effect that opposes h_c, $V_{\max}$, to s and γ on the first axis. This dichotomy can be interpreted as a difference between fast but cautious drivers and slow and less reactive ones. On the second axis, high reaction times and repulsiveness to the leader are opposed to low speed and speed difference perceptions. This axis clearly opposes very reactive to passive driving styles. Regarding variable correlations, previous conclusions are validated. There is a high negative correlation between s and $V_{\max}$ as well as γ and h_c. These conclusions are satisfactory since a high repulsiveness to the leader and hence a large safe headway can lead to a low perception of the speed differentials. Variables with 90 degree angles present no correlations and validate the previous analyses.

- IOVM : τ is not well represented by the first two factors and must be disregarded. The same structure as in the OVRV model is obtained but some parameters are different. On the first axis, drivers will present high γ and $V_{\max}$ values, which are not linked together. This axis opposes fast to slow drivers. It is noticeable that slow drivers will have high time gap values since variables T_0 and s_0 are highly correlated with the first axis. However, these two variables are not correlated to each other and are opposed on the second axis.

The performed multi-dimensional analyses and the analyses of the dependencies between parameters can serve as inputs for the estimation of joint density functions.

5.5 Joint estimation and sampling strategies

In this subsection, different strategies to estimate a joint parameters density function from the empirical marginals are presented. Based on these different estimation methods, sampling strategies can be discussed by comparing simulated trajectories with real and calibrated data. The objective of this section is to propose parameters density estimation techniques that will preserve the correlation structure of the original calibrated dataset [134].

5.5.1 Empirical distributions and joint estimation

The parameters distributions are observed *via* density histograms, as presented in the calibration section (figure 5.10). Most of the articles published on the topic are based on the assumption of normality (or log-normality) for the different distributions. However some parameters present very specific distributions far from the Gaussian assumption. In order to justify the criticism about the Gaussian hypothesis, particular attention is paid to two density histograms, which look like normal distributions: parameter T_1 for the IDM model and parameter $V_{\max}$ for the OVRV model. QQplots can be drawn (figure 5.12), and they consist in opposing the theoretical quantiles of the normal distribution to the empirical ones. The points are far from the right line: even the supposedly normal distributions are not normally distributed. This idea can be theoretically confirmed with a Shapiro-Wilk normality test [153] for which the hypothesis of a normal distribution is rejected with a p-value of 5.3e-06 for T_1 (IDM) and 2.72e-0.5 for $V_{\max}$ (OVRV).

In addition to the normal curve, non parametric density estimation has been performed for the different marginal distributions. These density estimations are much closer to the original distributions. It consists of a kernel based estimation where we compute the estimator of a moving window (from Rosenblatt) written as

$$\hat{f}_n(x) = \frac{1}{nh}\Sigma_{i=1}^{n} K(\frac{x - x_i}{h}), \tag{5.5}$$

where h is the class amplitude (a smoothing parameter), n the number of observations and K a kernel function that we take here to be Gaussian. $\hat{f}_n(x)$ is an arithmetic mean function that gives to the observations x_i a weight $1/h$ if it belongs to an interval centered to x. The reader can refer to [154] for more details and alternate choices for the Kernel function.

Following the analysis and estimation of marginal distributions, it is also possible to estimate joint parameter distributions. First, a multivariate

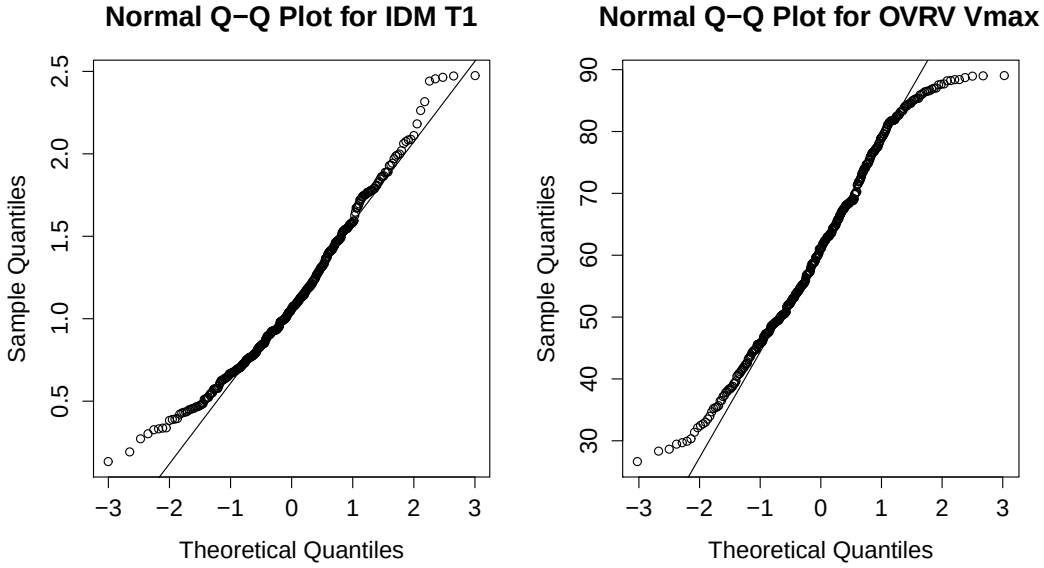

Figure 5.12: QQ plot of IDM T_1 and OVRV $V_{\max}$ parameters

normal distribution can be proposed, expressed as

$$f_x(x_1, ..., x_k) = \frac{1}{\sqrt{(2\pi)^k |\Sigma|}} exp(-\frac{1}{2}(x-\mu)^T \Sigma^{-1}(x-\mu)), \tag{5.6}$$

where $|\Sigma|$ is the determinant of the positive definite covariance matrix Σ and μ the mean. In order to go one step further, one could consider multivariate non parametric density estimations.

The extension of kernel density estimation to the multivariate case considers a set of random samples $X_1, X_2, ..., X_n$ distributed according to a certain density f. Next the kernel density is defined by

$$\hat{f}(x; H) = n^{-1} \Sigma_{i=1}^{n} K_H(x - X_i), \tag{5.7}$$

where $X_i = (X_{i1}, X_{i2}, ..., X_{id})^T, i = 1, 2, ..., n$. K is a density function and H the bandwidth matrix. As for the unidimensional case, some issues lie in the bandwidth parametrization. Figure 5.14 presents a joint kernel estimation for the parameters $V_{\max}$, τ and hc :

Thus, multivariate kernel density estimation technique provides an elegant way of modelling and representing a multivariate distribution without

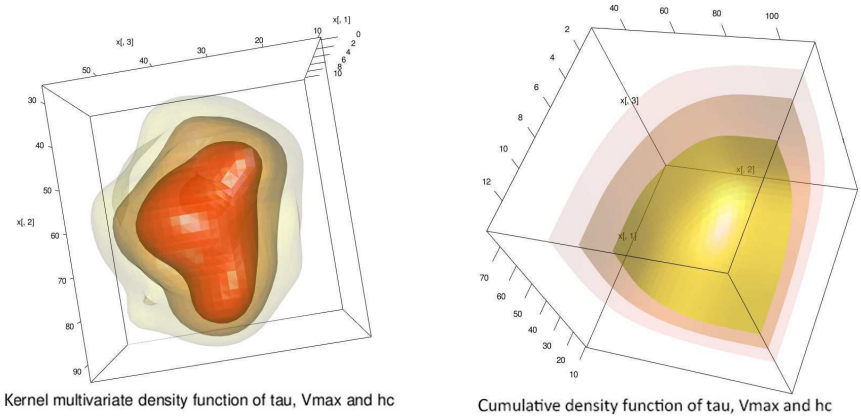

(a) (b)

Figure 5.13: Parameters $V_{\max}$, τ and h_c of the OVRV model: (a) density function, (b) cumulative density function.

any assumption on the parameter distribution. However, these refined multi-dimensional techniques need some sampling methodologies before generating random parameter sets and evaluating them.

5.5.2 Sampling strategies

It is clear that calibration processes are highly dependent on the datasets and such joint distribution estimations could be only useful in an ideal case where an empirical set is comprehensive and correct. Nevertheless, it is relevant to come up with some methodological and validation arguments regarding the sampling step, as discussed in [155]. The goal is to assess which one of the sampling techniques is the most suited to represent a realistic heterogeneous traffic flow. As the calibration effort focused on the speeds, the distribution of the relative velocities standard deviations is analyzed. For that, the leader-follower couples of lane 1 and lane 2 are picked (a total of 1004 couples for the two lanes). The trajectories of the leaders are taken from the empirical filtered speeds, and the followers' speeds are computed through the car-following models, using parameters that have been sampled from the consistent calibrated set. Then, the performances of the different sampling methods are compared with the original empirical filtered data.

For the sampling section, results are introduced for the OVRV model only, although similar results are available for the three models. More pre-

cisely, five different sampling methods are compared:

- *Method 1*: parameter sets are generated randomly, parameter by parameter, without taking into account the correlation structure.
- *Method 2*: parameter sets are generated randomly, parameter by parameter, taking into account the correlation structure (bootstrap with correlation, random rows are generated).
- *Method 3*: a 5-dimensionnal multivariate distribution is used to generate the dataset randomly. Several techniques exist then to sample from a multivariate normal distribution (Choleski decomposition, single value and eigenvalue decomposition). Here, the Choleski decomposition is used.
- *Method 4*: based on the correlation and multidimensional analyses, parameters γ and s are chosen randomly within their space. The three other parameters, τ, $V_{\max}$ and h_c, which are closer to a multivariate normal distribution and may be correlated, are modeled with a three-dimensional normal distribution.
- *Method 5*: Instead of using a 3d normal distribution in method 3, a multivariate kernel density estimation is performed for the three parameters. The cumulative density function $F(x)$ is the basis of an inverse sampling transform: a random number u is generated from a unifom distribution. Values of x are then computed such that $F(X) = u$. Finally, the resulting x is the random number taken from the multivariate kernel density of the three parameters.

Figure 5.14 shows distributions (of the relative speed standard deviation for leader-follower couples) for different sampling strategies for the OVRV model, figure 5.14a being the reference. Note that here the calibrated OVRV model tends to slightly underestimate the variation of relative velocities, and this would also be observable for the IOVM and IDM models. This is certainly due to observed variations which are not due to constrained driving (uncaptured behaviors by the models) or to possible overfiltered residual noises (which was unavoidable given the need to filter the observed spikes coming from data processing). Besides, as the goal is to accurately represent the heterogeneity of traffic, the different outputs are satisfactory and consistent with what could have been expected. The method 5 (multidimensional kernel density estimation) shows a good potential but concedes too much

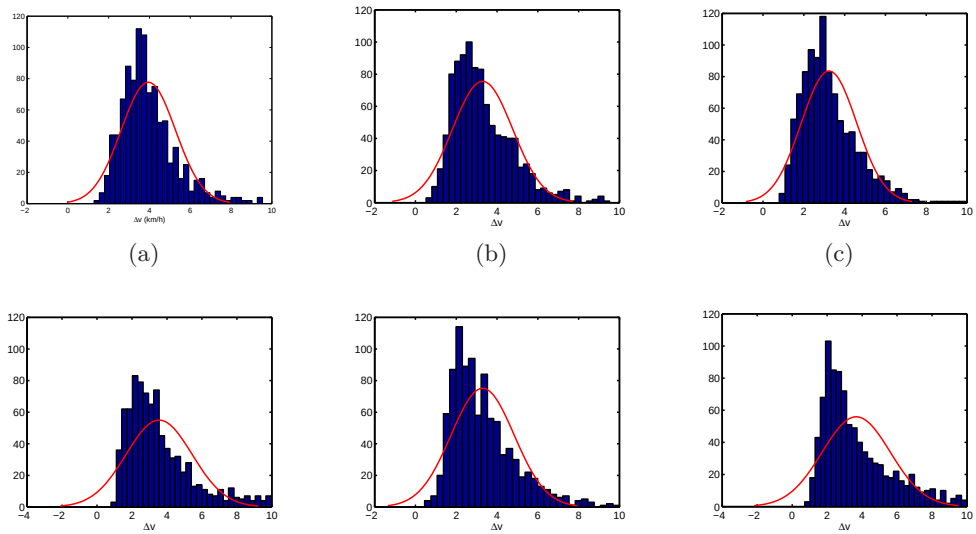

Figure 5.14: Distributions of the relative speeds standard deviations for the OVRV model and the following sampling methods: (a) empirical data, (b) method 1, (c) method 2, (d) method 3, (e) method 4, (f) method 5.

importance to extremes values, whereas the method 3 (5-dimensional multivariate normal distribution) relies on a wrong assumption (normality for all the parameters). The best methods are method 2 (bootstrap with correlation) and method 4 that models 3 parameters with a tri-variate normal distribution and 2 others with random correlated sampling. The conclusions are that a fine analysis of the parameters' marginal distributions is needed before carrying out a joint density estimation and that these results are a promising first step towards a robust sampling validation framework.

5.6 Conclusion

In this chapter, a comprehensive methodological chain was presented in order to be able to reproduce realistic traffic conditions from noisy trajectories: data filtering, calibration, parameters statistical analysis, sampling. Calibration uncertainties were discussed and robust sets of parameters that could be used for further analyses have been obtained. The joint distributions of the set of parameters were then estimated, and various sampling

methods discussed. There is no doubt that correlation plays a major role here and some recent findings [134, 98] have been confirmed. The proposed approach extends the analysis of microscopic parameters with more refined approaches. In addition to the estimation issue, sampling strategies are proposed and the results show that it is possible to adequately sample from multidimensional parameters estimation techniques. Perspectives of this work deals with a comparison of multiple estimation techniques (such as copulas, see [156]) as well as sampling strategies within a robust validation framework. However, good quality data must be a requisite in the future.

The ability to reproduce realistic traffic is fundamental for the testing of control algorithms, meaning that a realistic perturbated traffic can be chosen as the representation of the ground truth traffic. Besides, the emergence of communication systems reinforces the needs to understand microscopic physical behaviors, the simulation of realistic unpredictable or unexpected behaviors potentially helping the design of robust control algorithms [157]. Chapter 6 will focus on simulations that first validate the analytical developments of chapter 4, and then help draw conclusions about control algorithms using the results presented here in chapter 5 as inputs.

Chapter 6

Simulations and results analyses

This chapter gathers simulations studies to validate, evaluate and measure the performance of the developed cooperative models introduced in chapter 4. After introducing the simulation set-up, previous research concerning linear stability results as well as weakly non-linear stability results are validated. Besides, the integration of the driving behavior variability which was discussed in chapter 5 is a natural extension of this work and requires further simulation studies. Performance measures hereby referred as traffic indicators are defined, as they provide an evaluation of the traffic efficiency, homogeneity, and safety. This study shows how these indicators are related to each other. The influence of the number of needed cooperative vehicles in the car-following law, the fleet percentage of cooperative vehicles, the percentage of aggressive vehicles and the added control term are being tested in the light of these indicators and of previous analytical studies.

Contents

6.1 Simulation Set-up

6.1.1 Synthesis of calibration results and steady-state speed headway relation

The calibration of time continuous car-following models was performed in the previous chapter and the mean and standard deviation of the results are summarized in table 6.1. The models are calibrated under dense traffic conditions for a total of 417 sets of parameters for the IOVM model, 403 for the OVRV model and 374 for the IDM model. The mean and standard deviation of the results are presented in table 5.3.3.

The stability regime corresponding to the calibrated traffic conditions can be estimated by computing the steady-state speed and headway. The steady-state relations are expressed as

$$\text{OVRV:}\quad V_{eq} = \frac{V_{\max}}{2}\left(\tanh(sh_c) + \tanh(s * (\Delta x_{eq} - h_c))\right) \tag{6.1}$$

$$\text{IOVM:}\quad V_{eq} = \min\left(V_{\max}, \frac{\Delta_{eq} - s_0}{T_0}\right) \tag{6.2}$$

$$\text{IDM:}\quad \Delta x_{eq} = \sqrt{\frac{(s_1 + V_{eq}T_1)^2}{1 - (V_{eq} - V_{\max})^4}} + l \tag{6.3}$$

In order to have an idea on the traffic stability regime, the average of the observed headway and speed are computed for the calibrated period. This gives $\Delta x_{eq} = 15.9$ m and $V_{eq} = 37.4$ km/h, which corresponds to dense traffic conditions. Then, the stability values $f_1^2 - 2f_2 - 2f_1 f_3$ can be computed using the mean calibrated values of the parameters, and respectively gives -0.16 for the IDM with a steady-state headway of 16.7 m and a steady-state flow of 0.62 veh/s, -0.11 for the OVRV with a steady-state speed

Table 6.1: Calibrated parameters for different models

	Mean	Standard deviation
OVRV		
τ (s)	4.4	2.7
$V_{\max}$ (km/h)	67.2	16.4
γ	0.50	0.4
h_c (m)	11.1	3.4
s (m^{-1})	0.18	0.17
IOVM		
τ (s)	3.8	2.4
$V_{\max}$ (km/h)	70.0	16.4
γ	0.42	0.37
s_0 (m)	4.2	2.3
T_0 (s)	1.3	0.57
IDM		
a $(m.s^{-2})$	1.1	0.52
$V_{\max}$ (km/h)	109.0	28.9
b $(m.s^{-2})$	2.2	1.4
T_1 (s)	1.1	0.46
s_1 (m)	0.49	0.69

of 56.2 km/h and a steady-state flow of 0.98 veh/s, -0.13 for the IOVM with a steady-state speed of 33.7 km/h and a steady-state headway of 0.59 veh/s. Those results show that the traffic is comparably and globally string unstable, which was expected given the observed appearances of stop and go waves in the trajectories.

6.1.2 Practical design: discussion on agressiveness in lane changing maneuvers, emergency braking, cooperation for mixed traffic, and numerical scheme

The trajectories of a finite number of vehicles are simulated on a stretch of highway, for a given number of lanes. The car-following law is implemented for each following vehicle. The first leader evolves at the computed steady-state speed (equation 6.3), and see section 4.4.2 for the mathematical definition. It sould be mentioned that the first leader evolves at a constant speed has a stabilizing effect in the context of forward multi-anticipation. In

this chapter two types of perturbations are studied, provoked ones coming from a push forward or backward of a vehicle, and spontaneous ones coming from aggressive lane changes. The implemented lane-changing law is therefore introduced. The cooperative window is chosen as the cosine window described in section 4.5.4, however some precautions must be taken in the case of a mixed traffic. Moreover, in the case of a large interaction range and strong perturbations, the cooperative law can increase the collision risk as it makes vehicles drive close to each other. A Yukawa potential [158] is implemented as a smooth emergency braking to secure a collision-free traffic. Finally, the selected numerical scheme is specified.

Lane-changing model and aggressiveness

A realistic lane changing strategy is implemented in order to force sudden maneuvers to the observed vehicles, and thus, to introduce plausible perturbations to the traffic flow. In the numerical experiments the MOBIL strategy was used [159] to simulate lane changes. The symmetric overtaking MOBIL rule for a vehicle reads that provided that there was no lane change in a previous time frame T, a lane change is possible if

$$\bar{\ddot{x}}_n - \ddot{x}_n + p(\bar{\ddot{x}}_t - \ddot{x}_t + \bar{\ddot{x}}_c - \ddot{x}_c) > \Delta a_{th} \tag{6.4}$$

$$\bar{\ddot{x}}_n > -a_{saf} \tag{6.5}$$

where an acceleration $\bar{\ddot{x}}$ denotes the potential acceleration of a vehicle on the targeted lane - acceleration if the lane change occurs - and the coefficients t and c refer to the following vehicles in the target and current lanes respectively. Δa_{th} and a_{saf} are respectively the criterion for lane changing that denotes the permissiveness threshold of a lane change and the safe deceleration limit of the following vehicle in case a lane change occurs. p is a politeness factor, which weights the acceleration gain or loss of the targetted old and new followers. The vehicle is actually estimating an acceleration gain before proceeding to a lane change. If both conditions are satisfied, it changes its lane. One attracting feature of this law is that it directly deals with the acceleration. One can note that with a car following model, such as the optimal velocity model of Bando *et al.* [66], i.e. without the relative speed consensus term, the MOBIL model becomes a simple gap acceptance model. As specified in [159], the politeness factor p is used to vary the importance of the traffic situation of the followers from the point of view of the current vehicle. As it turns out, small or even negative values of p result in

greedy or even malicious lane-hopping behaviors. Malicious maneuvers are typically followed by sudden counter-actions from the other drivers, such as sharp decelerations to avoid collisions. Real egoistic behaviors happen when p is close to 0, i.e. the acceleration gain of the surrounding vehicles is not taken into consideration. Egoistic drivers are frequently observed in critical situations, when traffic is heterogeneous [160]. Finally, the recent thesis of Habtemichael [161] synthetizes research on the so-called driver aggressiveness. When Risser [162] states that in his study 18% of drivers are aggressive in their lane change, he adds that 25% of the drivers change lane in too hesitant a manner. A recent study by Guo and Fuang [163] comforts this idea, in which moderate risk and high risk drivers are said to represent 18% of the driving population.

In future developements, the numerical values will be taken as $a_{saf} = -3.5\ m.s^{-2}$ $\Delta a_{th} = 1.0\ m.s^{-2}$ and $p \in [0, 0.5]$, which corresponds to a realistic traffic, see [159] for more details.

Smooth emergency braking

A critical emergency braking is implemented for the three models as a repulsive function to prevent collision-prone situations due to cooperation, and converting the OVRV and IOVM models into collision-free models. The emergency braking function is chosen such as the Yukawa potential

$$Y(\Delta x_n) = -g^2 \frac{\exp(-k\Delta x_n)}{\Delta x_n}, \tag{6.6}$$

where g and k are scaling constants. For well-tuned parameters g and k (later taken such as $g = 15\ m.s^{-1}$ and $k = 1\ m^{-1}$), the Yukawa potential only has an influence in case of small headways, so that it will not modify the conditions for appearances of shock waves. It must also be reminded that small distances occur in a less frequent way for collision-free models like the IDM model which already contains a repulsive term.

Multi-anticipative law

Two remarks have to be made relatively to the multi-anticipative law. First, as soon as a vehicle is cooperative, it is assumed to be able to sense the headway and speed of the immediate leader and the immediate follower. As a result the immediate neighbors are always taken into consideration. Second, the interaction range is being scaled at the most remote detected cooperative vehicles in the predefined interaction range. For example, suppose that r

is the interaction range and $n + m_f$ the last cooperative vehicle in this interaction range, r is scaled so that $r = \Delta_T x_{n+m_f}$. Consequently, there is no scaling effect when normalizing the coefficients of cooperation. In future developments, the multi-anticipation will be successively refered to as the interaction range or the number of cooperative leaders m and number of cooperative followers m' considered in the cooperative law.

Numerical scheme

Regarding the selected numerical scheme, the mixed first order second order Euler scheme is chosen, as it was proven to be twice more efficient than the fourth order Runge Kutta scheme and three times more efficient than the simplest first order Euler scheme. Interested reader can refer to the recent book of Treiber and Kesting [64]. Speeds and positions are therefore derived from the continuous acceleration expression such as

$$\dot{x}_n(t + \Delta t) = \dot{x}_n(t) + f(\dot{x}_n, \Delta x_n, \Delta \dot{x}_n) \cdot \Delta t \tag{6.7}$$

$$x_n(t + \Delta t) = x_n(t) + \frac{\dot{x}_n + \dot{x}_n(t + \Delta t)}{2} \cdot \Delta t \tag{6.8}$$

6.2 Evidence of stability results

This section summarizes all the numerical experiments for validation of the stability analyses of chapter 4. In the next subsections the three models will be used successively to validate the analytical results, however any model can be used to prove each concept, except for the IOVM model which has all its second order partial derivatives equal to 0 and as a result must be discarded for the weakly non-linear stability analyses.

6.2.1 Validation of the linear stability threshold

The propagation of shock waves as a reaction to a small perturbation can be verified *via* simulation. The perturbation is introduced at time t=50 s, and consists of displacing the second vehicle by 2 meters backwards. Choosing the IOVM model, the set of parameters of table 6.1 is used, setting $\gamma = 0.2$. The steady-state traffic is computed according to section 6.1.1. This gives a stability value of $(f_1^2 - 2f_2 - 2f_1 f_3) = \epsilon^2 = -0.27$, chosen to be lower than the calibrated one in order to exhibit unstable effects.

Figure 6.1 shows the influence of the percentage of cooperative vehicles on the traffic stream. Cooperative vehicles are randomly generated, and

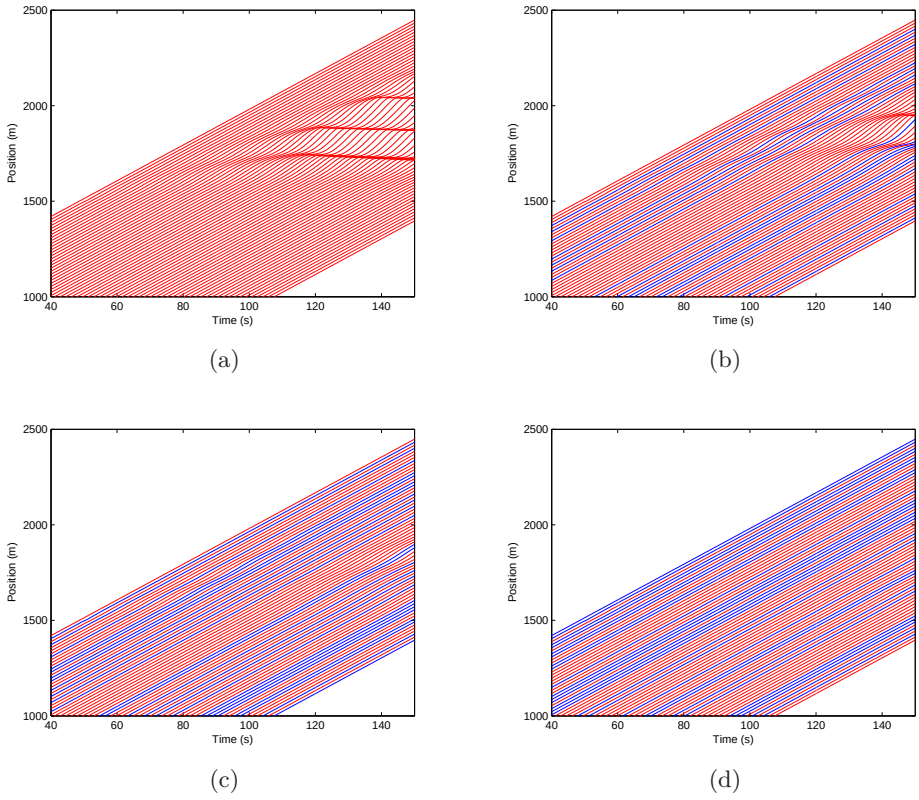

Figure 6.1: Time-space shock wave diagram for an interaction range of 120 m and for different cooperative vehicles penetration rate: (a) 0%, (b) 15%, (c) 30% and (d) 45%. Each line corresponds to a vehicle trajectory, blue for cooperative, red for non-cooperative.

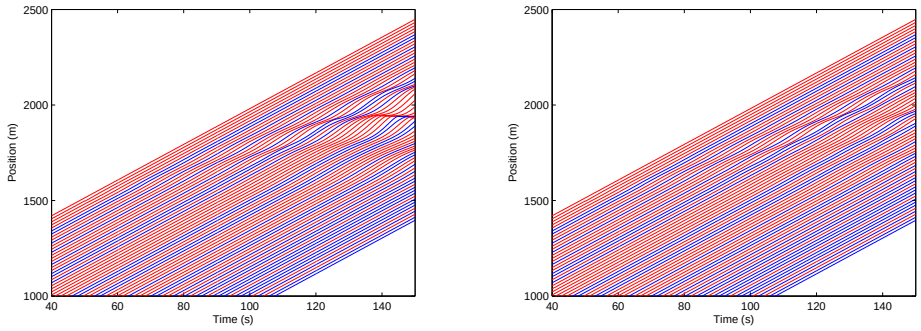

(a) (b)

Figure 6.2: Time-space shock wave diagram for 45% of cooperative vehicles and an interaction range of: (a) 50 m (b) 120 m. Each line corresponds to a vehicle trajectory.

move according to forward multi-anticipation. It appears that the generated shock wave is of the convective downstream type. The shock wave is being partially removed with a cooperative range of 30%, and totally with a cooperative vehicle of 45%. This is the illustration of the stability threshold being shift, and increasing the domain of stability, see figure 4.4. Differently, figure 6.2 highlights the importance of the interaction range in the cooperative framework. It appears here that an interaction range of 120 m (6 vehicles ahead) is more efficient to reduce the shock waves than an interaction range of 50m (3 vehicles ahead), in this configuration. A comparison between figures 6.1d and 6.2b allows to conclude over the importance of the cooperative vehicles positions in the stream (blue vehicle for cooeprative and red for non-cooperative). As they evolve closer to the perturbation, cooperatives vehicles will increase the chances of removing the shock waves. In contrast to figure 6.2b, the shock wave is being totally cleared in figure 6.1d, for the same random generation of cooperative vehicles. Here bilateral traffic was not considered, however some simulations easily confirm its stabilizing effect. Finally, and it will be illustrated later, it must be mentioned that cooperation can become critical in the case of a large interaction range as it may result in vehicles driving too close to each other, and that in the case of a highly unstable traffic and a bigger perturbation, the multi-anticipation can trigger other perturbations.

For the next two subsections, as non-linear effects are studied, a bigger size of perturbation (5 m) will be introduced at time t=50 s.

6.2.2 Weakly non-linear analyses: validation of the soliton sign

It was found out in equation (4.80) that a rather simple condition gives the sign of the soliton amplitude: it has the same sign as $C_2 = -f_{12}\frac{f_2}{f_1} + f_{22}$. Here the OVRV model is used in case of an upstream convective unstable traffic, for a calibrated pair of parameters in the presence of a shock wave: $\tau = 3.1$ s, $V_{\max} = 28.4$ m/s, $\gamma = 0.95$, $s = 0.19$ m^{-1}, and h_c is picked such as $h_c = \Delta x_{eq} \pm 1.5$ which gives $f_1^2 - 2f_2 - 2f_1 f_3 = -0.57$ for $\Delta x_{eq} = 33$ m, *i.e.* strong instabilities. For the OVRV model $C_2 = \frac{V''(\Delta x_{eq})}{\tau} = \frac{V_{\max}}{\tau} s^2 \tanh\left(s(\Delta x_{eq} - h_c)\right) \operatorname{sech}^2(\Delta x_{eq} - h_c)$. Figure 6.3 presents the variation of C_2 as a function of parameter h_c, the other parameters being set as above. Finally, in addition to the symmetry of the figure, it appears that $C_2 > 0 \Leftrightarrow\ h_c > \Delta x_{eq}$, and reciprocally for $C_2 < 0$.

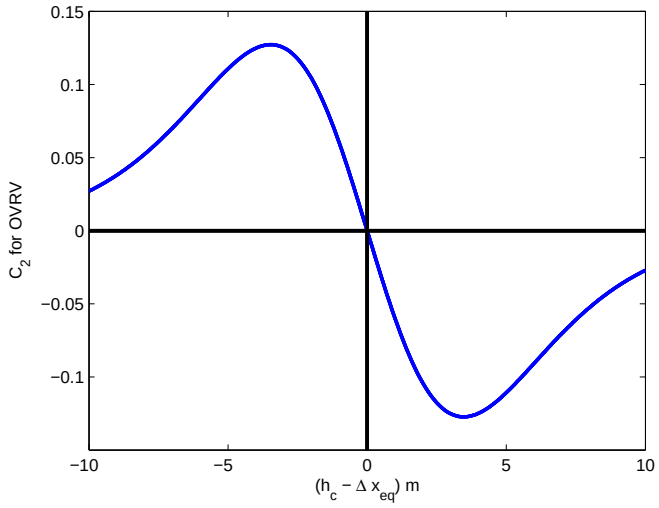

Figure 6.3: Sign of the leading edge of the soliton C_2 as a function of parameter h_c

Figures 6.4a, 6.4b correspond to $h_c = \Delta x_{eq} + 1.5$ m, *i.e.* $f_{22} > 0$. It is observable in figure 6.4b that the leading edge of the soliton amplitude is positive, as predicted by the theoretical equation (4.81). In figure 6.4a, it is shown in the time-space diagram that the leading edge of the shock wave is an acceleration regime. In the same vein, figures 6.4b, 6.5b are relative to $h_c = \Delta x_{eq} - 1.5$ m, *i.e.* $f_{22} < 0$. The soliton amplitude is negative and has the sign of f_{22}. Finally, and this is a new result as well, results are

valid independently of the sign of the initial perturbation (the vehicle can be displaced backwards or forwards), as displayed in figures 6.6a and 6.6b. It can be observed that the soliton has the same shape despite a major difference in the initial perturbation (10 m in terms of positions).

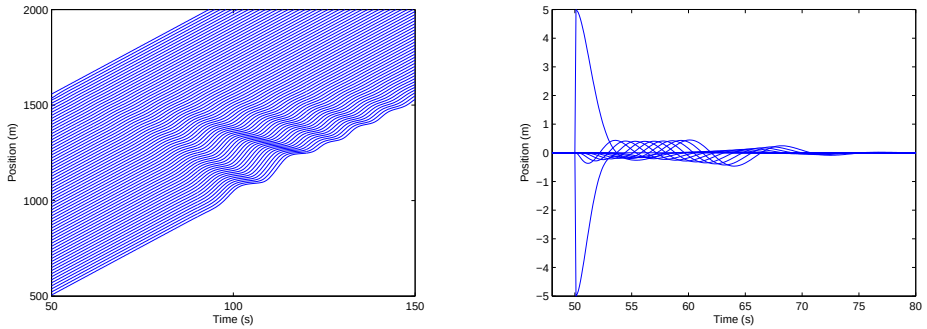

(a) (b)

Figure 6.4: Shape of the travelling wave for $h_c = \Delta x_{eq} + 1.5$ m ($f_{22} < 0$): (a) time space shock wave and (b) relative headway evolution Δ_y for the twelve first following vehicles.

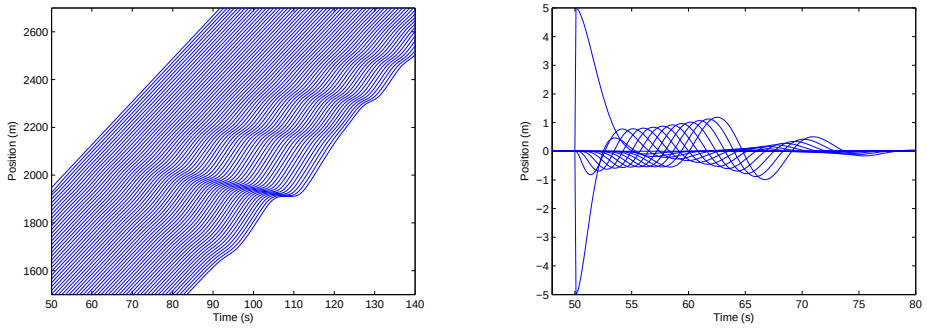

(a) (b)

Figure 6.5: Shape of the travelling wave for $h_c = \Delta x_{eq} - 1.5$ m ($f_{22} < 0$): (a) time space shock wave and (b) relative headway evolution Δ_y for the twelve first following vehicles.

Important and new results have therefore been verified: the sign of the amplitude does not depend on the initial perturbation sign as it only depends

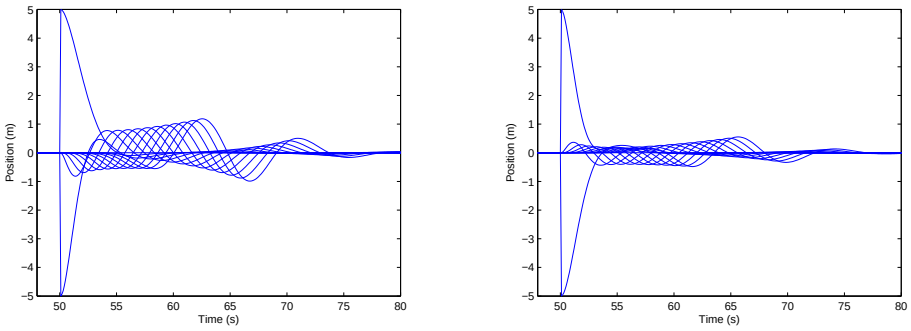

(a) (b)

Figure 6.6: Leading edge of the travelling wave for $h_c = \Delta x_{eq} - 1.5$ m ($f_{22} < 0$) for (a) negative initial perturbation (braking) (b) positive initial perturbation (acceleration)

on the C_2 value. This means that regardless of the nature of the perturbation (in terms of braking or accelerating), the leading edge of the stop and go wave will always be an acceleration ($C_2 > 0$) or deceleration ($C_2 < 0$) regime. This physical related result is counter intuitive and brings a better understanding of the appearance of traveling waves in presence of non-linearities.

6.2.3 Validation of the saturated amplitude value

It is now question of numerically validating equations (4.86) and (4.97), which give a relation between the speed and the amplitude of the soliton as well as the amplitude value. Here the IDM model is used with a steady state speed of 37.4 km/h and a set of parameters chosen relatively close to the neutral stability surface, with parameters $a = 1.6$ m/s^2, $V_{\max} = 100$ km/h, $b = 4.5$ m/s^2, $s_1 = 2.4$ m and $T_1 = 0.8$ s, which gives $f_1 = -0.25$, $f_2 = 0.29$, $f_3 = 0.57$, and $f_1^2 - 2f_2 - 2f_1 f_3 = -0.24$. The IDM model is the only model that does not have any of the partial derivatives $(f_{ij})_{0 \leq i,j \leq 3}$ equal to zero. For the sake of clarity, the first order partial derivatives for the IDM model

are written as

$$f_1 = -4a\frac{\dot{x}_{eq}^3}{V_{\max}^4} - \frac{2a\left(T_1 - \frac{\Delta\dot{x}_{eq}}{2\sqrt{ab}}\right)\left(s_1 + \dot{x}_{eq}T_1 - \frac{\dot{x}_{eq}\Delta\dot{x}_{eq}}{2\sqrt{ab}}\right)}{(\Delta x_{eq} - l)^2}, \tag{6.9}$$

$$f_2 = 2a\frac{\left(s_1 + \dot{x}_{eq}T_1 - \frac{\dot{x}_{eq}\Delta\dot{x}_{eq}}{2\sqrt{ab}}\right)^2}{(\Delta x_{eq} - l)^3}, \tag{6.10}$$

$$f_3 = \frac{a\dot{x}_{eq}\left(s_1 + \dot{x}_{eq}T_1 - \frac{\dot{x}_{eq}\Delta\dot{x}_{eq}}{2\sqrt{ab}}\right)}{\sqrt{ab}(\Delta x_{eq} - l)^2}, \tag{6.11}$$

the second order partial derivatives then being derivable from those expressions.

For the given perturbation of 5 m, the observed shock wave speed in the moving frame $v_{s,\text{obs}}$ and the observed saturated amplitude $\mathbf{A}_{\text{obs}}$ are respectively $v_{s,\text{obs}} \approx 63$ km/h, and $\mathbf{A}_{\text{obs}} \approx 0.6$ m, which is graphically estimated *via* figures 6.7a and 6.7b. Figures 6.7a and 6.7b show the variation of relative headway as a function of time and vehicle number in the moving frame (at the equilibrium speed).

The observed variations of speed in the moving frame and amplitude are roughly confirmed by the analytical expressions (4.97) and then (4.86). Numerical developments allow to compute the value $\mathbf{A} = 0.46$ m and according to (4.86) $v_s = 53.1$ km/h, which corresponds to the same order of magnitude. Note that the deviation was expected as the parameters were not chosen at the exact frontier of the neutral string stability surface ($\epsilon^2 = 0.24$).

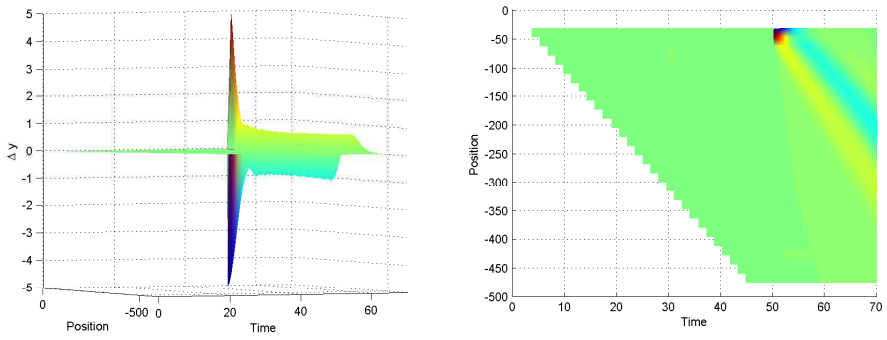

(a) (b)

Figure 6.7: 2D and 3D shock wave shape of a soliton in the moving frame for the IDM model, $f_1^2 - 2f_2 - 2f_1f_3 = -0.24$

6.3 Influence of driver behavior variability

In this section the driver behavior variability (results of chapter 5) is taken into consideration. The bootstrap sampling method is selected (random samping without replacement) to generate the sets of the three calibrated car-following models. The impact of the multi-anticipation and of the control terms is investigated in the light of described traffic indicators. This is a first step towards the introduction of the multi-agent framework, where the confidence between agents (vehicles) will be modelled, see chapter 7.

6.3.1 Traffic indicators

A series of traffic indicators is introduced in this subsection. Four concepts are of interest: traffic efficiency, traffic stability, homogeneity, and traffic safety. Traffic efficiency will be measured by the time-space diagram, which can be useful for graphical analyses, and the travel time distribution. The traffic stability and homogeneity, which are two related features, are embodied by the acceleration trajectories, and by the group disagreement value. The group disagreement value G_d was introduced by Choi *et al.* [164] and is expressed as

$$G_d = \frac{1}{4} \sum_{(i,j)\in\mathcal{N}^2} a_{ij}(\dot{x}_j - \dot{x}_i)^2, \tag{6.12}$$

where a_{ij} is the binary adjacency value (0 if not in the interaction range and 1 otherwise), and $\mathcal{N}$ is the set of vehicles on the road section. As for traffic safety, the Time to Collision (TTC) and the Post-Enroachment Time (PET) are selected, as they were the two indicators used by the USDOT Federal Highway administration for the Surrogate Safety Assessment Model (SSAM) [165] and as they account for information on homogeneity and danger (TTC) and direct collision (PET). The TTC is the ratio of the headway and relative velocity between a vehicle and its leader. Basically, if the drivers keep driving with the same speeds, they will collide in a certain amount of time: the TTC. The PET is the time needed for a driver to meet the exact position of the leader. A PET of 0 seconds is equivalent to a collision. For an application to the safety assessment of autonomous cruise control systems, the reader can refer to [166].

Starting from that, a few parameters are supposed to have a relevant impact on traffic flow and will be investigated. The number of cooperative vehicles m for forward multi-anticipation, the number of cooperative followers m' for bilateral cooperation, the percentage of cooperative vehicles, and

the percentage of aggressive drivers will be studied. The IOVM and IDM models will be used in the next subsections.

6.3.2 Default parameters values, interaction range and first analyses

The IOVM and IDM models are used in the coming developments, with bootstrap sampled parameters as specified in section 5.5.2. The time step, which is of critical importance, will be set equal to 0.4 s. The default percentage of egoistic/aggressive drivers ($p = -0.1$) is set to be 25%, in compliance with previous works [161]. The remaining drivers have a classical coefficient of $p = 0.5$, see [167]. The vehicles positions are initialized with steady-state headway and speeds. For the IOVM model, the steady-state headway is taken as the mean headway of the observed traffic, and the steady state speed is computed via the steady-state relation (6.2). For the IDM model, the steady-state speed is taken as the mean speed of the observed traffic, and the steady state headway is computed via the steady-state relation (6.3).

Interaction range and number of information data points in the car-following law

In this section, for the sake of simplicity, the cooperative vehicles in the car-following law share their downstream headway (relatively to their leader) in case of forward multi-anticipation and share their upstream headway in case of backward multi-anticipation. The interaction range r used in the cosine window is first intuitively defined as $r = (C_o + 30)$ m (where C_o is the percentage of cooperative vehicles) to avoid scaling effects, and is being re-scaled depending on a defined number of considered cooperative leaders and followers (as specified in 6.1.2). For example, if m is set to be the number of forward information data points to be considered in the cooperative car-following law, $n + m_{f1}$ is the indice of the $m_f + 1$ detected cooperative vehicle, so that $r = \min(r, \Delta_T x_{n+m_{f1}})$. The varying interaction range is chosen to avoid that the detection of a distant cooperative vehicle causes equal weights for the first cooperative leaders, and therefore increases the risk of collision. It means that for $m = 2$, at least 3 cooperative vehicles are detected, and 2 leaders have a weight in the cosine window.

To first analyze the simulated trajectories, the percentage of cooperative vehicles, and the numbers m and m' of forward and backward information data points are being analyzed in the light of the standard deviations of the speed and travelled distance distributions. The travelled distance is

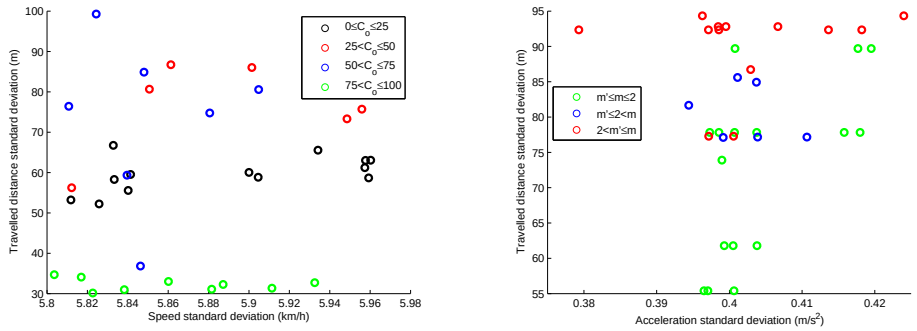

(a) (b)

Figure 6.8: IDM model: scatter plots for the standard deviation of thespeed, acceleration and travelled distance distributions: (a) influence of the percentage of cooperative vehicles; (b) influence of number of information data points m and m'

the distance travelled by vehicles during the simulation time: it is directly related to the travel time. For the analysis, the default values are 50% for the percentage of cooperative vehicles, 25% for the percentage of aggressive drivers, and $m = 2$ and $m' = 2$ for the number of forward and backward cooperative vehicles, and the simulation time is 90s. In figure 6.8, it is clearly obervable that the travel time distribution is very sensitive to both the percentage of cooperative vehicles and the number of considered cooperative vehicles. The speed information (and the acceleration information which is not traced) is not as meaningful as the travel time information. Two early conclusions can be drawn. It seems that only a high percentage of cooperative vehicles (above 75%) will lead to a significant change in the travel time distribution, whereas low and average percentages do not seem to have a positive effect. It is also highlighted that a large number of forward and backward cooperative vehicles will increase the heterogeneity of traffic flow. Adaptive cooperative strategies are therefore the answer to achieve traffic flow homogeneity.

Discussion on initial conditions

The vehicles positions are initialized with steady-state headway and speeds. The steady-state headway -or speed- is taken as the mean headway -or speed- of the observed traffic, and the steady-state speed -or headway- is computed

via the steady-state relations (6.2), (6.3) and using the mean values of the 5 sampled parameters. Computing a global steady-state headway-or speed- instead of computed steady-state headways -or speeds- per vehicle is equivalent to introducing perturbations at time t= 0 s, equal to the individual steady-state headway -or speed- minus the global steady-state headway -or speed-. Those perturbations will propagate under linear unstable conditions and metastable conditions depending on their magnitude.

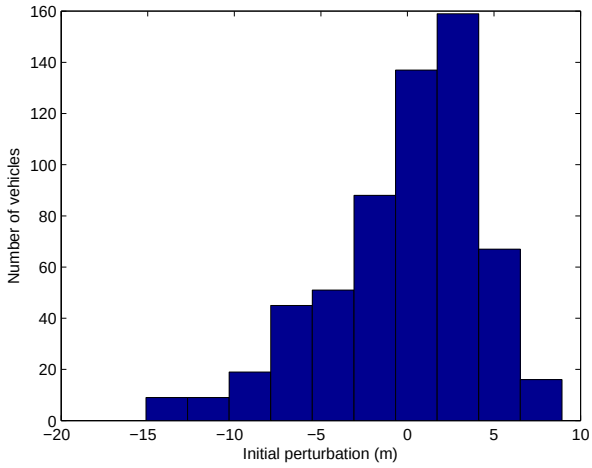

Figure 6.9: Distribution of perturbations at time t=0s.

Figure 6.9 displays the distribution of initial perturbations for the IDM model and for 600 vehicles, in which the perturbations consists in displacing vehicles forward (positive perturbation) or backward (negative perturbation). It is noticeable that most perturbations are under 5 m of absolute value, however some high perturbations likely to trigger non-linear phenomena exist.

6.3.3 Forward multi-anticipation: benefits and limitations

One first and important observation is that forward multi-anticipation is only helpful within a small interaction range, *i.e.* a small number of considered cooperative vehicles in the cooperative law (m and m'). Beyond that interaction range, cooperation can trigger dangerous situations as it makes vehicles drive too close to each other. If this was already highlighted in the previous subsection, it can also be validated by looking at the TTC and PET indicators. In this regard, figure 6.10 shows the possible negative effect of co-

operation. The traffic is safer for m=3 (2 leaders have weight). Even though there are 75% of equipped vehicles, beyond $m = 2$ an increasing number of forward information data points will oppose to a safe traffic. It can be verified that the cooperative law does not bring stability and homogeneity for increasing m either, as for $m > 2$ it causes more critical situations. This is an important result: when the drivers behavior variability is considered, forward multi-anticipation must be limited to $m \leq 2$ for the IOVM model, in this traffic configuration.

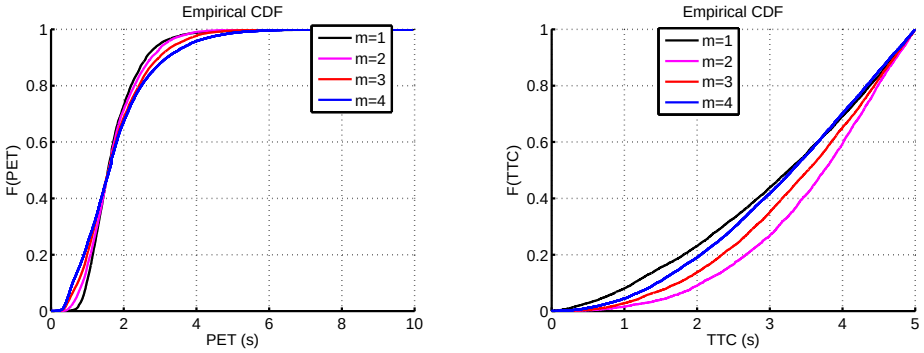

(a) (b)

Figure 6.10: Simulated PET and TTC for the IOVM model and 75% of cooperative vehicles and $m \in \{1, 4\}$

A similar analysis can be carried out for the IDM model and it leads to the same conclusion: when the drivers behavior variability is considered, forward multi-anticipation must be limited to $m \leq 2$ for the IDM model, in the calibrated traffic configuration. This could also be confirmed by considering other indicators, such as the group disagreement value and the travel time distribution.

Figure 6.11 displays the time-space diagrams for 50% of cooperative vehicles and increasing interaction range, for both IOVM and IDM models. First the diagrams confirm that the same traffic physics has been calibrated and is being simulated. However the accelerations are sharper in the case of the IOVM model, which is probably due to the lack of an equivalent to the comfortable acceleration term of the IDM model. Actually, for the IOVM model, the added term to compensate the non-completeness of the OVRV model makes vehicles react promptly to velocity differences, which is observable in the red patterns.

Finally the time-space diagrams also show that the cooperative law does

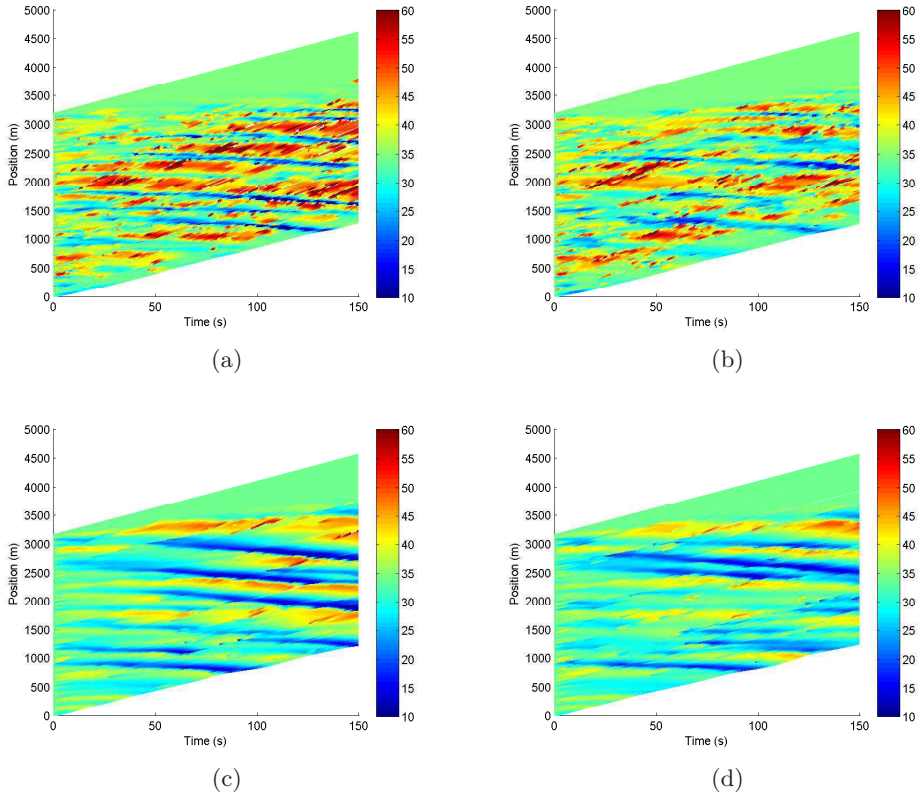

Figure 6.11: IOVM and IDM simulated trajectories for 50% of cooperative vehicles and number of cooperative leaders (a) $m = 1$ (IOVM), (b) $m = 2$ (IOVM), (c) $m = 1$ (IDM), (d) $m = 2$ (IDM).

not remove all the instabilities and therefore must be refined. Forward multi-anticipation is not satisfactory.

6.3.4 Positive influence of bilateral multi-anticipation

Bilateral multi-anticipation plays an important role. The root locus analysis detailed in section 4.5.5 can be used as a basis for the design of a bilateral cooperative strategy. The trade-off is to secure long-wavelength linear string stability, have a satisfactory safety margin for short-wavelength linear string stability, and limit the number of cooperative vehicles in the multi-anticipative law. For the mean of set of sampled parameters, the partial

derivatives are being computed, which gives $f_1 = -0.22$, $f_2 = 0.19$ and $f_3 = 0.39$, and $C_2 = -\frac{f_{12}}{f_2 f_1} + f_{22} = -0.49$.

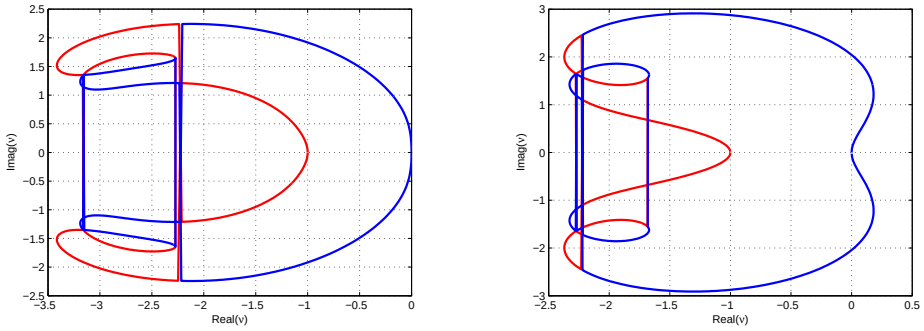

(a) (b)

Figure 6.12: IDM model: root locus analysis and different number of cooperative leaders and followers (a) $m = 2$ and $m' = 2$, (b) $m = 2$ and $m' = 0$

Figure 6.12 exposes the root locus for two multi-anticipative strategies: $m = 2$ and $m' = 0$, $m = 2$ and $m' = 2$. Two relevant observations must be made at this stage. First, for forward multi-anticipation a number of $m = 2$ of forward information data points integrating into the car-following model does not secure long-wavelength linear string stability. It means that with an increasing number of forward cooperative vehicles, the cooperative strategy makes vehicles drivers closer to each other, which will provoke braking reactions and then generate perturbations that will propagate. Secondly, on the contrary, the bilateral multi-anticipation strategy secures long-wavelength stability while guaranteeing short wavelength stability with a safety margin $S_D = 1$. Finally, in regard to non-linear instabilities, it is observed that the leading edges of the travelling waves are always of the same sign (and independently of the sign of the perturbations), which was expected given equation (4.80) and the negative sign of C_{22}.

Figure 6.13a and 6.13b show the time space diagrams of the multi-anticipative law designs for 75% of cooperative vehicles. It appears that instabilities are being totally removed for $m = 2$ and $m' = 2$. In figure 6.14 the corresponding group disagreement values (equation 6.12) are being traced for the same traffic configurations (same seeds in the random distributions), and it confirms that bilateral traffic plays a fundamental role as it divides the group disagreement value by a factor of 3.

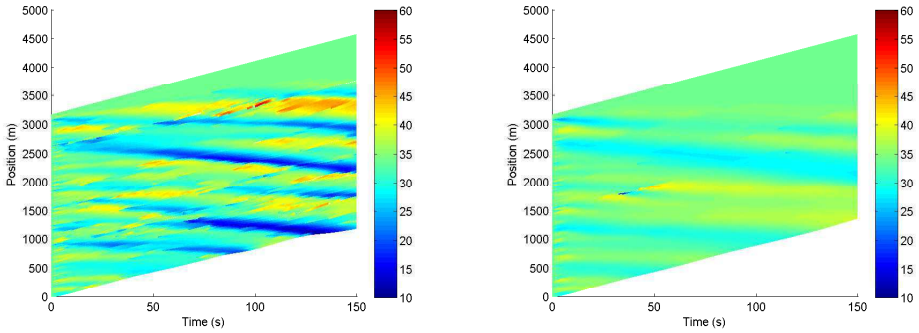

(a) (b)

Figure 6.13: IDM model simulated trajectories on lane 2 for 75% of cooperative vehicles: (a) $m = 2$ $m' = 0$, (b)$m = 2$ $m' = 2$

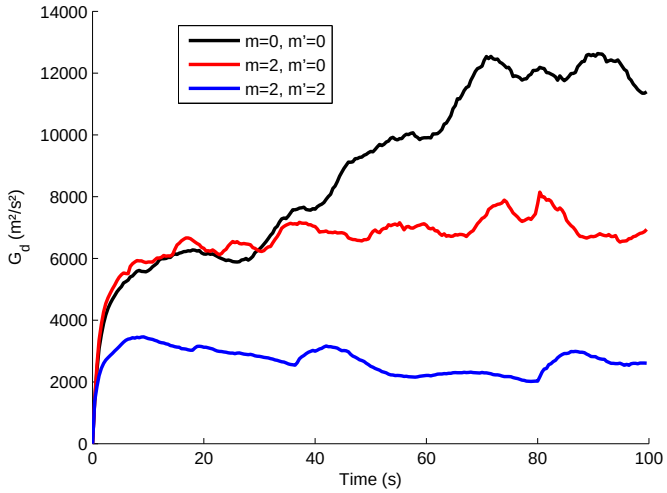

Figure 6.14: Evolution in time of the group disagreement values for 75% of cooperative vehicles: $m = 0$, $m' = 0$ (black); $m = 2$, $m' = 0$ (red); $m = 2$, $m' = 2$ (blue)

6.3.5 Potential negative influence of bilateral cooperation and positive influence of added linear control terms

It was highlighted previously (in section 4.3.5) that an added linear control term has a positive effect on string stability. For the tuning of the control

terms parameters c_1 and c_2, a rapid optimization is performed with the objective function selected as the product of the acceleration profiles standard deviation times the standard deviation of the traveled distance. For 25% of cooperative vehicles, Δx_d and $\dot{x}_d$ being the estimated steady-state headway and speed, the obtained values are $c_1 = 1.5$, $c_2 = 0$, which confirms the theoretical findings observed in figure 4.6, *i.e.* the system goes faster towards stability if c_2 is held to 0. The c_1 gain is being limited, as larger gains lead to oscillating trajectories around the $\dot{x}_{eq}$ value, which influences the acceleration trajectories. The gain threshold above which oscillatory trajectories are observed depend on the percentage of cooperative vehicles. Besides, for larger percentages of cooperative vehicles, if the indicator of interest is set to be the PET, positive values of c_2 tend to brings more safety as they remove the outliers which consist of low PET values. In this section, the c_2 gain will be set equal to zero in the cooperative law. Figure 6.15 synthetizes the results for 5 cooperative strategies, the black trajectory being the reference (no cooperation). It is seen that bilateral traffic is deterioring traffic flow without an adding control term: this is an important result that was already foreseen in the scatter plot analysis, see figure 6.8.

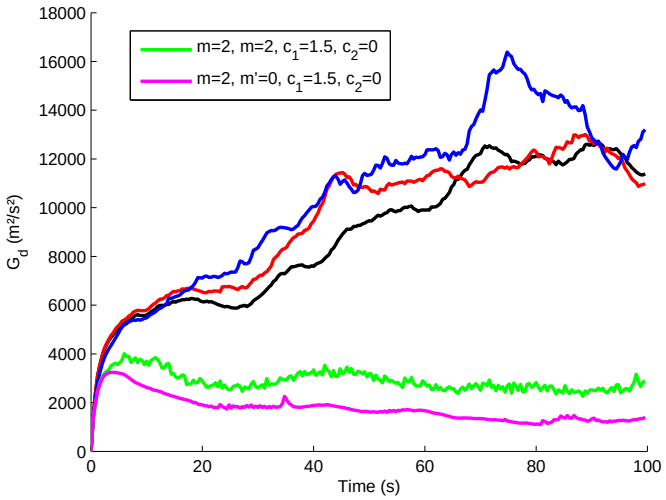

Figure 6.15: Evolution in time of the group disagreement values for 25% of cooperative vehicles with added control term: $m = 0$, $m' = 0$ (black); $m = 2$, $m' = 0$ (red); $m = 2$, $m' = 2$ (blue); $m = 2$, $m' = 0$ + control terms (magenta); $m = 2$, $m' = 2$ + control terms (green)

For this traffic configuration, it can be verified that a forward multi-anticipative traffic is more efficient than a bilateral multi-anticipative traffic for less than 60% of cooperative vehicles. This has a logical explanation. Under a small percentage of cooperative vehicles, the number of considered vehicles in the cooperative law is smaller. If the root locus analysis is performed, it is stated that a simple bilateral traffic (with one vehicle backward) does not secure long wavelength linear stability, which in addition to the non-linear instabilities contributes to the propagation of perturbations. Besides the multi-anticipative law is coupled with a lane changing strategy that does not take into account the eventual loss in the acceleration gain of the MOBIL formula (6.4) due to bilateral multi-anticipation. For example, the lane change of a non-cooperative vehicle introduces a perturbation for the leading cooperative vehicle which can propagate. In [64], the described Improved IDM model implemented for ACC systems aims at correcting such stong reaction to lane changes. To address this problem, the linear control term defined in section 4.3.5 allows to increase the linear string stability domain, and it is clear with the green curve which divides the group disagreement value by a factor 4 compared to the simple forward multi-anticipative strategy. With only 25% of cooperative vehicles, it is observed that a multi-anticipative strategy does not bring any increase of the homogeneity value, and the bilateral multi-anticipative strategy has a negative impact. The forward multi-anticipative strategy with control terms appears more efficient than the bilateral multi-anticipative strategy with control terms, however this is case dependent and they both exhibit low group disagreement values.

Finally, to verify and attest the validity of the cooperative law design, the PET indicator is displayed in figure 6.16a. It is noticeable that the distribution is being centered with an increasing rate of cooperative vehicles. As defined earlier, the PET is a relevant indicator as it directly measures the risk of collision: traffic is more homogeneous and safer with an increasing percentage of cooperative vehicles. Figure 6.16b display the scatter plots of the traveled distance and the acceleration profiles standard deviations, which were already presented in figure 6.8. It is observed that the designed cooperative car-following law leads to a more efficient traffic while keeping comparable acceleration profiles. Note that the standard deviation of the traveled distance can be divided by 6 with the introduction of cooperation. An increasing percentage of cooperative vehicles potentially has a positive effect on an heterogeneous traffic.

Finally, the recommended approach to design the best multi-anticipative strategy starting from trajectory data should follow the steps:

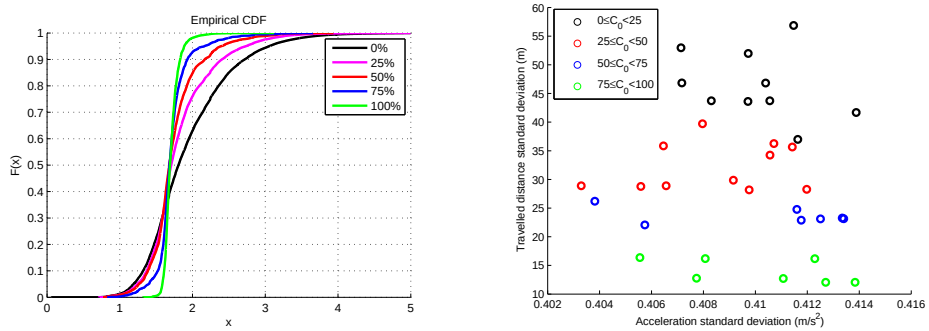

(a) (b)

Figure 6.16: Increasing coverage of cooperative vehicles (0 to 100%): (a) PET indicator, (b) Scatter plot of acceleration and travelled distance standard deviations

- If trajectories are available, apply the parameters identification methodology of chapter 5 to sample realistic sets of parameters. Better use the IDM model or the improved IDM (see [64]).
- Compute the mean calibrated values, estimate the steady-state headway and speed, and compute the partial derivatives of funtion f.
- Fix a limit on the number of forward and backward information data points m and m' *via* sensitivity analyses.
- From the computed partial derivatives, perform root locus analysis: secure the long-wavelength linear stability and apply the safety margin method. Combine with previous sentivity analyses to determine the best cooperative strategy,
- Tune the linear control gains to increase string stability despite law coverage of cooperative vehicles.

Chapter 7

Multi-agent modelling framework

Previous chapters, 5 and 6, were partially motivated by the multi-agent paradigm. In this chapter, an introduction to a multi-agent framework is proposed, with the underlying idea being to monitor and detect unreliable cooperative vehicles sensors and thereafter organize a safe and efficient traffic flow. After a literature review on the use of agents for traffic modelling, a three-layers multi-agent framework is described. The structure, as well as the graphical interface, are presented. Discussions on the learning layer are provided, and conclusions over the ongoing work, the potential and perspectives of this approach are drawn.

Contents

7.1 Intelligent agents, multi-agent systems and their potential applications to the transportation field

Intelligent agents have emerged as an accepted modelling concept in the Artificial Intelligence (AI) field. The fundamental role of action in intelligence calls for the design of intelligent agents [168]. An intelligent agent is defined as a system that acts in an environment in a intelligent way (Poole et al., [169]). Intelligent agents appear in many subfields of science, some applications including robotic vehicles, speech recognition, video games, spam fighting, and robotics, among others. The fields of control and robotics are much concerned by the concept of physical agents. In fact, the progress made in solving subproblems of the AI field encourage the coupling of those sub-systems in a whole-agent view perspective [170, 171], which as a consequence brings intelligent agents applications closer to fields like control and economics. For instance, robotic vehicles need to learn the sensing technology known not to be perfectly reliable and to coordinate it with the physical task -a vehicle is moving-. The internet field also serves the agent view paradigm, and software agents have acquired the name of softbots. Etzioni and Weld [172] introduced the term when they designed a softbot that dynamically helped satisfy a high level request by the user by using facilities such as archie, netfind and effectors such as ftp and mail. Among other applications, learning algorithms were tested to filter spams in E-mail messages [173]. Robotics vacuum cleaners have already been commercialized by the company iRobot. Google recently acquired an AI start up with the aim of developing their speech and image recognition software.

7.1.1 Definition of an agent

The following description is influenced by the book of Russell and Norwig [170]. The agent interacts with its environment through sensors and actuators, perceiving through sensors and acting through actuators. The past observations of an agent are the history of all the information collected by its sensors up to date. An agent that operates autonomously, perceives the environment he is part of, acts so as to achieve a good outcome while adapting to the environment changes is said to be rational. A good outcome can be defined as a desirable measure of performance achievable in the environment. Basically, the rational agent can be seen as a black box, where the prior knowledge of the environment, the past experiences, the observations and the goals of the agent are taken into consideration to generate some action (figure 7.1).

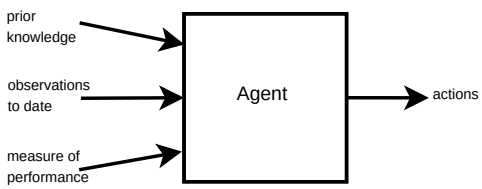

Figure 7.1: A rational agent

A few concepts can be developed from this definition. Omniscience happens when agents maximize the actual performance, in contrast with rationality where the expected performance is maximized. Autonomous agents rely more on observations than on their prior knowledge of the environment. Learning can increase the prior knowledge of the environment.

Different sorts of agents are chosen depending on applications. In the control theory field a very precise knowledge of the environment and of the consequences of some determined actions is required. Classical controllers force the system to converge towards a desired performance value, Bode and Nyquist analyses being widely used tools for convergence and stability of linear systems. Optimal control consists in chosing the optimal control policy by minimizing a cost function under specific constraints, relying on the Hamilton-Jacobi-Bellmann equation or on the Pontryagin principle. Stochastic control allows to deal with incertainties in the environment, *i.e.* partial observations. Adaptive and robust controls aim at designing appropriate controllers that deal with the incertainties of the estimated controlled agent parameters. In most of these control theory applications agents are controllers and physical agents. The fields of behavioral and cognitive psychology helped bring the notion of reflex and goal based agents that would later be used in a broad range of scientific applications. We can name the autonomous planning agent controlling the NASA Deep Space One spacecraft, and the autonomic computing concept that corresponds to the idea of achieving self-management in interconnected and distributed computing systems [174] via learning agents. Multi-agent systems (MAS) refer to interacting autonomous agents and their environment. If those agents are often software agents they can also be physical ones, and their sometimes simple interactions can generate emergence and self-organization [175]. The notion of emergence refers to the creation of identified and complex patterns out of relatively simple interactions, while self-organization can be defined as the creation of a desired global order -highly robust to unexpected perturbations- out of multiple and local interactions.

7.1.2 Agents in vehicular traffic

The field of transportation is well suited to agent technology deployment because of its distributed and dynamic nature, its partially observable environment, and the possible and sometimes needed flexible interactions between all its subsystems. An extensive review of the use of the agent computing paradigm in the field of traffic and transportation was made by Chen and Cheng (2010) [176].

Agents are first widely used as software and infrastructure agents for traffic management and decision support systems for traffic control. Garcia Serrano *et al.* designed Track-R agents according to the Foundation for Intelligent Physical Agent (FIPA) standard. Track-R agents are responsible for a geographical zone and send route choice recommendation to drivers and other agents [177] under particular meteorological incidents [178]. The MAS can be seen as a coordinating system for various traffic management centers. Another FIPA compliant system, the mobile-C platform, was developed and used to design the agent-based real time traffic detection and management system (ABRTTDMS) [179]. Mobile agents (vehicles) check the data acceptability of the laser detector stationary agents (part of the laser-based highway detection system [180]). Agencies corresponding to stationary agents process data from all sorts of detectors and track real time conditions while they are dynamically grouped by a higher level agency in order to assign and coordinate subtasks within subnetworks. Wang [181] proposed a three-layer architecture for agent based control of networked transportation systems separating task planning, coordination and running of control agents. Ossowski *et al.* presented the TRYSA$_2$ decision support system [182], which is split in an indivual stage where individual agents goals are generated, a social stage where conflicts and interactions are treated according to bargaining theory and a normative stage which permits/prohibits control actions in relation to traffic situations, *e.g.* congestion warning. The basic idea is that control algorithms are like control agents that can be activated on demand. Still with the idea of an urban traffic control (UTC), a traffic data management MAS was used for global visualization of spatial temporal traffic states in the city of Beijing [183].

Traffic signal control and intersection control are relevant applications of agent-based modelling in transportation. Choy *et al.* [184] divided the problem in high level and lower level agents to coordinate the real time traffic signal control of a traffic network. Intelligent agents operate from the network level to the intersection level, and their design based on fuzzy logic and neural network theories provide learning and adaptive facilities

to changes in the environment. A cooperative ensemble (CE) is introduced in [185]: link relationships between agents (intersections) are evaluated to form cooperative zones, so that agents within a same cooperative zone make a group decision to generate control outputs at each optimization stage. Intelligent intersection agents are also used in [186]. Their components are included in three categories: the data layer, which allows communication and data process, the processing layer which keeps the knowledge of past experiences, predicts traffic volumes and weights the importance of each intersection and the decision layer which integrates information from the processing layer to act upon the cycle, split and offset of traffic signals. These systems are close to the system for autonomous agent-based UTC proposed by Roozemond [187], which consists of authorities agents, intersection traffic signalling agents (ITSA), and road segment agents. ITSA have the central role of predicting traffic, adapting control strategies and sacrificing performance to achieve self-organization. At the network level, the coordination and synchronization should be based on heuristic methods that take into account constantly changing and sometimes conflicting goals of various ITSAs.

Agents can also be used as physical agents to examine the dynamic routing of vehicles in an urban network. An agent-based extension of the microscopic simulation model DRACULA is proposed in [188] to investigate the influence of information on departure time and route choice behavior. Dia and Panwai [189] interfaced a neural network agent-based route choice model with a microsimulation model to assess the compliance rate to travel information in the city of Brisbane. The Cooperative Traffic Management and Route Guidance System (CTMRGS) is used to explore the dynamic routing by simulating negotiation between in vehicle route guidance systems that integrate the traveller's needs and its position in the network, and the information service providers in charge of traffic estimation and trip planning which receive network information as well as desirable control strategies from a traffic management center [190].

Finally, agents can serve traffic simulation purposes especially by integrating ITS communication capabilities. The COSY agent architecture and DASEDIS multi-agent system were used [191] to model the driver-vehicle elements as agents, so that sensors gather data that is treated in a cognition module to achieve appropriate actions, a list of five traffic states being linked to intended execution scripts. Tactical drivers -agents- that assess the driving decisions based on internal parameters, *e.g.* car-following parameters and desire to exit, and external parameters such as influence weight of vehicles in the global system [192]. Those parameters are learned via the

evolutionary population Based Incremental Learning (PBIL) algorithm to avoid collisions, missed exits and deviation from desired speeds. A STEAM-based multi-agent framework was used for platoon coordination, stating that a teamwork agent based model increases the safety, time and communication efficiency of platoon formation [193]. Regarding platoon formation and control of automated vehicles, we saw that most of the work had been achieved along the Automated Vehicle and Highway System (AVHS) effort from California PATH [194, 195, 196, 197, 198, 199], while other works focused on conditions to obtain string stable and collision free motion [200, 201].

7.1.3 Towards traffic flow homogeneization: from control of vehicle formation to self-organization

Those traffic applications being listed, traffic flow homogeneization is another topic of significant interest to both control and multi-agent communities. Thanks to communication facilities, connected vehicles are now able to send, receive and forward information within an interaction range. Then, if some vehicles are doted of such communications capabilities, the idea is to coordinate and control their movement to ideally remove accident and congestion prone microscopic -or mesoscopic- traffic situations.

Achieving good synchronization and homogenization of any traffic stream through vehicle sensing brings us back to the field of control of vehicle formations. Tools from both graph and control theory were merged in [202] to determine a Nyquist stability criterion for stabilization of a linear system, linking graph Laplacian eigenvalues with the topology of formation dynamics. The flocking framework described by Olfati El Saber [95] and introduced in section 3.2.3 is inspired by the movement of birds. Related work on flocking theory concluded over the importance of parameters in the design of the system pairwise potential energy to obtain cohesive groups of particles [203]. Choi *et al.* [164] used a similar dynamical system, in which each agent cooperatively updates its own estimate of the field of interest based on noisy measurements. The ODE Ljung approach [204] allows proving the convergence of the stochastic algorithm. Limitations of this research reside in the use of static and symmetric communication graph. Dynamic and switching topologies were introduced for a simpler dynamical model in [205] where a Lyapunov-Krasovkii function is used to perform stability analysis. In [206], the authors develop a nonlinear leader-follower architecture where the linear matrix inequalities (LMI) method helps obtain the asymptotical stability conditions. These results provide important insights on the potential of communication in terms of control of vehicle formation.

However, it can be argued that such approaches are rigid and not well suited to traffic flow control, as traffic exhibits multiple sources of uncertainties. A multi-agent self-organizational structure [207] may appear to be more flexible when the goal of a system is to reach an organization through autonomous internal processes. Notions such as emergence of -desired- structures, adaptivity and self-maintenance characterize self-organization. Most existing approaches provide mechanisms that dynamically alter the structural relations between agents either through bio-inspired mechanisms or through the use of some specified transformation rules. More specifically, a particular attention was recently given to mutual influence between informational and behavioral levels [208, 209]. Trust and reputation-based systems [210] are often well used to relate these two levels, as the informational flow must be organized to effectively exploit the information and to ensure the reliability of this information which is used at a behavioral level. The interested reader can refer to literature reviews by Sen [211] and Alzaid *et al.* [212], those systems being mainly used to help reinforce insufficient protection by cryptographic mechanisms in Wireless Sensors Networks. Finally, Sabater and Sierra [213] proposed a classification of trust systems using the following criteria: the model type (game-theoretical or cognitive), the diversity of information sources (direct, witnessed or indirect, and sociological, prejudice), the visibility type (global/public or local/private), the model granularity (context dependent or not), the behavioral assumptions (whether cheating behavior is allowed or not), the type of exchanged information (boolean or continuous measures), and the existence of a trust reliability or confidence measure. In the case of a highway traffic with unreliable cooperative vehicles (faults in sensors), the collective task is to make traffic evolve in the stability regime while guaranteeing a sufficiently safe traffic. The approach that is developed in the next section takes over the trust system concept with the specificity of using a trust layer, which can be seen as the learning layer to detect unreliable sensors, and which acts as a top layer over the physical and communication layers.

7.2 A three layers multi-agent framework

Incertainties coming from fault in sensors or poor parameters estimation can cause major breakdowns of the highway traffic if not monitored in real time. The goal of each agent -vehicle- is to cooperatively evolve towards a stable and homogeneous traffic despite such incertainties. To achieve this goal, a three layer architecture is proposed with physical, communication and

trust layers. The communication and trust layers interact with the physical layer by managing information exchanges and information reliability and by using this information to influence the vehicles dynamics described at the physical layer. From a control perspective, the purpose is to use the reliable information to influence the movements of vehicles while limiting traffic disturbances, and hence homogenize traffic flow. Figure 7.2 presents the interaction between the three layers. The physical layer concerns the vehicle dynamics rules and estimates on its dynamics. The communication layer governs the information exchanges through proximity and reliability rules, which are traduced into probabilities. The trust layer models the quality of the exchanged information and then influences the physical layer through the communication layer.

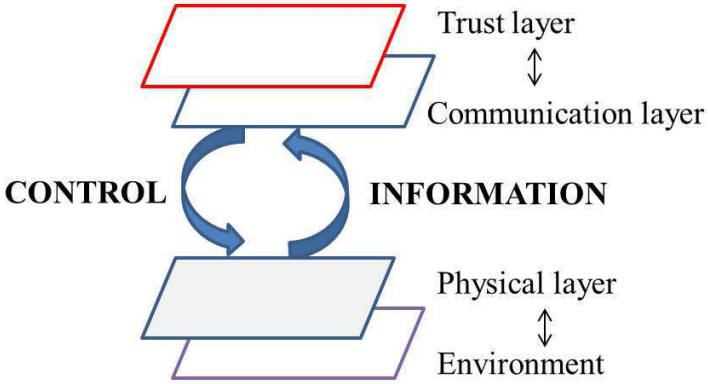

Figure 7.2: Interacting layers

7.2.1 Conception

The interacting layers are here described in detail for a highway traffic with open boundaries, *i.e.* when the vehicles are not circulating in a ring. The simulated traffic consists of a finite number of vehicles evolving on a stretch of highway with a finite number of lanes. The environment, the physical, communication and trust layers are introduced with their specificities. Figure 7.3 illustrates the studied traffic configuration.

Yellow lines correspond to in-vehicle sensors (radars, cameras) that are able to detect neighboring headways, relative speeds and speeds while the red dotted line corresponds to radio communication. The objective of a multi-agent framework is to build a robust framework to integrate communication

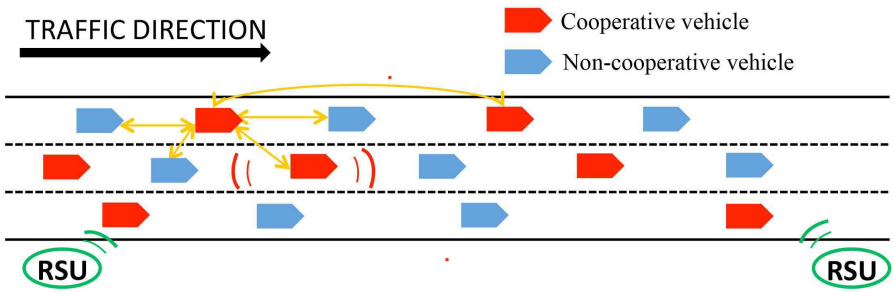

Figure 7.3: Example of a mixed highway traffic of cooperative and non-cooperative vehicles

for traffic flow homogeneization.

Hypothesis

The estimation of car-following and lane-changing parameters is not performed online but in a static way prior to the simulation, applying the methodology of chapter 5. Each agent has a full knowledge of its parameters, and a noise (incertainty) could be associated to this knowledge.

Environment

The environment consists of Road Side Units (RSU), which are part of the infrastructure along the road, and of vehicles which could be cooperative or non-cooperative. Both cooperative vehicles and RSU are doted with radio communication abilities and are able to send and receive information within a given communication range at every communication time step. As specified earlier, cooperative vehicles also dispose of radars or lasers that are able to sense the headway and relative velocities with surrounding vehicles (yellow lines in figure 7.3). Each cooperative vehicle is assigned an initial measurement error $\mathcal{E}_n$ which takes the following form for a vehicle n

$$\mathcal{E}_n \begin{pmatrix} \dot{x}_n \\ \Delta x_n \\ \Delta \dot{x}_n \end{pmatrix} = n_f \begin{pmatrix} \dot{x}_{eq} \\ \Delta x_{eq} \\ \dot{x}_{eq} \end{pmatrix}, \tag{7.1}$$

where n_f is a noise factor weighting the error in function of the global steady-state values. Note that the parameters estimation errors are not being covered in this study, however since the measurement noise is set to

impact the three variables of the car-following law ($\dot{x}_n, \Delta x_{n+j}, \Delta \dot{x}_{n+j}$), an equivalence can be made with the reliability of parameters estimation and the same methodology applied.

Physical layer

The non-cooperative vehicles are moving according to the IDM model, with the sampled distributions of calibrated parameters of chapter 5 (using random sampling without replacement). The cooperative vehicles are also moving based on the sampled sets of parameters, but also according to the bilateral multi-anticipation law with added control terms. There is a need to integrate the trust value computed from information reliability considerations. Let a_{ij} be the coefficient of the weighted information between agents i and j. If the lane change, which is chosen to remain non cooperative, does not apply, the longitudinal behavior is defined as

$$\ddot{x}_n = f_c(\dot{x}_n, \sum_j a_{nj}\Delta x_{n+j}, \sum_j a_{nj}\Delta \dot{x}_{n+j}), \tag{7.2}$$

$$\ddot{x}_n < acc_{\max}, \tag{7.3}$$

$$\ddot{x}_n > acc_{\min}, \tag{7.4}$$

where f_c' is chosen as the IDM model with added control terms c_1' and c_2' (see (4.39)) that are defined in the communication layer. The interaction range is selected to be equal to

$$r = 4 \cdot \Delta x_{eq,e}, \tag{7.5}$$

where $\Delta x_{eq,e}$ is the steady-state headway estimated by the RSU, which is chosen to be the average of speeds sent by cooperative vehicles in the three lanes over the last five communication steps and within a radius of 300 m (150 m upstream and 150 m downstream). The term $4 \cdot \Delta x_{eq,e}$ was calibrated to avoid scaling effects when computing the cooperative coefficients, in the case of $m = 2$, see section 6.3.2.

Figure 7.4 illustrates the interactions for vehicle n as well as the definition of the interaction range r. The condition $m = 2$, $m' = 2$ discussed in chapter 6, is here applied and expressed as the exchange of 2 measurements, and these measurements are taken as close as possible to the vehicle n to increase its immediate knowledge and increase safety. Consequently, forward cooperative leaders will communicate the headway in relation with their follower, and backward cooperative leaders will communicate the headway in relation with their leader.

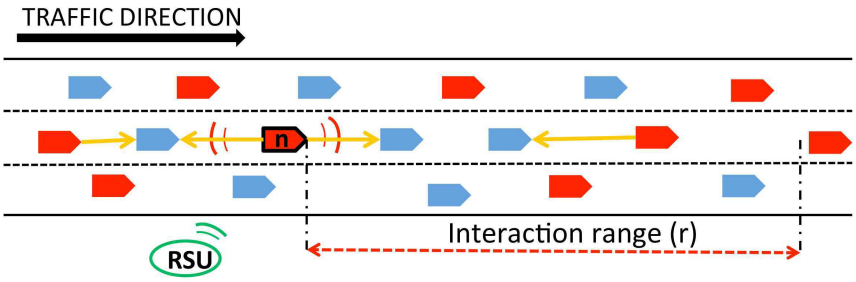

Figure 7.4: Considered interactions (two informations) for cooperative vehicle n.

Communication layer

The communication task is split into two categories: static and mobile agents. First, static agents are RSU units that are in charge of collecting information in their geometric areas to compute global steady-state values $(\dot{x}_{eq}, \Delta x_{eq})$. The highway section is divided into RSU sections that estimate in real time the average speed in their assigned geometric section. The IDM steady-state headway is then computed according to relation (6.3), and both steady-state headway and speed are sent to cooperative vehicles. Note that the stability value $f_1^2 - 2f_1 - 2f_1 f_3$ can be associated to each computed global steady-state value, and therefore an adapted control (dependent control gains c_1 and c_2) could be applied to change the global steady state values to modify that stability value while homogeneizing traffic flow.

Secondly, the cooperation between mobile agents is set to follow two rule: the proximity rule and the reliability rule. As for the proximity rule, a coefficient (p_{ij}) represents the proximity of information weight, as it was introduced in equation 4.106 for constant coefficients:

$$P_{ij} = 1/2\left(1 + \cos\left(\pi\frac{(x_j - x_i)}{r}\right)\right), \; j = i - m' \ldots, i + m, \tag{7.6}$$

$$p_{ij} = \frac{P_{ij}}{\sum_l P_{il}}, \tag{7.7}$$

where the cosinus window is used, as it is the window that minimizes the possible unsafe situations due to cooperation, while guaranteeing an increase of string stability, see section 4.5.4 and r is the interaction range.

As for the reliability rule, a trust value (T_{ij}) between agent i and j is computed as a measure of the information reliability. Coefficients p_{ij} should

then be designed to reduce the breakdown induced by poor information reliability and at the same time to increase traffic string stability. The strategy to determine the best coefficient a_{ij} is written

$$A_{ij} = p_{ij} \cdot T_{ij}, \tag{7.8}$$

$$a_{ij} = \frac{A_{ij}}{\sum_l A_{il}}, \tag{7.9}$$

where a multiplication is performed between weights of proximity and reliability rules. Finally, two last considerations have their importance. First, it is a question of not breaking the root locus analysis conjecture of section 4.5.2, stating that a_{ij} must decrease with j. Consequently, the following condition to the introduction of weigthing coefficients is added:

$$a_{i(i+1)} > \max_{j \in \{i+1, i+i_m\}} a_{ij}, \tag{7.10}$$

where $i + i_m$ is the index of the last considered cooperative vehicle in the cooperative law. Secondly, the low T_{ij} values should be disregarded even though condition (7.10) is fulfilled. A second condition to the introduction of cooperation, which is complementary to equation 7.10, is written

$$\max_{k \in \mathcal{I}_i} T_{ki} > \delta, \tag{7.11}$$

where $\mathcal{I}_i$ is the set of agents that sense the same information as agent i at the same time step, including vehicle i, with $i \in \mathcal{N}$ and δ is a reliability threshold above which value the information can be taken into consideration. Finally, the added linear control terms are written

$$c_1' = \max_{k \in \mathcal{I}_i} T_{ki} \cdot c_1, \tag{7.12}$$

$$c_2' = \max_{k \in \mathcal{I}_i} T_{ki} \cdot c_2. \tag{7.13}$$

Trust layer

The definition of the information reliability can be twofold. First, each agent measures the confidence made in the received information as well as the confidence it has in itself (in its own sensors). A cooperative agent is able to sense all its surrounding vehicles via sensing devices, e.g. radars, lasers, cameras. It compares this sensed information with comparable information coming from other agents, and then is able to share it with others

agents, allowing the computation of a trust value. Secondly, each cooperative agent can estimate its car following parameters based on its trajectory data. Another reliability value can, therefore, be computed depending on the robustness of the parameters identification, for example, its variability and the quantity of information available to perform the estimation. As specified earlier, only the errors coming from sensors will be part of the trust system.

Following the work of Sabater and Sierra [213], a classification of the trust system to be built can be made. It is a game theoretical system as it computes probability that will weight the information. The information sources are chosen to be direct and indirect. Direct information embodies the information that is sensed by one agent and possibly directly comparable with other agents. At a given time step, agents sense the speed, headway and relative velocities of their immediate neighbors. A same information that is shared between an agent i and an agent j allows the computation of a direct trust DT_{ij}. Indirect information refers to the information that is shared by other agents, so that indirect trust between an agent i and an agent j IT_{ij} is computed by using the direct trust of the past direct communicants k with agent j (which were able to compute a direct trust T_{kj}). The visibility type is private, given that each agent only communicates the direct trust it has in another agent with agents in its communication range, and that the confidence an agent has in itself is never shared. The trust system is set not to be context dependent, and cheating behavior is not allowed. Finally, the measures of trust information are continuous, and there is no trust confidence value given that the parameters identification incertainties will not be considered.

The direct trust DT_{ij} between an agent i and an agent j is deduced from the Euclidean norm of the measurement noise m_{ij} in the vector space defined by the three variables $(\dot{x}_n, \Delta x_n, \Delta\dot{x}_n)$ of the car-following law. The measurement noise is written

$$m_{ij} = \frac{||\mathcal{E}_j - \mathcal{E}_i||_2}{||(\dot{x}_{eq}, \Delta x_{eq}, \dot{x}_{eq})||_2} \ , \tag{7.14}$$

which can be seen as a normalized value compared to the computed equilibrium values by the RSU. Note that for the sake of simplicity, the measurement noise is written is one dimension (instead of three), *i.e.* it is assumed that each sensor has identical noises for the three measurements (or the same sensor is used to measure the three variables and therefore exhbits identical noises).

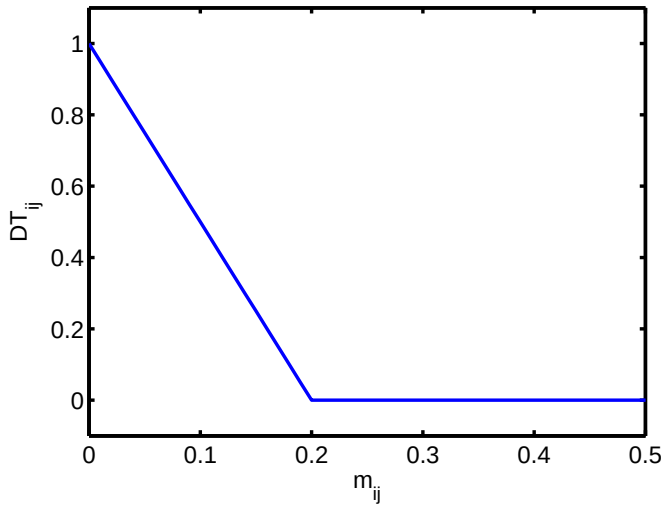

Figure 7.5: Relation between computed measurement noise and direct trust, with $\sigma = 5$.

Figure 7.5 illustrates a simple way of linking the direct trust DT_{ij} with the measurement noises m_{ij}, the slope of the curve being σ. The error m_{ij} decreases until it reaches the threshold error $m_{ij} = 0.15$ above which the direct trust is equal to 0. Different slopes σ can be selected, and the relation between m_{ij} and DT_{ij} is simply written:

$$DT_{ij} = \max(1 - m_{ij}\sigma, 0). \tag{7.15}$$

As a second step, if and once the direct trust values have been computed, the computation of the indirect trust IT_{ij} is possible and is written as

$$IT_{ij} = \frac{\Sigma_{k \in \mathcal{N}_{ij}} T_{ik} T_{kj}}{\Sigma_{k \in \mathcal{N}_{ij}} T_{ik}}, \tag{7.16}$$

where $\mathcal{N}_{ij}$ is the set of agents k of cardinal n_{ij} that have previously compared direct information with both agents j and i and hence updated trust values T_{ik} and T_{kj}. Thus, IT_{ij} is an indirect trust i has in j based on a mean trust of agents agents i and j previously compared information with.

After these two computations, the agent i can compute the trust value T_{ij} as a weighted average between the direct trust and the indirect trust

$$T_{ij} = \frac{T_{ii} DT_{ij} + IT_{ij}}{T_{ii} + 1}. \tag{7.17}$$

Finally, the self trust an agent i has in itself can be viewed as an average trust the agents that have interacted with it have in him, as follows:

$$T_{ii} = \frac{\Sigma_{k \in \mathcal{N}_i} T_{kk} T_{ki}}{\Sigma_{k \in \mathcal{N}_i} T_{kk}}, \tag{7.18}$$

where $\mathcal{N}_i$ is the set of past direct communicants with agents i, of cardinal n_i. This self trust directly interacts with the final trust T_{ij} for the computation of coefficients p_{ij} defined in equations (7.9).

7.2.2 Pseudocode and graphical interface

In this section, the general code structure, pseudocode and graphical interface are presented. The program was all written in Matlab, and the data stored during the simulation to allow posttreatment. Figure 7.6 first introduces a graphical representation of the simulation program, where the simulator is divided into two parts: an initialization and a run stage.

The figure shows the sequence of instructions in the program, which indicates the series of tasks involving the three different layers of the simulator. The perception stage precedes the physical behavior update which has to go through the communication rules and use the knowledge of the just-computed trust values. The pseudocode is now introduced to detail data structures.

Pseudocode

Phase 1: Initialization

1. *Loading:* load calibrated parameters, empirical trajectories.

2. *Set global parameters:* simulation time step, vehicle length, percentage of aggressive lane changing parameters, percentage of perturbed sensors, percentage of cooperative vehicles, interaction range, maximum number of considered vehicles in the cooperative law, apply bilateral control or not, control gain values.

3. *Set initial conditions:* compute steady-state headway and speed from empirical data and prior calibrated parameters, select the number of lanes and the number of simulated vehicles.

4. *Create data structures:* store initial conditions in a map NotUpdated-Data(id) (key:id, value: time, position, speed, acceleration, headway, relative speed). Store vehicle data in a map Vehicle(id) (key: id,

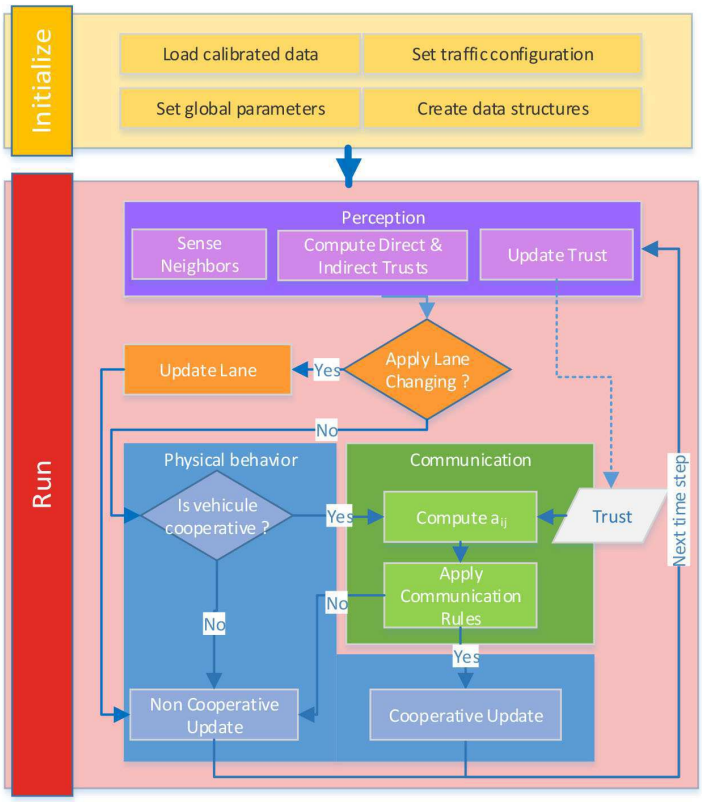

Figure 7.6: Principal tasks in the code structure.

value: car following parameters, lane changing politeness parameter, cooperative vehicle or not). Initialize the Graph Trust (matrix Tij(id,id)), the direct measurement matrix DT(ij,ij), the direct adjacency matrix DTAdj(id,id), the indirect measurement matrix IT(ij,ij), the indirect adjacency matrix ITAdj(id,id) and the sensors Noise (map SensorsNoise(id)).

Phase 2: Run

At a given time step t, perform:

1. *Perception stage:* loop on ids of map NotUpdatedData(id). Each cooperative vehicle senses its immediate behavior and update its direct measurement matrix DT(ij,ij) and the corresponding adjacency matrix DTAdj(id,id), its indirect measurement matrix IT(ij,ij) and the corresponding indirect adjacency matrix ITAdj(id,id), and finally update

the matrix Tij(id,id) by integrating direct and indirect measurements.

2. *Action stage:* loop on ids of map NotUpdatedData(id). If the vehicle does not have any leader, maintain the same speed.

   a. Apply lane changing model if possible, and compute the updated data as map UpdatedData(id), otherwise;

   b. Update the acceleration according to the cooperative law or the non-cooperative law (depending on the vehicle and trust characteristics, using map Vehicle(id) and matrix Tij(id,id)). Compute the updated data as map UpdatedData(id).

3. *Update stage:* store UpdatedData(id) in GlobalData(id) and equal NotUpdatedData(id) to UpdatedData(id). Go to time step t+1.

Graphical interface

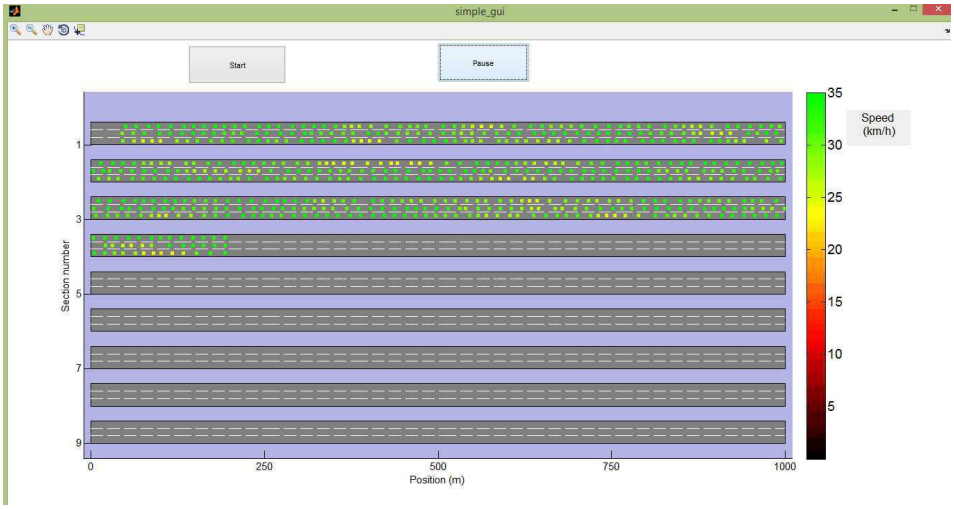

Figure 7.7: Screenshot of the Guide graphical interface. Colors indicate vehicle speeds.

A simple graphical interface was implemented using the GUIDE interface of Matlab, as shown in figure 7.7. Vehicles evolve from the top left to the bottom right, each horizontal line corresponding to a 3 lane highway section of 1000 m. Here vehicles are represented in a scale color corresponding to their speeds, which enables the observation of the stop and go phenomenom.

However colors could be used to represent other features (cooperative vehicle or not, reliable sensors, accelerations).

Generally speaking, this interface enables a simple and quick visualization of the simulated traffic, and can be used for multi-purposes (for instance collision avoidance, observation of local instabilities, detection of perturbed sensors).

7.3 Simulations

In this section, simulations are first run to test the communication and trust layers in a static way, *i.e.* without the trust dynamic update rules. In this static configuration, vehicles are assumed to have the knowledge of their sensors faults, and a trust value is associated to the mesaurement errors using formula 7.15. The robustness of the cooperative strategy to faults in sensors is first being investigated. Parameters to be tested are parameter δ, which is the self-confidence threshold above which a vehicle should not have a cooperative update law (equation 7.11), and parameter σ, which is the slope relating the measurement error and the direct trust value (figure 7.5). Finally, first results on the dynamic estimation of perturbed and defective sensors as well as perspectives of improvements are discussed.

In the next subsections, a sensor is said to be a perturbed sensor if it has a trust value ranged in the open interval $[0, 1[$, and is said to be a defective sensor if it has a trust value of 0.

7.3.1 Simulations: static trust layer

In this subsection the noise factor n_f of equation 7.1 is chosen to be following a uniform distribution centered in 0 and taking values in the interval $[-n_f/2, n_f/2]$, which corresponds to measurement errors in the interval $[-\frac{\Delta x_{eq}}{2}, \frac{\Delta x_{eq}}{2}]$ for headways and in the interval $[-\frac{\dot{x}_{eq}}{2}, \frac{\dot{x}_{eq}}{2}]$ for speeds and relative speeds.

Robustness of strategies: time-space diagram

It is first a question of looking at the impact of a cooperative strategy in the presence of perturbed sensors. A first time-space diagram helps verify the efficiency of the defined communication and trust layers. Figure 7.8 displays the time-space diagrams for respectively 0 and 60% of perturbed sensors, with 60% of coperative vehicles, using rule 7.9, and $\delta = 0.7$, $\sigma = 5$. It is obvious that no shock waves appear, so that the cooperative strategy is still

efficient with 60% of perturbed sensors (assuming that a prior knowledge on the sensors quality is possible).

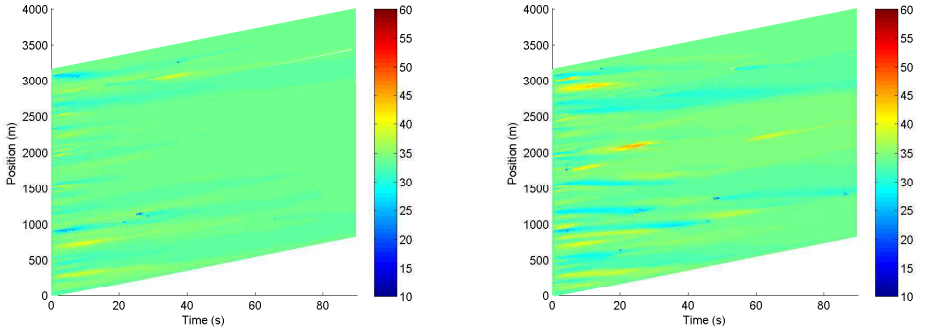

(a) (b)

Figure 7.8: Simulation with 60% of cooperative vehicles, $\delta = 0.7$, $\sigma = 5$, and (a) 0% of unrealiable sensors (b) 60% of perturbed sensors.

Besides, with 100% of faults in sensors and 60% of cooperative vehicles, it is still possible to go towards traffic flow stabilization. Figure 7.9 shows the time-space diagrams for 0% and 60% of cooperative vehicles (100% of them perturbed).

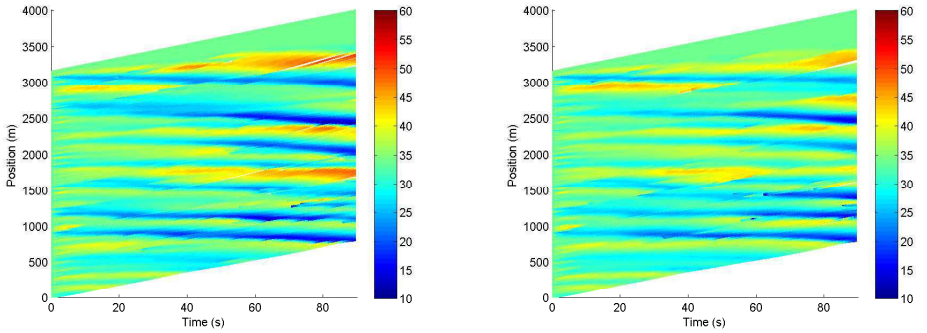

(a) (b)

Figure 7.9: Time-space diagrams with $\delta = 0.7$, $\sigma = 5$, $c_1 = 1.1$, $c_2 = 0.4$ and (a) 0% of cooperative vehicles (b) 60% of cooperative vehicles (100% of them are perturbed).

The same obervations can be reinforced when looking at the value of the

PET indicator (which is shown later). It appears clear that the successive inclusions of equations (7.9), (7.10), (7.11) increase traffic flow safety and efficiency to eventually reach the homogeneous traffic flow observed in figure 7.8b. The construction of the communication and trust layers are part of a robust framework which allows to preserve a homogeneous traffic flow even when 60% of cooperative vehicles are doted with perturbed sensors.

Discussion on parameters δ and σ

Two parameters are of relevant importance: the self-trust threshold parameter δ and the decreasing slope relating the measurements and the direct trust σ. The number of critical safety situations are chosen to be the ones with PET < 0.5s. Let N_c be the number of occurences of such critical situations, while TD is the the travelled distance standard deviation of the vehicles. Figure 7.11 displays the values of these two indicators in a color scale as a function of the two varying coefficients δ and σ, again for 60% of cooperative vehicles and for 60% of perturbed sensors.

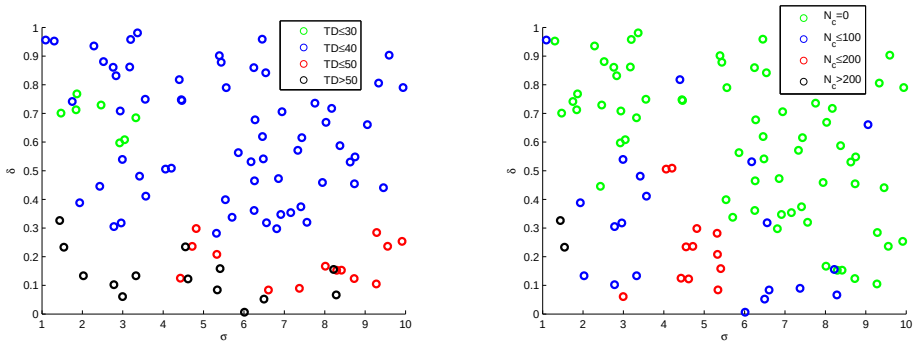

(a) (b)

Figure 7.10: Simulation with same random distributions for 60% of cooperative vehicles and 60% of perturbed sensors: (a) Traveled distance scatter plots; (b) PET scatter plots.

It appears that combined low values of coefficients σ and δ lead to instabilities. This is due to a bad design of cooperation: a low value of σ tends to underestimate the impact of measurement errors whereas a low value of δ means that vehicles with low self-trust values can use a cooperative car-following law. It is also observed that values of δ so that $0.6 < \delta < 0.8$, and values of σ so that $1 < \sigma < 3$ lead to a good trade-off for both indicators.

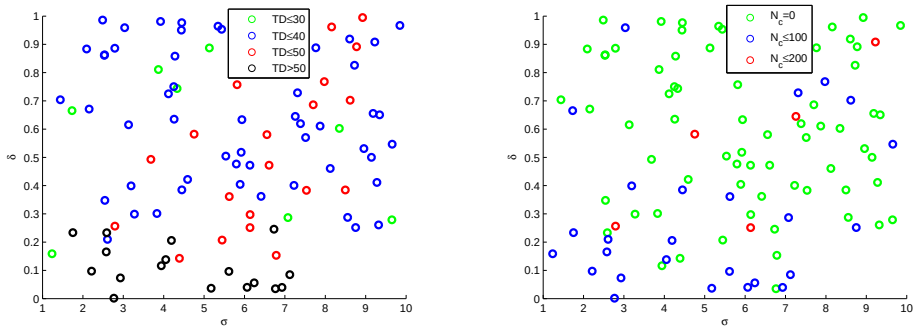

(a) (b)

Figure 7.11: Replications with 60% of cooperative vehicles and 60% of perturbed sensors: (a) Traveled distance scatter plots; (b) PET scatter plots.

Higher values of δ degrade the indicators as it means that no cooperation is introduced even though the sensor is only slightly defective (law percentage of errors according to equation 7.14). From now on, the parameters will be set so that $\delta = 0.7$ and $\sigma = 2$. For $\sigma = 2$, a noise factor above 0.5 leads to a nil trust value, see figure 7.5.

Variation of measurement errors in time

To go further in the analysis, it is interesting to observe how a mixed traffic composed of cooperative vehicles with perturbed sensors reacts to a change of trust values, *i.e.* when a deviation is observed in the sensors measurements, for example, caused by a bad response to adverse weather conditions. Here the noise factor is gradually changing in time from 0 to 0.25, which corresponds to a trust decrease from 1 to 0.5, and the consequences on traffic flow are investigated.

In figures 7.13 and 7.12 the temporal evolution of the statistical whiskers of the PET and speed distributions are displayed, where the first and last quartile, the median, and the extreme values that are not considered as outliers are displayed in boxes. The noise factor linearly grows in time to eventually reach a 0.5 trust value, *i.e.* below the δ threshold of cooperation (equation 7.11). The stabilization effect of the introduction of cooperation is well observable. While a non-cooperative traffic exhibits a spread of the distribution quartiles, as shock and go waves propagate and as such instabilities result in a more heterogenous traffic, a cooperative traffic appears

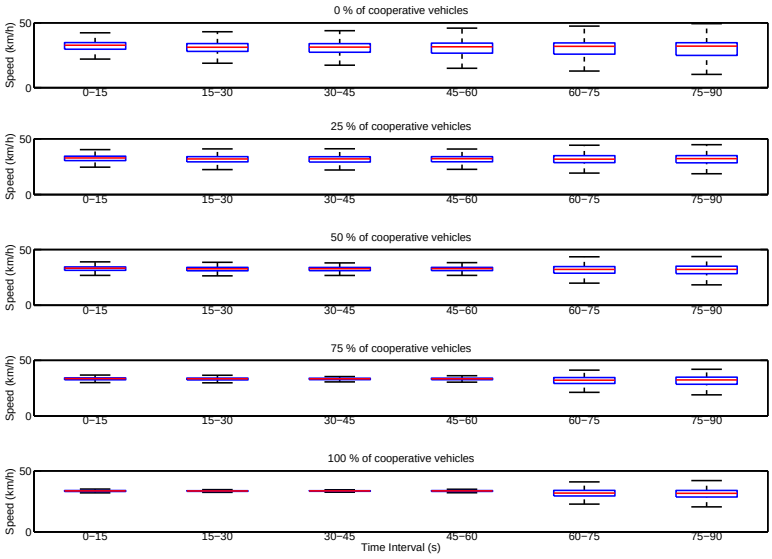

Figure 7.12: Temporal evolution of the speed distribution for decreasing trust values and different cooperative vehicles rate.

more resilient to the propagation of such instabilities.

At the beginning, cooperation contracts both speeds and PET distributions to a certain extent, especially high values for the PET. The higher the percentage of cooperation is, the more contracted the speed and PET distribitions are. For non-cooperation, the distributions progressively spread with time. Then, when the trust reaches the value of 0.7 (corresponding to the δ threshold of cooperation), which happens right before time step t=60s, the traffic heterogeneity starts increasing. If a degradation of the trust values barely leads to a growth of the traffic heterogenity (*i.e.* a spread of the PET and speed distributions), the transition is easily observable for the threshold delimiting cooperative *vs* non-cooperative traffic. This tendency is clearly confirmed by the time-space diagrams of figure 7.14, where for either 25% or for 100% of cooperative vehicles, new shock waves are created when trust values pass the δ threshold, which certifies the transition cooperative *vs* non-cooperative traffic. More specifically, in figure 7.14b, for 25% of cooperative vehicles, the percentage of cooperation is not sufficient to remove all sort of instabilities but at the same time, prevents them from growing, see the corresponding evolution of the speed and PET distributions in figures 7.13,7.12.

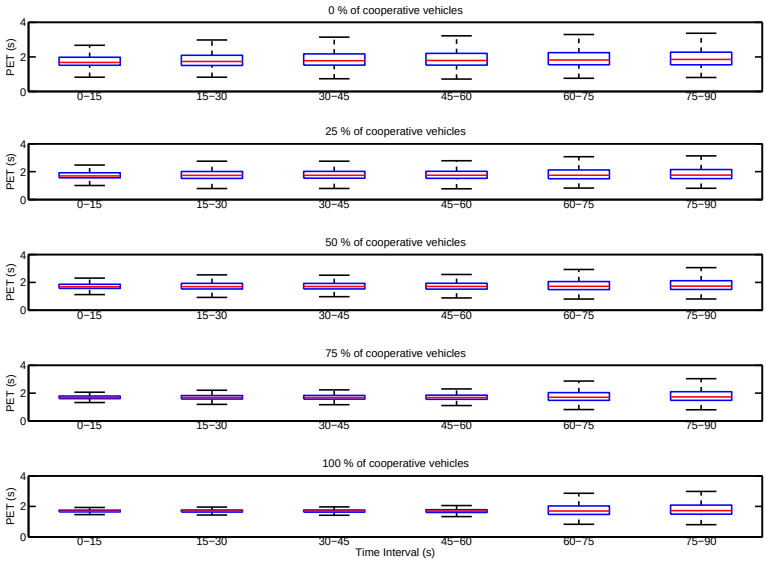

Figure 7.13: Temporal evolution of the PET distribution for decreasing trust values and different cooperative vehicles rate.

Then, when the δ threshold is reached, new shock waves are added to the previous ones.

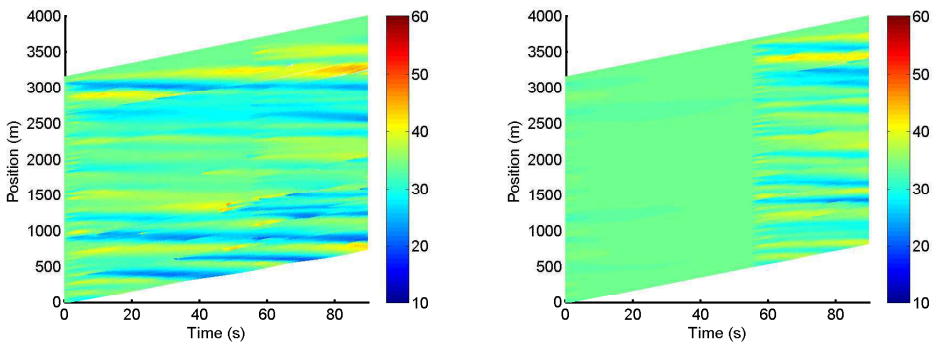

(a) (b)

Figure 7.14: Time-space digrams with 25% of cooperative vehicles and 100% of cooperative vehicles.

Finally, one can imagine that when a cooperative vehicle is ruled out, the driver present in the car can take over the driving task. Consequently, an intelligent cooperative vehicle could adapt its car-following parameters to the driving characteritics of its driver in order to secure smooth transitions between driving task and automatic task. Reciprocally, a cooperative vehicle could train a driver to modify its driving behavior.

7.3.2 Simulations: dynamic learning layer

In the dynamic case, there is no prior knowledge on the quality of sensors, and they are all initialized to be reliable. This learning step is fundamental as the detection of defective sensors would avoid possible dramatic effects on traffic flow. This section emphases that the built-in trust layer requires a minimum number of information exchanges to be accurate.

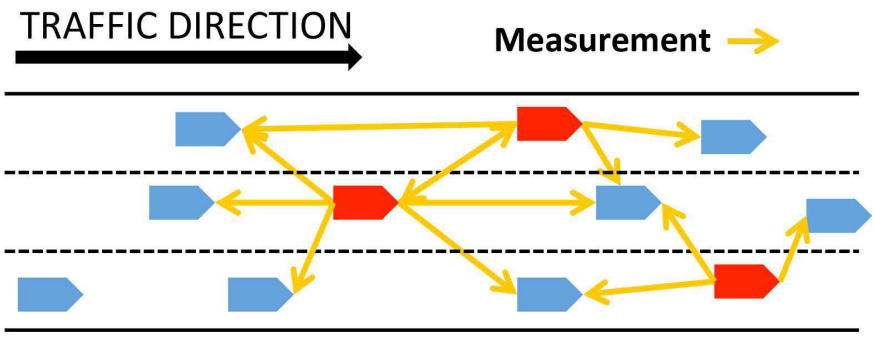

Figure 7.15: Sensing abilities of cooperative vehicles (in red).

First, the physics of information exchanges has to be defined. Figure 7.15 illustrates the potential exchanges for a cooperative vehicle that are possible at any communication time steps -possibly different to simulation time steps. A cooperative vehicle is able to sense its leaders and followers in its lane and its two adjacent lanes. This could be considered at a worst case scenario as in some clear circumstances a vehicle might be able to sense further vehicles (for instance its second leader).

The first configuration consists in setting the noise factor following an uniform distribution between 0 and 0.5, so that the trust varies from 0 to 1 in an uniform way. ϵ_T is chosen to be the difference between the computed trust an agent has in itself and the "true"trust of this agent (computed via

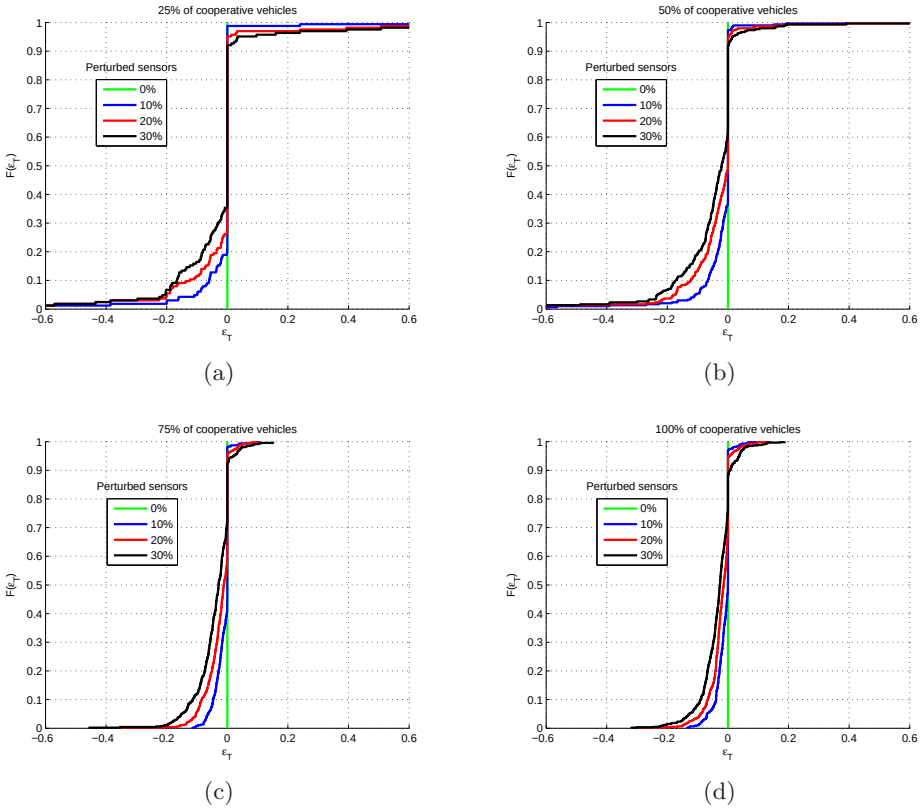

Figure 7.16: Cumulative distribution functions of ϵ_T after 75 communication time steps for various percentage of cooperative vehicles: (a) 25%; (b) 50%; (c) 75% and (d) 100%

equation 7.14 and 7.15). It appears obvious from the cumulative distribution functions of figure 7.16 that low and medium coverage of cooperative vehicles (below 75%) do not allow a full learning of perturbed sensors in the selected time period, which is of 75 seconds. The high values of ϵ_T are due to the lack of interaction between vehicles, as the traffic is very dense and the time interval is not sufficient to allow a large enough amount of direct trust computations.

Figure 7.17 corroborates these observations, where here the unreliable sensors are all set to be defective (corresponding trust value of 0). The number of unsatisfying detections is set to be the total number of cooperative vehicles with a computed ϵ_T for the self-trust higher than 10%, meaning

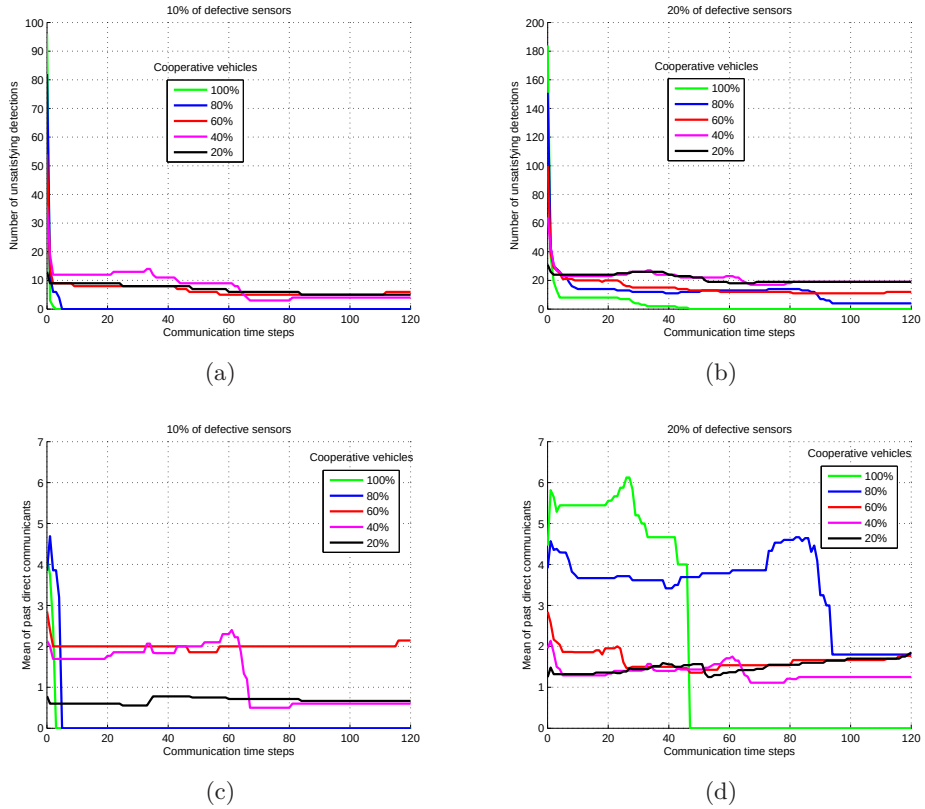

Figure 7.17: Number of unsatisfying detections and mean number of past direct communicants for unsatisfying detections for (a), (c) 10% of unreliable sensors; (b), (d) 20% of unreliable sensors.

that the computed trust is accurate within a confidence interval of 10%. A correlation between the average number of direct trust comparisons and the number of unsatisfying detections appear immediate. Each time the mean value of past direct interactions exceeds 2 (where a vehicle interacts with himself and with another vehicle), new defective sensors are detected and the number of unsatisfying detections decrease. However, similarly to figure 7.16, the dense simulated traffic appears to limit the number of direct trust computations and, as a result, the accurate detection of trust values. For example, in figure 7.17b and for 75% of cooperation, the non-detected unreliable sensors are probably due the open boundaries simulation, when a very limited number of cooperative vehicles are stuck on the boundary of the

section. This allows a simple criterion to be given: the trust model is said to be effective for agent i provided that agent i has interacted in a direct way with a large enough number of cooperative vehicles, which appears to be 3 in this configuration but may also depend on the percentage of perturbed or defective sensors.

The main advantage of errors coming from sensors measurements lies in their non-reproducibility between agents. The quality of the estimates does not rely on a binary value but on a measurement, so that is very unlikely to observe a same deviation for two different sensors, which as a result would estimate themselves to be reliable even though they are not. Finally, the trust model appears well suited to the detection of measurement errors. The building of a trust layer for online trust estimation highlighted promising results, and was only compromised by the lack of direct information exchanges. Last but not least, the relatively low computational time of the global simulation, including the dynamic trust layer is also very promising, as the CPU time of the implemented program is of 0.99572s to run one simulation step (in this case merged with the communication time step) with a processor Intel Xeon 2.67 GHz with 24.0 Go of RAM.

Chapter 8

Conclusion and perspectives

The subject of this dissertation work was motivated by the recent investment of car manufacturers and institutions in smart technologies, with the ideal outcome being a zero accident and zero emission traffic within the next few decades. This unprecedent technological explosion is expected to cause extensive changes in the field of traffic engineering, probably even more challenging than the early developments of traffic theory, as ITSs bring together fields like sociology, robotics, informatics, telecommunication, and network optimization.

The preceding research investigates the effects of configuring a mixed traffic on highways, made up of cooperative vehicles, which may be controlled by automatic devices, and vehicles operated by normal drivers, who adopt their own particular behaviors. Controlled cooperative vehicles must not be the cause of any traffic disturbances, including those caused by normal drivers surprised by unusual cooperative behaviors, but should act as smoothing agents in the traffic stream. Therefore, cooperative vehicles have to behave similarly to normal vehicles but differently enough in order to homogenize traffic flow.

In order to manage traffic flow one must first understand the mechanisms of congestion, especially non-recurrent congestion, as it is intuitively the most responsive to cooperative strategies. The microscopic modelling scale was selected to effectively integrate the microscopic form of communication exchanges. The preliminary approach adopted to understand the formation of instabilities in traffic flow consists of investigating the impact of small perturbations in a steady-state traffic. In order to achieve this, a mathematical framework for linear stability analyses inspired by the work of Wilson and Ward, Treiber and Kesting was developed for the time-continuous

class of car-following models. Contributions include the extension of the linear stability analysis to forward and backward multi-anticipation, with the addition of a control term to increase linear string stability, and the graphical root locus method to analyze linear stability for all wavelengths. For larger perturbations, it was demonstrated that for a specific type of traffic condition close to the string stability fronteer, the KdV equation could be derived for time continuous car-following models, with and without forward and backward multi-anticipation. This important result reveals the acceleration regime of the leading edge of the travelling wave, *i.e.* whether vehicles are likely to first brake or accelerate when caught in a perturbation. Numerical simulations confirm the magnitude range of the analytical speed and amplitude.

The limits of stability analyses unequivocally come from its total determinism. In realistic traffic, car following parameters depend on each driver's behavior, and may vary along a trajectory. As a first step towards the evaluation of cooperative strategies as a function of the distribution of those parameters, realistic traffic conditions were reproduced from noisy data trajectories: data filtering, calibration, parameters statistical analysis, sampling, to produce a comprehensive methodological chain. Calibration uncertainties were discussed to obtain a robust set of parameters that proved useful for further analyses. This made it possible to estimate the joint distributions of the set of parameters and discuss various sampling methods. The proposed approach allows the analysis of microscopic parameters to be further refined and extended.

The ability to reproduce realistic traffic is fundamental for the testing of control algorithms so that a realistic perturbed traffic can be chosen as the representation of the ground truth traffic. A natural development of the previous research consisted in the validation of the analytical results with realistic calibrated values on a highway section. While all analytical results were confirmed, for instance, the relevance of bilateral cooperation, it was also demonstrated that 25% of cooperative vehicles can remove instabilities for the specific calibrated traffic flow configuration, with an appropriate car-following law design. Simulation results exceed expectations as the cooperation strategy can cope well with driving behaviors variability.

Finally, a multi-agent approach was proposed as a self-organization paradigm to homogenize traffic flow. The multi-agent framework combines three modelling layers and the environment. The physical layer is responsible of the physical behavior of vehicles, made of normal and cooperative vehicles. The communication layer services cooperative vehicles by distributing information through reliability and proximity rules. The trust layer performs real

time estimates of information reliability, which is then transmitted to the communication layer, and which in turn clouts -controls- the physical layer. When investigating the robustness of this framework to perturbed or defective sensors it was observed that the definition of appropriate communication and trust rules made the model perfectly robust to noise measurements. The results concluded that the modeling framework facilitates improved traffic safety and efficiency, while dealing with communication noises. An approach to dynamic estimation of perturbed and defective sensors concluded the discussion, providing very satisfactory results and highlighting the importance of the number of direct interactions between vehicles to accurately detect unreliable sensors.

Perspectives of the presented research are numerous and can be listed by theme. First, recommendations for future developments on stability analyses include: analytical developments to other types of car-following models such as time delay car-following models that capture physical characterics of vehicles, in order to verify whether similar effects are observable; non-linear stability analyses of car-following models, as very few analytical results are available in the non-linear domain; and Lyapunov's analyses of car-following models to evaluate criteria for traffic flow homogenization. Then, with regards to the reproduction of realistic car-following behavior from data trajectories, perspectives comprise: analyses of multiple estimation techniques and sampling strategies within a robust validation framework, the sampling procedure being strengthened, for example, by methodically analyzing the consistency of the simulated microscopic traffic with real traffic; the study of confidence areas around the found minima, which may reveal the robustness quality of car-following models, when a particular driving behavior corresponds to a particular set or range of parameters; the assessment of the extent to which the quantified uncertainties of parameters identification deform the statistical features of the car-following parameters; the study of online car-following parameters identification algorithms, which would favor control applications. Finally, recommendations for future developments on multi-agent and control algorithms are multiple, among them feature: a dynamic estimation of car-following parameters that allows cooperative vehicles to adapt to their drivers behavior and to the vehicle characteristics, and subsequently enables the tuning of adaptive cooperative strategies in real time; the design of cooperative lane changing models, which should be coupled with the cooperative car-following dynamics, to prevent sudden decelerations caused by a lane change, and to favor necessary lane changing maneuvers without perturbing traffic flow; a geometric extension of this work to small networks, which has been dedicated to highway sections; the design

of tailored control strategies to modify the global steady state equilibrium of the system towards a more string stable system, thereby anticipating a change of traffic conditions, for instance due to changing weather conditions.

Bibliography

[1] T. Hey, S. Tansley, and K. Tolle, editors. *The Fourth Paradigm: Data-Intensive Scientific Discovery*. Microsoft Research, Redmond, Washington, 2009.

[2] M. Parent. Automated vehicles: Autonomous or connected? In *Mobile Data Management (MDM), 2013 IEEE 14th International Conference on*, volume 1, pages 2–2, 2013.

[3] *Advanced Driver Assistance Systems Report*. SupplierBusiness, 2011.

[4] D. Schrank and T. Lomax. *The 2000 urban mobility report*. Texas Transportation Institute, TX, 2009.

[5] M. E. Hallenbeck, J. M. Ishimaru, and J. Nee. Measurement of recurring versus non-recurring congestion. *Washington state department of Transportation*, 2003.

[6] P. Ricoeur. *Freedom and nature: the voluntary and the involuntary*. Northwestern University press, 1950.

[7] `http://select.nytimes.com/gst/abstract.html?res=F10C13FE395916738DDDAF0894DE405B808AF1D3`.

[8] `http://www.eurekanetwork.org/project/-/id/45`.

[9] `http://www.path.berkeley.edu/PATH/Research/Demos/`.

[10] A. De la Fortelle. *Habilitation à diriger des recherches*. Université Paris VI, 2008.

[11] `http://www.etsi.org/index.php/news-events/news/226-press-release-30th-september-2008`.

[12] F. Bai, H. Krishnan, V. Sadekar, G. Holland, and T. ElBatt. Towards characterizing and classifying communication-based automotive applications from a wireless networking perspective. In *Proceedings of IEEE Worshop on Automotive networking and applications (AUTONET)*, 2006.

[13] K. A. Brookhuis, D. Waard, and D. H. Janssen. Behavioral impacts of avanced driver assitance systems- an overview. *EJTIR*, 1(3):245 – 253, 2001.

[14] L. Guvenc, I.M.C. Uygan, K. Kahraman, and R. Karaahmetoglu. Cooperative adaptive cruise control implementation of team mekar at the grand cooperative driving challenge. *Intelligent Transportation Systems, IEEE Transactions on*, 13(3):1062–1074, 2012.

[15] Institution of Mechanical Engineers (Great Britain). *Advanced driver assistance systems (ADAS) : vehicle control for the future*. Bury St. Edmunds : Professional Engineering Pub. for the Institution of Mechanical Engineers, 1999.

[16] `http://transport.epfl.ch/systems-support-networked-automated-driving`.

[17] `http://www.car-to-car.org/`.

[18] `http://www.its.leeds.ac.uk/festa/`.

[19] `http://www.fotsis.com/`.

[20] `http://www.drive-c2x.eu/`.

[21] Y. Suzuki, H. Ishizaka, A. Sakuma, H. Kawashima, K. Aoki, M. Aki, K. Nakano, and Y. Suda. Development of braking systems for platoon-driving - development of energy-saving ITS technologies. In *Intelligent Transportation Systems (ITSC), 2011 14th International IEEE Conference on*, pages 1138–1143, 2011.

[22] `http://www.cvi-utc.org/?q=node/26`.

[23] `http://www.safetypilot.us/`.

[24] B. D. Greenshields. The photographic method of studying traffic behavior. In *PhD thesis, University of Michigan*, 1934.

[25] M. J. Lighthill and G. B. Whitham. On kinematic waves. I. Flood movement in long rivers. *Proceedings of the Royal Society of London. Series A. Mathematical and Physical Sciences*, 229(1178):281–316, 1955.

[26] M. J. Lighthill and G. B. Whitham. On kinematic waves. II. A theory of traffic flow on long crowded roads. *Proceedings of the Royal Society of London. Series A. Mathematical and Physical Sciences*, 229(1178):317–345, 1955.

[27] P. I. Richards. Shock waves on the highway. *Operations Research*, 4(1):42–51, 1956.

[28] D. Helbing. Traffic and related self-driven many-particle systems. *Rev. Mod. Phys.*, 73:1067–1141, Dec 2001.

[29] S. P. Hoogendoorn and P. H. L. Bovy. State-of-the-art of vehicular traffic flow modelling. *Proceedings of the Institution of Mechanical Engineers – Part I*, 215(4):283–303, 2001.

[30] F. Van Wageningen-Kessels. Multi-class continuum traffic flow models: analysis and simulation methods. In *PhD thesis, Delft University of Technology*, 2013.

[31] D. Ni. Multiscale modeling of traffic flow. *Mathematica Aeterna*, 1(1):27–54, 2011.

[32] B. S. Kerner. Phase transitions in traffic flow. In *Traffic and Granular Flow 99*, pages 253–283. Springer Berlin Heidelberg, 2000.

[33] R. J. Leveque. Numerical methods for conservation laws. *Birkhauser Verlag, Basel, Switzerland*, 1992.

[34] L. A. Pipes. An operational analysis of traffic dynamics. *Journal of Applied Physics*, 24(3):274–281, 1953.

[35] G.F. Newell. A simplified theory of kinematic waves in highway traffic, part II: Queueing at freeway bottlenecks. *Transportation Research Part B: Methodological*, 27(4):289 – 303, 1993.

[36] C. F. Daganzo. The cell transmission model, part II: network traffic. *Transportation Research Part B: Methodological*, 29(2):79 – 93, 1995.

[37] C. Daganzo. On the variational theory of traffic flow: well-posedness, duality and applications. *Networks and heterogeneous media*, 1(4):601, 2006.

[38] H. Greenberg. An analysis of traffic flow. *Operations Research*, 7(1):79–85, 1959.

[39] M. Van Aerde. Multivariate calibration of single regime speed-flow-density relationships. *In 74th Annual Meeting of the Tranportation Research Board*, 1995.

[40] R. Underwood. Speed, volume, and density relationships: quality and theory of traffic flow. *Yale Bureau of Highway Traffic*, pages 141–188, 1961.

[41] Y. Wang and M. Papageorgiou. Real-time freeway traffic state estimation based on extended kalman filter: a general approach. *Transportation Research Part B: Methodological*, 39(2):141 – 167, 2005.

[42] Traffic Flow Theory and Characteristics Committee of the Transportation Research Board. 75 years of the fundamental diagram for traffic flow theory: Greenshields symposium. TRB Transportation Research Electronic Circular E-C149:, 2011.

[43] R. Courant and D. Hilbert. Methods of mathematical physics: Partial differential equations, volume II. 1969.

[44] S. Blandin. Modelling, estimation and control of distributed parameter systems: application to transportation networks, Ph.D. thesis. 2012.

[45] R. J. Leveque. Springer, Series Lectures in Mathematics. ETH Zurich, 1992.

[46] W. J. M. Rankine. On the thermodynamic theory of waves of finite longitudinal disturbance. *Proceedings of the Royal Society of London*, 18:pp. 80–83, 1869.

[47] A. Aw and M. Rascle. Resurrection of "second order" models of traffic flow? *SIAM J. APPL. MATH*, 60:916–938, 1999.

[48] H. M. Zhang. A non-equilibrium traffic model devoid of gas-like behavior. *Transportation Research Part B: Methodological*, 36(3):275 – 290, 2002.

[49] R. Jiang, Q.-S. Wu, and Z.-J. Zhu. A new continuum model for traffic flow and numerical tests. *Transportation Research Part B: Methodological*, 36(5):405 – 419, 2002.

[50] R. Billot, C. Chalons, F. De Vuyst, N.-E. El Faouzi, and J. Sau. A conditionally linearly stable second-order traffic model derived from a Vlasov kinetic description. *Comptes Rendus Mecanique*, 338(9):529 – 537, 2010.

[51] C. F. Daganzo. Requiem for second-order fluid approximations of traffic flow. *Transportation Research Part B: Methodological*, 29(4):277 – 286, 1995.

[52] H. J. Payne. Models of freeway traffic and control. *Math. Models Publ. Sys*, 28:51–61, 1971.

[53] E. Godlewski and P. A. Raviard. Hyperbolic systems of conservation laws. *Collection Mathématiques et Applications de la SMAI, Ellipse*, 1991.

[54] J.-P. Lebacque, S. Mammar, and H. Haj-Salem. The aw-rascle and zhang's model: Vacuum problems, existence and regularity of the solutions of the riemann problem. *Transportation Research Part B: Methodological*, 41(7):710 – 721, 2007.

[55] R. Billot. Analyse et modélisation de l'impact de la météorologie sur le trafic routier, Ph.D. thesis. 2010.

[56] M. Ben-Akiva, M. Bierlaire, H.N. Koutsopoulos, , and R. Mishalani. Dynamit: A simulation-based system for traffic prediction and guidance generation. *Proceedings of the 3rd Triennial Symposium on Transportation Systems*, 1998.

[57] R. Jayakrishnan, H. S. Mahmassani, and T.-Y. Hu. An evaluation tool for advanced traffic information and management systems in urban networks. *Transportation Research Part C: Emerging Technologies*, 2(3):129 – 147, 1994.

[58] I. Prigogine and R. Herman. Kinetic theory of vehicular traffic. *American Elsevier Pub. Co.*, 1971.

[59] R. Illner, C. Kirchner, and R. Pinnau. A derivation of the Aw-Rascle traffic models from Fokker-Planck type kinetic models. *Quart. Appl. Math.*, 67:39–45, 2009.

[60] D. Ngoduy, S. P. Hoogendoorn, and R. Liu. Continuum modeling of cooperative traffic flow dynamics. *Physica A: Statistical Mechanics and its Applications*, 388(13):2705 – 2716, 2009.

[61] A. Klar and R. Wegener. Kinetic derivation of macroscopic anticipation models for vehicular traffic. *SIAM J. Appl. Math.*, 60(5):1749–1766, 2000.

[62] A. Klar and R. Wegener. Enskog-like kinetic models for vehicular traffic. *J. Stat Phys.*, 87:9–1, 1997.

[63] S. P. Hoogendoorn. Multiclass continuum modelling of multilane traffic flow. *Delft University Press*, 1999.

[64] M. Treiber and A. Kesting. *Traffic flow dynamics: data, models and simulation*. Springer, 2013.

[65] A. Kesting, M. Treiber, and D. Helbing. Enhanced intelligent driver model to access the impact of driving strategies on traffic capacity. *Philosophical Transactions of the Royal Society*, A 368:4585–4605, 2010.

[66] M. Bando, K. Hasebe, A. Nakayama, A. Shibata, and Y. Sugiyama. Dynamical model of traffic congestion and numerical simulation. *Phys. Rev. E*, 51(2):1035–1042, 1995.

[67] A. Kesting and M. Treiber. Calibrating car-following models using trajectory data: Methodological study. *Journal of the transportation research Board*, 2088:148, 2008.

[68] A. Kesting, M. Treiber, and D. Helbing. General lane-changing model mobil for car-following models. *Transportation Research Record: Journal of the Transportation Research Board*, Volume 1999:86–94, 2005.

[69] M. Treiber and A. Kesting. Validation of traffic flow models with respect to the spatiotemporal evolution of congested traffic patterns. *Transportation Research Part C: Emerging Technologies*, 21(1):31 – 41, 2012.

[70] J. Monteil, R. Billot, D. Rey, and N-E. El Faouzi. Distributed and centralized approaches for cooperative road traffic. *Procedia - Social and Behavioral Sciences*, 48:3198–3208, 2012.

[71] R. Jiang, Q. Wu, and Z. Zhu. Full velocity difference model for a car-following theory. *Phys. Rev. E*, 64:017101, 2001.

[72] G.F. Newell. A simplified car-following theory: a lower order model. *Transportation Research Part B: Methodological*, 36(3):195 – 205, 2002.

[73] H. Rakha and B. Crowther. Comparison of Greenshields, Pipes, and Van Aerde car-following and traffic stream models. *Transportation Research Record*, 1802(1):248–262, 2002.

[74] H. Greenberg. An analysis of traffic flow. *Operations Research*, 7(1):79–85, 1959.

[75] A. D. May. *Traffic flow fundamentals*. Prentice Hall, 1990.

[76] M. Van Aerde and H. Rakha. Multivariate calibration of single regime speed-flow-density relationships. In *Vehicle Navigation and Information Systems Conference, 1995. Proceedings*, pages 334–341, 1995.

[77] H. Rakha, P. Pasumarthy, and S. Adjerid. A simplified behavioral vehicle longitudinal motion model. *Transportation letters*, 1:95–110, 2009.

[78] H. Rakha and K. Ahn. Integration modeling framework for estimating mobile source emissions. *Journal of transportation engineering*, 130:183–193, 2004.

[79] G. F. Newell. Nonlinear effects in the dynamics of car following. *Operations Research*, 9(2):209–229, 1961.

[80] E. Sueli and D. Mayers. *An Introduction to Numerical analysis*. Cambridge: Cambridge University Press. x, 433 p., 2003.

[81] S. Ahn, M. J. Cassidy, and J. Laval. Verification of a simplified car-following theory. *Transportation Research Part B: Methodological*, 38(5):431 – 440, 2004.

[82] K. Nagel and M. Schreckenberg. A cellular automaton model for freeway traffic. *Journal de Physique I*, 2(12):2221–2229, December 1992.

[83] C. Quek, M. Pasquier, and B. Lim. A novel self-organizing fuzzy rule-based system for modelling traffic flow behaviour. *Expert Syst. Appl.*, 36(10):12167–12178, December 2009.

[84] T. Schulze and T. Fliess. Urban traffic simulation with psycho-physical vehicle-following models. In *Proceedings of the 29th Conference on Winter Simulation*, WSC '97, pages 1222–1229, Washington, DC, USA, 1997. IEEE Computer Society.

[85] D. Ngoduy. Analytical studies on the linear instabilities of heterogeneous intelligent traffic flow. *Communications in Nonlinear Science and Numerical Simulation*, 388(18):2838 – 2851, 2013.

[86] D. Ngoduy. Platoon based macroscopic model for intelligent traffic flow. *Transportmetrica Part B*, (1):153–169, 2013.

[87] D. Ngoduy and R. E. Wilson. Multi-anticipative nonlocal macroscopic traffic model. *Computer-Aided Civil and Infrastructure Engineering*, 2013.

[88] A. Kesting, M. Treiber, and D. Helbing. Enhanced intelligent driver model to access the impact of driving strategies on traffic capacity. *Philosophical Transactions of the Royal Society A: Mathematical, Physical and Engineering Sciences*, 368(1928):4585–4605, 2010.

[89] S. P. Hoogendoon, S. Ossen, and M. Schreuder. Emprirics of multi-anticipative car-following behavior. *Transportation Research Record: Journal of the Transportation Research Board*, (1965):112–120, 2006.

[90] H. X. Ge, S.Q. Dai, and L. Y. Dong. An extended car-following model based on intelligent transportation system application. *Physica A: Statistical Mechanics and its Applications*, 365(2):543 – 548, 2006.

[91] M. Treiber, A. Kesting, and D. Helbing. Delays, inaccuracies and anticipation in microscopic traffic models. *Physica A: Statistical Mechanics and its Applications*, 360(1):71–88, 2006.

[92] W. K. Potts. The chorus-line hypothesis of manoeuvre coordination in avian flocks. *Nature*, (309):344–345, 1984.

[93] T. J. Pitcher, B. L. Partridge, and C. S. Wardle. A blind fish can school. *Science*, (194):963–968, 1976.

[94] Craig W. Reynolds. Flocks, herds and schools: A distributed behavioral model. *SIGGRAPH Comput. Graph.*, 21(4):25–34, 1987.

[95] R. Olfati-Saber. Flocking for multi-agent dynamic systems: Algorithms and theory. *IEEE Transactions on Automatic Control*, 51:401–420, 2006.

[96] J. LaSalle. Some extensions of liapunov's second method. *Circuit Theory, IRE Transactions on*, 7(4):520–527, 1960.

[97] C. Nowakowski, S. E. Shladover, and D. Cody. Cooperative adaptive cruise control: Testing drivers' choices of following distances. *California Path research report*, 2010.

[98] M. Treiber and A. Kesting. Microscopic calibration and validation of car-following models : A systematic approach. *Procedia - Social and Behavioral Sciences*, 80(0):922 – 939, 2013. 20th International Symposium on Transportation and Traffic Theory (ISTTT 2013).

[99] R. E. Wilson and J. A. Ward. Car-following models: fifty years of linear stability analysis - a mathematical perspective. *Transportation Planning and Technology*, 34(1):3–18, 2011.

[100] E. N. Lorentz. Deterministic nonperiodic flow. *J. Atmos. Sci.*, (20):130–141, 1963.

[101] B. Mandelbrot. How long is the coast of Britain? Statistical self-similarity and fractional dimension. *Science*, 156(3775):636–638, 1967.

[102] J. Yi, H. Lin, L. Alvarez, and R. Horowitz. Stability of macroscopic traffic flow modeling through wavefront expansion. *Transportation Research Part B: Methodological*, 37(7):661 – 679, 2003.

[103] J. Yi and R. Horowitz. Macroscopic traffic flow stability for adaptive cruise controlled (ACC) vehicles. *Proceedings of the IEEE Conference on Decision and Control*, 1(1):893–899, 2003.

[104] D. Helbing and A. Johansson. On the controversy around Daganzo's requiem for and Aw-Rascle's resurrection of second-order traffic flow models. In *Modelling and Optimisation of Flows on Networks*, Lecture Notes in Mathematics, pages 271–302. Springer Berlin Heidelberg, 2013.

[105] R. E. Wilson. Mechanisms for spatio-temporal pattern formation in highway traffic models. *Phil. Trans. R. Soc. A*, 366(1872):2017–2032, 2008.

[106] R. E. Wilson. An analysis of Gipps' car-following model of highway traffic. *IMA Journal of Applied Mathematics*, (66):509–537, 2000.

[107] M. Treiber and A. Kesting. Evidence of convective instability in congested traffic flow: A systematic empirical and theoretical investigation. *Transportation Research Part B: Methodological*, 45(9):1362 – 1377, 2011. Selected Paper from the 19th ISTTT.

[108] B. S. Kerner. Analytical calculation of critical perturbation amplitudes and critical densities by non-linear stability analysis of a simple traffic flow model. *The European Physical Journal B*, 69:551–581, 2009.

[109] B. S. Kerner. Experimental features of self-organization in traffic flow. *Phys. Rev. Lett.*, 81:3797–3800, Oct 1998.

[110] T. Taniuti. Reductive perturbation method and far fields of wave equations. *Progress of Theoretical Physics Supplement*, 55:1–35, 1974.

[111] H. C. Fogedby. Solitons and diffusive modes in the noiseless burgers equation: Stability analysis. *Phys. Rev. E*, 57:2331–2337, 1998.

[112] R. A. Kraenkel, J. G. Pereira, and M. A. Manna. The reductive perturbation method and the Korteweg-de Vries hierarchy. *Acta Applicandae Mathematicae*, 39:389–403, 1995. 10.1007/BF00994645.

[113] H. Leblond. The reductive perturbation method and some of its applications. *Journal of Physics B: Atomic, Molecular and Optical Physics*, 41(4):043001, 2008.

[114] P. G. Drazin and R. S. Johnson. *Solitons : an introduction / P.G. Drazin, R.S. Johnson.* Cambridge University Press, Cambridge [England] ; New York, 1989.

[115] H. Demiray. An application of modified reductive perturbation method to long water waves. *International Journal of Engineering Science*, 49(12):1397 – 1403, 2011.

[116] M. Muramatsu and T. Nagatani. Soliton and kink jams in traffic flow with open boundaries. *Phys. Rev. E*, 60:180–187, Jul 1999.

[117] H. X. Ge, R. J. Cheng, and S. Q. Dai. KdV and kink and antikink solitons in car-following models. *Physica A: Statistical Mechanics and its Applications*, 357:466 – 476, 2005.

[118] Y. Li, H. Zhu, M. Cen, Y. Li, R.i Li, and D. Sun. On the stability analysis of microscopic traffic car-following model: a case study. *Nonlinear Dynamics*, 74(1-2):335–343, 2013.

[119] F. Losilla, A.-J. Garcia-Sanchez, F. Garcia-Sanchez, J. Garcia-Haro, and Z. J. Haas. A comprehensive approach to WSN-based ITS applications: A survey. *Sensors*, 11(11):10220–10265, 2011.

[120] M. C. Cross and P. C. Hohenberg. Pattern formation outside of equilibrium. *Rev. Mod. Phys.*, 65:851–1112, 1993.

[121] M. Hărăguş-Courcelle and D. H. Sattinger. Inversion of the linearized korteweg-de vries equation at the multi-soliton solutions. *Z. Angew. Math. Phys.*, 49(3):436–469, May 1998.

[122] W. R. Evans. Graphical analysis of control systems. *American Institute of Electrical Engineers, Transactions of the*, 67(1):547–551, 1948.

[123] R. C. Dorf and R. H. Bishop. *Modern control systems*. Reading, Mass. Addison-Wesley, 1995.

[124] J. Sau, J. Monteil, R. Billot, and N.-E. El Faouzi. Design of cooperative car-following models using root locus analysis. *Submitted to Tranportmetrica B: Tranport Dynamics*, 2013.

[125] `http://ngsim-community.org/`.

[126] V. Punzo, D. J. Forminaso, and V. Torrieri. Nonstationary kalman filter for estimation of accurate and consistent car-following data. *Proceedings of the 84th Transportation Research Board Annual Meeting*, 2005.

[127] S. H. Hamdar and H. S. Mahmassani. Driver car-following behavior: From discrete event process to continuous set of episodes. *Proceedings of the 87th Transportation Research Board Annual Meeting*, 2008.

[128] V. Punzo, M. T. Borzacchiello, and B. Ciuffo. On the assessment of vehicle trajectory data accuracy and application to the Next Generation Simulation (NGSIM) program data. *Transportation Research Part C: Emerging Technologies*, 19(6):1243 – 1262, 2011.

[129] F. Marzack and C. Buisson. New filtering method for trajectory measurement errors and its comparison with existing methods. *Transportation Research Record: Journal of the Transportation Research Board*, 2315:35–46, 2012.

[130] H. Rakha, F. Dion, and H.-G. Sin. Using global positioning system data for field evaluation of energy and emission impact of traffic flow

improvement projects: Issues and proposed solutions. *Transportation Research Record: Journal of the Transportation Research Board*, Volume 1768(1):210–223, 2001.

[131] A. Kesting and M. Treiber. Calibrating car-following models using trajectory data: Methodological study. *Transportation Research Record: Journal of the Transportation Research Board*, 2088(6):148–156, 2008.

[132] C. Thiemann, M. Treiber, and A. Kesting. Estimating acceleration and lane-changing dynamics from next generation simulation trajectory data. *Transportation Research Record: Journal of the Transportation Research Board*, 2088, 2008.

[133] V. Punzo, B. Ciuffo, and M. Montanino. May we trust results of car-following models calibration based on trajectory data? *Proceedings of the 91st Transportation Research Board Annual Meeting*, 2012.

[134] J. Kim and H. S. Mahmassani. Correlated parameters in driving behavior models: Car-following example and implications for traffic microsimulation. *Transportation Research Record: Journal of the Transportation Research Board*, 2249:62–77, 2011.

[135] P. E. L. Zhang and V. G. Kovvali. Freeway gap acceptance behaviors based on vehicle trajectory analysis. *Proceedings of the 86th Transportation Research Board Annual Meeting*, 2007.

[136] T. Toledo, C. Choudhury, and M.-E. Ben-Akiva. Lane-changing model with explicit target lane choice. *Transportation Research Record: Journal of the Transportation Research Board*, Volume 1934:157–165, 2005.

[137] L. Leclerq, N. Chiabaut, J. A. Laval, and C. Buisson. Relaxation phenomenon after changing lanes: Experimental validation with NGSIM data set. *Transportation Research Record: Journal of the Transportation Research Board*, 1999:79–85, 2007.

[138] Methods and tools for supporting the use, calibration and validation of traffic simulation models (MULTITUDE). http://www.multitude-project.eu/, 2013.

[139] A. Amer, H. Rakha, and I. El-Shawarby. Agent-based stochastic modeling of driver decision at onset of yellow light at signalized intersections. *Transportation research record*, (2241):68–77, 2011.

[140] L. Ljung. *System identification: theory for the user*. Prentice-Hall, Inc., Upper Saddle River, NJ, USA, 1986.

[141] I. D. Landau and G. Zito. *Digital Control Systems*. Springer, 2006.

[142] W. T. Eadie and F. James. *Statistical methods in experimental physics*. World Scientific, 2006.

[143] F.. James. *Statistical methods in experimental physics*. World Scientific, 2006.

[144] Minuit, cernlib 1994. http://hep.fi.infn.it/minuit.pdf/, 1994.

[145] V. Punzo and M. Montanino. Making NGSIM data usable for studies on traffic flow theory: Multistep method for vehicle trajectory reconstruction. *Proceedings of the 91th Transportation Research Board Annual Meeting*, 2013.

[146] Inc. Lindo Systems. Lindo API user manual 2.0, 2003.

[147] H. Rakha and W. Wang. Procedure for calibrating Gipps' car-following model. *Transportation Research Record: Journal of the Transportation Research Board*, 2124:113–124, 2009.

[148] M. Kendall and A. Stuart. *The advanced theory of statistics. Inference and relationship (4th edition)*. New York : Macmillan 2, 1979.

[149] B. Schweizer and E. F. Wolff. On nonparametric measures of dependence for random variables. *The annals of statistics*, pages 879–885, 1981.

[150] H. Hotelling and M. R. Pabst. Rank correlation and tests of significance involving no assumption of normality. *The Annals of Mathematical Statistics*, 7(1):29–43, 1936.

[151] G. Govaert. *Data analysis*, volume 136. Wiley. com, 2010.

[152] I. T. Jolliffe. *Principal component analysis*. Springer, 2002.

[153] S. S. Shapiro and M. B. Wilk. An analysis of variance test for normality (complete samples). *Biometrika*, 52(3/4):591–611, 1965.

[154] R. O. Duda, P. E. Hart, and D. G. Stork. *Pattern classification*. John Wiley & Sons, 2012.

[155] V. Punzo. Trajectory-based and aggregate measures-based calibration of traffic simulation models: a cross-comparison exploratory study. Reliability and Statistics in Transportation and Communication International Conference - RelStat'12, Riga, Latavia, October 19th, 2013.

[156] R. B. Nelsen. *An introduction to copulas*. Springer, 1999.

[157] M. Wang, M. Treiber, W. Daamen, S. P. Hoogendoorn, and B. Van Arem. Modelling supported driving as an optimal control cycle: Framework and model characteristics. *Procedia - Social and Behavioral Sciences*, 80(0):491 – 511, 2013. 20th International Symposium on Transportation and Traffic Theory (ISTTT 2013).

[158] Hideki Yukawa. On the interaction of elementary particles. I. *Progress of Theoretical Physics Supplement*, 1:1–10, 1955.

[159] M. Treiber and A. Kesting. Modeling lane-changing decisions with mobil. In *Traffic and Granular Flow 07*, pages 211–221. Springer Berlin Heidelberg, 2009.

[160] J. Laval, M. Cassidy, and C. Daganzo. Impacts of lane changes at merge bottlenecks: A theory and strategies to maximize capacity. In *Traffic and Granular Flow 05*, pages 577–586. Springer Berlin Heidelberg, 2007.

[161] F. Habtemichael. Improved active traffic management system for motorway safety and efficiency: Benefits of reducing the driving task difficulty, Ph.D. thesis. 2014.

[162] Ralf Risser. Behavior in traffic conflict situations. *Accident Analysis and Prevention*, 17(2):179 – 197, 1985.

[163] F. Guo and Y. Fang. Individual driver risk assessment using naturalistic driving data. *Accident Analysis and Prevention*, 2012.

[164] J. Choi, S. Oh, and R. Horowitz. Distributed learning and cooperative control for multi-agent systems. *Automatica*, 45(12):2802–2814, December 2009.

[165] SSAM, software user manual. http://www.fhwa.dot.gov/publications, 2008.

[166] M. M. Minderhoud and P. H.L. Bovy. Extended time-to-collision measures for road traffic safety assessment. *Accident Analysis and Prevention*, 33(1):89 – 97, 2001.

[167] A. Kesting, M. Treiber, and D. Helbing. General lane-changing model mobil for car-following models. *Transportation Research Record: Journal of the Transportation Research Board*, Volume 1999:86–94, 2005.

[168] J. McCarthy. Programs with common sense. In *Semantic Information Processing*, pages 403–418. MIT Press, 1968.

[169] D. Poole, A. Mackworth, and R. Goebel. *Computational Intelligence: a logical approach*. Oxford University Press, Oxford, 1998.

[170] S. J. Russell and P. Norvig. *Artificial Intelligence: A Modern Approach*. Pearson Education, 2003.

[171] A. Newell. *Unified Theories of Cognition (The William James Lectures)*. Harvard University Press, October 2002.

[172] O. Etzioni and D. Weld. A softbot-based interface to the internet. *Commun. ACM*, 37(7):72–76, July 1994.

[173] M. Sahami, S. Dumais, D. Heckerman, and E. Horvitz. A bayesian approach to filtering junk e-mail, 1998.

[174] Dynamic reconfiguration: Basic building blocks for autonomic computing on IBM pSeries servers - Author Bios.

[175] J. M. E. Gabbai, Y. Hujun, W. A. Wright, and N. M. Allinson. Self-organization, emergence and multi-agent systems. In *Neural Networks and Brain, 2005. ICNN B '05. International Conference on*, volume 3, pages nil24–1863, 2005.

[176] B. Chen and H. H. Cheng. A review of the applications of agent technology in traffic and transportation systems. *Trans. Intell. Transport. Sys.*, 11(2):485–497, June 2010.

[177] A. M. Garcia-Serrano and D. Teruel Vioque. FIPA-compliant MAS development for road traffic management with a knowledge-based approach: the track-r agents. In *the TRACK-R agents, Challenges in Open Agent Systems '03 Workshop*, 2003.

[178] V. R. Tomás and L. A. García. Agent-based management of non urban road meteorological incidents. In *Proceedings of the 4th international Central and Eastern European conference on Multi-Agent Systems and Applications*, CEEMAS'05, pages 213–222, Berlin, Heidelberg, 2005. Springer-Verlag.

[179] B. Chen, H. H. Cheng, and J. Palen. Integrating mobile agent technology with multi-agent systems for distributed traffic detection and management systems. *Transportation Research Part C: Emerging Technologies*, 17(1):1 – 10, 2009.

[180] H. H. Cheng, B. D. Shaw, J. Palen, B. Lin, Bo Chen, and Z. Wang. Development and field test of a laser-based nonintrusive detection system for identification of vehicles on the highway. *Trans. Intell. Transport. Sys.*, 6(2):147–155, June 2005.

[181] F.-E. Wang. Agent-based control for networked traffic management systems. *IEEE Intelligent Systems*, 20(5):92–96, September 2005.

[182] S. Ossowski, J. Cuena, and A. García-Serrano. A case of multiagent decision support: Using autonomous agents for urban traffic control. In *Proceedings of the 6th Ibero-American Conference on AI: Progress in Artificial Intelligence*, IBERAMIA '98, pages 100–111, London, UK, UK, 1998. Springer-Verlag.

[183] H.-S. Zhang, Y. Zhang, Z.-H. Li, and D.-C. Hu. Spatial-temporal traffic data analysis based on global data management using mas. *Trans. Intell. Transport. Sys.*, 5(4):267–275, December 2004.

[184] M. C. Choy, D. Srinivasan, and R.L. Cheu. Cooperative, hybrid agent architecture for real-time traffic signal control. *Systems, Man and Cybernetics, Part A: Systems and Humans, IEEE Transactions on*, 33(5):597–607, 2003.

[185] D. Srinivasan and M. C. Choy. Cooperative multi-agent system for coordinated traffic signal control. *Intelligent Transport Systems, IEE Proceedings*, 153(1):41–50, 2006.

[186] R. S. Chen, D. K. Chen, and S. Y. Lin. Actam: Cooperative multiagent system architecture for urban traffic signal control. E88D, 2005.

[187] A. R. Danko. Using intelligent agents for pro-active, real-time urban intersection control. *European Journal of Operational Research*, 131(2):293 – 301, 2001. Artificial Intelligence on Transportation Systems and Science.

[188] R. J. F. Rossetti, S. Bampi, Ronghui L., D. Van Vliet, and H. B. B. Cybis. An agent-based framework for the assessment of drivers' decision-making. In *Intelligent Transportation Systems, 2000. Proceedings. 2000 IEEE*, pages 387–392, 2000.

[189] H. Dia and S. Panwai. Modelling drivers' compliance and route choice behaviour in response to travel information. *Nonlinear Dynamics*, 49(4):493–509, 2007.

[190] J. L. Adler, G. Satapathy, V. Manikonda, B. Bowles, and V. J. Blue. A multi-agent approach to cooperative traffic management and route guidance. *Transportation Research Part B: Methodological*, 39(4):297 – 318, 2005.

[191] B. Burmeister, A. Haddadi, and G. Matylis. Application of multi-agent systems in traffic and transportation. *Software Engineering. IEE Proceedings*, 144(1):51–60, 1997.

[192] R. Sukthankar, S. Baluja, and J. Hancock. Multiple adaptive agents for tactical driving. *Applied Intelligence*, 9(1):7–23, July 1998.

[193] S. Hallan and B. Chaib-draa. A collaborative driving system based on multiagent modelling and simulations. *Transportation Research Part C: Emerging Technologies*, 13(4):320 – 345, 2005. Agents in Traffic and Transportation: Exploring Autonomy in Logistics, Management, Simulation, and Cooperative Driving.

[194] P. Y. Li, R. Horowitz, L. Alvarez, J. Frankel, and A. M. Robertson. An automated highway system link layer controller for traffic flow stabilization. *Transportation Research Part C: Emerging Technologies*, 5(1):11 – 37, 1997.

[195] P. Varaiya. Smart cars on smart roads: problems of control. *Automatic Control, IEEE Transactions on*, 38(2):195–207, 1993.

[196] U. Karaaslan, P. Varaiya, and J. Walrand. Two proposals to improve freeway traffic flow. In *American Control Conference, 1991*, pages 2539–2544, 1991.

[197] J. Lygeros, D. N. Godbole, and S. Sastry. Verified hybrid controllers for automated vehicles. *Automatic Control, IEEE Transactions on*, 43(4):522–539, 1998.

[198] S. E. Shladover, C. A. Desoer, J. K. Hedrick, M. Tomizuka, J. Walrand, W.-B. Zhang, D.H. McMahon, H. Peng, S. Sheikholeslam, and N. McKeown. Automated vehicle control developments in the PATH program. *Vehicular Technology, IEEE Transactions on*, 40(1):114–130, 1991.

[199] J.G. Bender. An overview of systems studies of automated highway systems. *Vehicular Technology, IEEE Transactions on*, 40(1):82–99, 1991.

[200] P. Li, L. Alvarez, and R. Horowitz. Ahs safe control laws for platoon leaders. *Control Systems Technology, IEEE Transactions on*, 5(6):614–628, 1997.

[201] C. Canudas de Wit and B. Brogliato. Stability issues for vehicle platooning in automated highway systems. In *Control Applications, 1999. Proceedings of the 1999 IEEE International Conference on*, volume 2, pages 1377–1382 vol. 2, 1999.

[202] J. A. Fax and R. M. Murray. Information flow and cooperative control of vehicle formations. *IEEE Transactions on Automatic Control*, 49:1465–1476, 2004.

[203] Y.-L. Chuang, M. R. D'Orsogna, D. Marthaler, A. L. Bertozzi, and L. S. Chayes. State transitions and the continuum limit for a 2D interacting, self-propelled particle system. *Physica D: Nonlinear Phenomena*, 232(1):33 – 47, 2007.

[204] L. Ljung. Analysis of recursive stochastic algorithms. *Automatic Control, IEEE Transactions on*, 22(4):551–575, 1977.

[205] L. Peng and Y. Jia. Average consensus in networks of multi-agents with both switching topology and coupling time-delay. *Physica A: Statistical Mechanics and its Applications*, 387(1):303 – 313, 2008.

[206] J. Qiang, K. S. T. Wallace, and A. H. Wolfgang. Leader Following of Nonlinear Agents With Switching Connective Network and Coupling Delay. *IEEE Transactions on Circuits and Systems I-regular Papers*, 58:2508–2519, 2011.

[207] R. Holzer and H. de Meer. On modeling of self-organizing systems. In *Proceedings of the 2nd International Conference on Autonomic Computing and Communication Systems*, Autonomics '08, pages 29:1–29:6, ICST, Brussels, Belgium, Belgium, 2008. ICST (Institute for Computer Sciences, Social-Informatics and Telecommunications Engineering).

[208] O. Lefevre, F. Armetta, G. Clair, and S. Hassas. MANA: A new multi-agent approach for complex assignment problems. In *Proceed-*

ings of the 2009 Computation World: Future Computing, Service Computation, Cognitive, Adaptive, Content, Patterns, COMPUTATIONWORLD '09, pages 167–172, Washington, DC, USA, 2009. IEEE Computer Society.

[209] S. Abdallah and V. Lesser. Multi-agent reinforcement learning and self-organization in a network of agents. In *Proceedings of the 6th international joint conference on Autonomous agents and multiagent systems*, AAMAS '07, pages 39:1–39:8, New York, NY, USA, 2007. ACM.

[210] S. P. Marsh. *Formalising Trust as a Computational Concept.* PhD thesis, University of Stirling, April 1994.

[211] J. Sen. A survey on reputation and trust-based systems for wireless communication networks. *CoRR*, 2010.

[212] H. Alzaid, M. Alfaraj, S. Ries, A. Josang, M. Albabtain, and A. Abuhaimed. Reputation-based trust systems for wireless sensor networks: A comprehensive review. In *Trust Management VII*, volume 401 of *IFIP Advances in Information and Communication Technology*, pages 66–82. Springer Berlin Heidelberg, 2013.

[213] J. Sabater and C. Sierra. Review on computational trust and reputation models. *Artificial Intelligence Review*, 24:33–60, 2005.